The Pennsylvania State University
The Graduate School

NITRIC OXIDE-PRODUCING INTERNEURONS CONTROL BASAL AND EVOKED BLOOD FLOW IN SOMATOSENSORY CORTEX

A Dissertation in

Bioengineering

by

Christina Echagarruga

Submitted in Partial Fulfillment
of the Requirements
for the Degree of

Doctor of Philosophy

August 2019

The dissertation of Christina Echagarruga was reviewed and approved* by the following:

Patrick Drew
Associate Professor, Engineering Science and Mechanics, Neurosurgery
Dissertation Advisor
Chair of Committee

Nanyin Zhang
Professor of Biomedical Engineering and Electrical Engineering

Kevin Alloway
Professor, Neural and Behavioral Sciences,
College of Medicine Chair of Graduate Program in Neuroscience

Bruce J. Gluckman
Associate Director, Penn State Center for Neural Engineering
Professor of Engineering Science and Mechanics, Neurosurgery, and Bioengineering

William Hancock
Chair of the Intercollege Graduate Program in Bioengineering
Professor of Bioengineering

*Signatures are on file in the Graduate School

Abstract

Changes in cortical neural activity are coupled to changes in local arterial diameter and blood flow. However, the neuronal types and the signaling mechanisms that control the basal diameter of cerebral arteries or their dilations are not well understood. Using chronic two-photon microscopy, electrophysiology, chemogenetics, and pharmacology in awake, head-fixed mice, I dissected the role of multiple neuron subtypes and their signaling mechanisms in controlling the basal diameter and evoked dilation in cortical arteries. I found that modulation of overall neural activity up or down caused corresponding increases or decreases in basal arterial diameter. Surprisingly, modulation of pyramidal neuron activity had minimal effects on basal or evoked arterial dilation. Instead, the neurally-mediated component of arterial dilation was largely regulated through nitric oxide released by neuronal nitric oxide synthase (nNOS)-expressing neurons, whose activity was not reflected in electrophysiological measures of population activity. Our results show that cortical hemodynamic signals are not controlled by the average activity of the neural population, but rather the activity of a small 'oligarchy' of neurons.

Contents

List of Figures

List of Tables

List of Abbreviations

ACA	anterior cerebral artery
MCA	middle cerebral artery
MLCK	myosin light chain kinase
αSMA	α-smooth muscle actin
LFP	local field potential
MUA	multi-unit activity
VGAT	Vesicular GABA Transporter
ChR2	channelrhodopsin
AA	arachidonic acid
EETs	epoxyeicosatrienoic acids
NO	nitric oxide
NOS	nitric oxide synthase
SOM	somatostatin
NPY	neuropeptide y
ACh	acetylcholine
NE	norepinephrine
5HT	serotonin
BF	basal forebrain
NK1R	neurokinin 1 receptor
NBM	nucleus basalis of Meynert
TRPV4	transient receptor potential vanilloid 4
mGluR	metabotropic glutamate receptors
Kir	inward rectifying potassium channel
BOLD	blood-oxygen-level dependent
fMRI	functional magnetic resonance imaging
sGC	soluble guanalyl cyclase
7NI	7-Nitroindazole
HBOCs	hemoglobin-based oxygen carriers
mAChR	Muscarinic acetylcholine receptor
CNO	clozapine-n-oxide
GIRK	G-protein inwardly rectifying K^+ channels
aCSF	artificial cerebrospinal fluid

Acknowledgements

First and foremost, I'd like to thank my mentor, Patrick Drew, for his support, guidance, and insight over the past four years. From the moment I began in the Drew lab, Patrick's enthusiasm for his research and the success of his students made a strong impression on me. Patrick invested so much time and effort on my behalf that it motivated me to work hard. I worked hard both to meet his implicit expectations, but also because his excitement rubbed off and spurred excitement within me.

I would like to thank numerous members of the Drew lab for their support and guidance. Qingguang Zhang has been a fantastic mentor to me as the postdoc in the lab and I have been motivated by his enthusiasm, efficiency, and work ethic. Kyles Gheres was the biggest help in developing my project both conceptually and by physically helping me with experiments. He has provided invaluable help in understanding neuroscience concepts.

Along with Kyle, Jordan Norwood, Ravi Kedarasetti, and Davis Haselden have been the best labmates I could hope for; Together they were very important in keeping me happy in State College. Thank you to Aylin Dincer and Deborah Anderson, who were in the lab when I joined and helped keep the lab running over the first few years of my PhD.

I'd like to thank my thesis committee: Nanyin Zhang, Kevin Alloway, and Bruce Gluckman for comments and support, and helping to keep me on the right track. Thanks for happily engaging in collaboration and for adding productive criticisms during all of my committee meetings.

I'd like to thank my family for their support. Mom and Dad, thank you for always being unconditionally supportive for all decisions I have made. They have helped me at every step of the way, with both motivation and love. Thanks to the rest of my family, especially my siblings, Lourdes, Alicia, Eddy, Natalia, and Victoria for always being there for me.

Lastly, I owe everything to my amazing husband, Samuel Cohen, who initially pushed me to join Penn State and motivated me every day. This time apart will have been worth it. This dissertation is dedicated to him.

Chapter 1 | Background

1 Introduction

Cortical neural activity is related to local blood flow, but the cellular sub-types and the signaling that regulate the cerebral arteriole diameter and dilations are not completely clear. I aimed to separate the role of neuron subtypes and their signaling in controlling arteriole basal diameter and evoked dilations.

1.1 The cerebral vasculature is necessary to maintain neural metabolic need

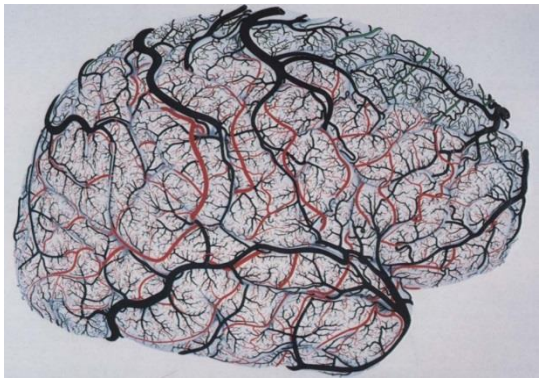

Figure 1.1 **Cortical pial vessels of the human brain.**
Branches of the middle cerebral artery in *red*. Branches of the anterior cerebral artery in *green*. Branches of the posterior cerebral artery in *blue*. Veins are in *black*. Adapted from "Cortical blood vessels of the human brain" by Duvernoy, H. et al. *Brain Research Bulletin* (1981)

The vascular system in the brain is an intricate and specialized system (Figure 1.1) that couples the energy needs of neural and non-neural cells with blood flow (Roy and Sherrington, 1890; Purves and Williams, 2001; Iadecola, 2004; Raichle and Mintun, 2006). As neural populations that perform specific computational tasks can occupy small spatial volumes, the coupling between neurons and blood vessels needs to be spatially and temporally specific to support the delivery of nutrients and removal of cellular metabolites from these active populations. Neurovascular coupling describes the mechanisms that transduce

local activation of neurons into increases in cerebral blood volume. Though well studied, there are many aspects of neurovascular coupling that are not well understood. Resolving how neural populations communicate their activity to control the volume of the vasculature at a cellular level is essential for understanding the basis of healthy cerebral perfusion, for neuropathologies where effective perfusion breaks down, and for neuroimaging modalities that rely on hemodynamics signals to determine brain activity.

1.2 **The architecture of the cerebral vasculature**

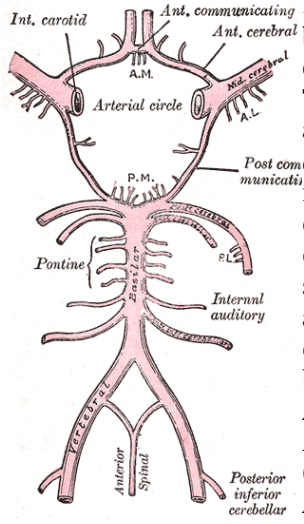

Figure 1.2 **Major arteries of the brain branching from the Circle of Willis.**
The anterior and middle cerebral artery (*ant. cerebral* and *mid. cerebral* in figure) arise from the internal carotid artery and circle of Willis. The branches supply the cortex and deeper brain structures. The posterior cerebral artery supplies the posterior cortex, midbrain, and the brainstem.
Adapted from *Anatomy of the Human Body*. Henry Vandyke Carter - Henry Gray (1918) Gray's Anatomy, Plate 519

The brain receives blood through a network of arteries that have intricate connections across the brain (Blinder *et al.*, 2013; Gao, Greene and Drew, 2015). The supply of blood flow enters the brain from the internal carotid artery and the vertebral artery (Purves and Williams, 2001). These two major arteries come together to form the Circle of Willis on the ventral surface of the brain (Figure 1.2). From the Circle of Willis, arises the anterior cerebral artery (ACA), the middle cerebral artery (MCA), and the posterior cerebral artery (PCA). These arteries branch from the Circle of Willis to supply blood to different brain regions, like the cortex and the deep structures of the brain (basal ganglia, thalamus, etc.).

1.2.1 **Structure of cerebral blood vessels**

The cerebral vasculature is organized into three different vessel types (arteries, capillaries, and veins), that are broadly distinguishable based on morphology, cellular subtypes, and dynamic responses. In the cortex, the vasculature is composed of large pial arteries that cover the surface of the brain and branch into smaller arteries. These smaller arteries penetrate into the brain becoming smaller as they descend. The intracortical arteries turn into the capillary network (Zhao *et al.*, 2006; Nishimura *et al.*, 2007) (Figure 1.3). The capillaries feed into veins and emerge from cortex as pial venules.

Each part of the vasculature responds to neural activity in different ways. Arteries dilate, capillaries have faster blood flow through them, and veins have a small and delayed dilatory response (Huo, Gao and Drew, 2015). There is still contention in the field about whether dilations initiate in arterioles or capillaries in response to neural activity in cortex (Hall *et al.*, 2014; Hill *et al.*, 2015). The differential responses to changes in neural activity are highly connected to morphology and structure of the vessels (Duvernoy, Delon and Vannson, 1981; Blinder *et al.*, 2013). Pial arteries are composed of endothelial cells and multiple layers of vascular smooth muscle. Penetrating arteries have endothelial cells and a

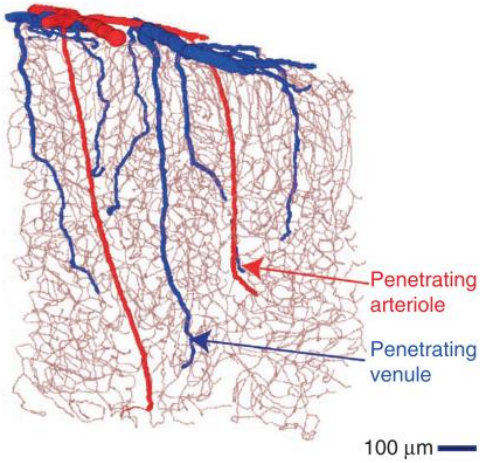

Figure 1.3 **Vascular network through cortex.**
Example of vasculature through the depth of cortex. Surface and penetrating arterioles are colored red, venules blue. Adapted from "The cortical angiome: an interconnected vascular network with noncolumnar patterns of blood flow" by Blinder P., *Nature Neuroscience*, 2013.

single layer smooth muscle. Capillaries have endothelial cells and pericytes, and veins have endothelial cells.

The arteries are composed of an inner layer of endothelial cells and outer layers of smooth muscle cells (Greensmith and Duling, 1984). Vessel diameter is determined by the contractile properties of the smooth muscle cells that surround arteries and microvessels. Increases in arteriole diameter lead to increases in local blood flow, where a single penetrating arteriole contributes to supplying a cylinder of about 350um in diameter in the cortex (Nishimura *et al.*, 2007). Both arterioles and venules have smooth muscle cells surrounding them (Hill *et al.*, 2015), but express different smooth muscle morphology. These differences in morphology dictate their distinct contractile properties. Briefly, arteriole dilations are active because they are mediated by the relaxation of the surrounding smooth muscle cells, while venules have thinner walls and limited contractile properties, and so display a passive dilation (Duvernoy, Delon and Vannson, 1981; Huo, Greene and Drew, 2015).

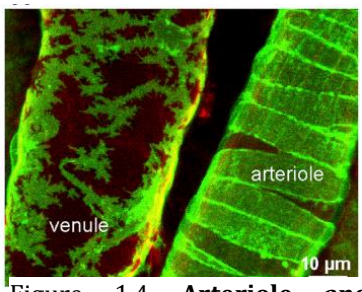

Figure 1.4 **Arteriole and venule smooth muscle.**
In vivo image captured from the cortex of smooth muscle cells on arterioles and venules in *green*
Adapted from "Regional Blood Flow in the Normal and Ischemic Brain Is Controlled by Arteriolar Smooth Muscle Cell Contractility and Not by Capillary Pericytes" by Hill R., *Neuron*, 2015.

On pial and penetrating arteries, the smooth muscle cells envelope the circumference of the vessel in a band-like morphology (Figure 1.4) (Hill *et al.*, 2015). The smooth muscle cells constrict or dilate around the circumference of the arteriole wall. The depolarization of smooth muscle cells increases intracellular Ca^{2+} concentrations. Myosin light-chain kinase (MLCK) phosphorylates myosin in a calcium-dependent manner which in turn interacts with smooth muscle actin

(αSMA). This interaction elicits constriction, which leads to decreased blood flow (Hamilton, Atwell and Hall, 2010). In contrast, smooth muscle cell relaxation happens when there are low intracellular Ca^{2+} levels and decreased MLCK activity. This inhibits interactions with αSMA, leading to relaxation. The band-like smooth muscle cells surrounding cerebral arteries also contributes to spontaneous, low-frequency oscillations in vessel diameter that are not see in capillaries or veins (Drew, Shih and Kleinfeld, 2011).

The wall morphology and dilation properties of arteries change as the vessel diameter does, so smaller arterioles dilate proportionally more than larger arterioles (Iadecola *et al.*, 1997; Drew, Shih and Kleinfeld, 2011). The constriction around the edges of the arteriole walls may not be symmetrical, leading to changes in shape (Greensmith and Duling, 1984).

1.2.2 **Functional properties of cerebral blood vessels**

While arterioles dilate within seconds of increased neural activity, venule distention is on the time scale of tens of seconds (Huo, Greene and Drew, 2015) and the amplitude of this dilation does not depend on vessel diameter (Drew, Shih and Kleinfeld, 2011). Passive dilation of veins is believed to be a response to increased mechanical forces associated with increased blood flow after prolonged stimulus (Duvernoy, Delon and Vannson, 1981; Huo, Greene and Drew, 2015). Although the dilation response of veins is not as large in magnitude as in arteries, the arterial dilation dynamics correlate strongly with blood flow changes seen in veins (Hillman *et al.*, 2007).

Sensory stimulation causes reliable increases in capillary red blood cell velocity, and dilations of surface and penetrating arteries (Drew, Shih and Kleinfeld, 2011). Traditionally, the vascular responses to stimuli are measured at the level of the arterioles (Zhao *et al.*, 2006; Hillman *et al.*, 2007; Cauli and Hamel, 2010; Mishra *et al.*, 2016), but it is still unknown where along the vascular tree blood flow changes are initiated. The timing of neuronal, pericyte, and smooth muscle cell activation alongside vessel diameter changes and capillary blood velocity measurements have shown that functional hyperemia is regulated at the pre-capillaries (Fernandez-Klett *et al.*, 2010; Hill *et al.*, 2015). Pre-capillaries are the region between arteries and capillaries (Rungta *et al.*, 2018).

Researchers speculate that capillaries regulate local changes, while arteriole response is spatially broader and might be driven by different signaling pathways (Mishra *et al.*, 2016). Many recent studies have concentrated on the role of capillaries in the active regulation of cerebral blood flow. Based on *in vivo* and brain slice experiments, some speculate the hemodynamic response initiates in the capillaries, with increases in capillary blood flow and even capillary dilations (Stefanovic *et al.*,

2008; Hall *et al.*, 2014). As capillaries lack smooth muscle cells, the control of diameter in the capillary bed occur through contractile pericytes (Hamilton, Atwell and Hall, 2010; Biesecker *et al.*, 2016; Mishra *et al.*, 2016). Pericytes surround the capillary and are located between the endothelial cells and the parenchyma (Hamilton, Atwell and Hall, 2010). Similar to smooth muscle cells in arteries, the capillaries dilate in response to sensory stimulation causing transients in Ca^{2+} concentrations leading to interactions with αSMA. Capillaries are spatially well-situated for controlling blood flow, as capillaries are in close proximity to active neurons and astrocytes (<15um) (Kim and Ogawa, 2012). The capillary walls consist of only one layer of endothelial cells and pericytes, so are ideal for the metabolic exchange between the blood and the brain.

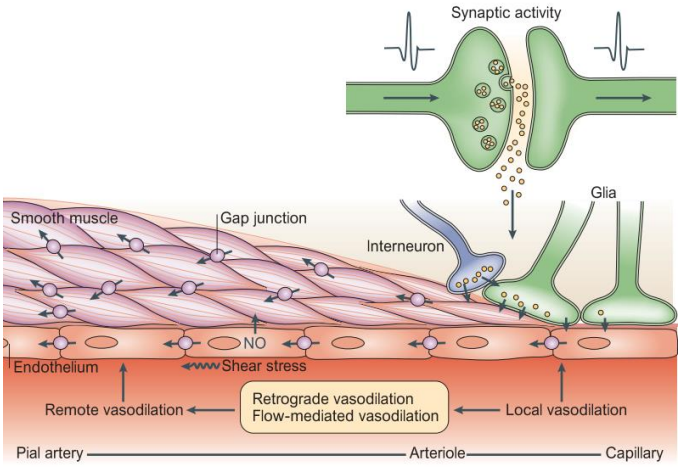

Figure 1.5 **Hypothesized mechanism for the vasodilation propagation in vessels.**
Cellular mechanisms for the propagation of vasodilation from arterioles and capillaries to pial arteries. Glia, representing the end-feet extensions, are associated with neuronal axon terminals. Smooth muscle relaxation is produced by local release of vasoactive agents and propagates upstream through the intercellular gap junctions between endothelial cells and smooth muscle cells.
Adapted from "Neurovascular regulation in the normal brain and in Alzheimer's disease." by Iadecola C., *Nature Reviews Neuroscience*, 2004.

Others have shown using GFP-labeled pericytes *in vivo*, that capillaries do not actively dilate in response to a stimulus as arteries do (Fernandez-Klett *et al.*, 2010). Instead, capillaries dilate passively after increased perfusion pressure elicited by arteriole dilation indicating they do not play a major role in neurovascular coupling.

Blood flow is dynamically regulated in the brain, and the vasculature is sensitive to the chemical and mechanical environment to alter diameter, either in the capillary or arterioles. This dynamic regulation also involves the propagation of a hyperpolarizing signal along the vascular tree. Both arterioles and capillaries are surrounded by endothelial cells. The endothelial cell signals are coupled together through tight and gap junctions, so synaptic activation triggers an electrical signal that propagates backward along the vascular tree through the gap junctions (Iadecola *et al.*, 1997; Chen *et al.*, 2014; Longden *et al.*, 2017).

1.2.3 **Spatial propagation of the dilation response**

Endothelium-dependent hyperpolarization involves the propagation of a vasodilation up the interconnected vascular network. Both arteriole and capillary endothelial cells can sense chemical changes in the local environments (Sonkusare *et al.*, 2016; Longden *et al.*, 2017). The hyperpolarizing signal propagates between endothelial gap junctions of capillary and arteriole endothelial cells up to surface arterioles (Emerson and Segal, 2000; Wölfle *et al.*, 2011). The endothelial-dependent hyperpolarization signal is independent of vasoactive nitric oxide (NO) or prostanoids (Griffith, 2004). Selective damage to endothelial cells, but not smooth muscle cells, interrupts the conduction of hyperpolarization and the dilation response up the vascular tree (Emerson and Segal, 2000; Wölfle *et al.*,

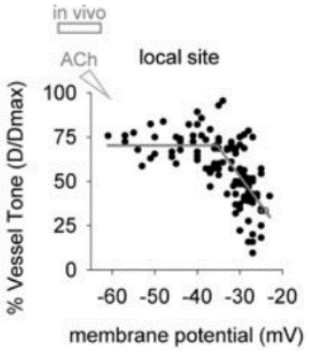

Figure 1.6 **Non-linear relationship between membrane potential and vessel tone.** Simultaneous recordings of vessel tone and membrane potential at the local site, before and during ACh stimulation. Adapted from "Non-linear relationship between hyperpolarization and relaxation enables long distance propagation of vasodilatation." By Wolfe S, *Journal of Physiology*. 2011

2011; Chen *et al.*, 2014). The propagating hyperpolarization signal through endothelial cells decreases intracellular Ca^{2+} in the smooth muscle cells via the deactivation of voltage-dependent Ca^{2+} channels. The absence of any Ca^{2+} influx leads to smooth muscle relaxation and arteriole dilation (Iadecola and Nedergaard, 2007).

The vessels in the deeper layers of cortex dilate faster in response to a sensory stimulus (Uhlirova, Kılıç, *et al.*, 2016). This suggests the vascular response initiates in the deeper layers and then propagates up the penetrating arteriole for a hemodynamic response to neural activity that could extend over 1 mm, depending on the length constant of the arteriole (Figure 1.6) (Desai *et al.*, 2010; Wölfle *et al.*, 2011; Scott and Murphy, 2012; Vazquez *et al.*, 2014).

1.3 **Physics of Cerebral Circulation**

Blood flow is governed by laws that dictate the balance between changes in volume and pressure of arterial blood, venous blood, and cerebral spinal fluid. The blood vessel walls can accommodate the force exerted by the movement of blood.

Blood flow is the movement of blood volume (ΔV) through a specific point in the vasculature during a period of time (Δt):

$$\text{Flow}=\Delta V/\Delta t.$$

Poiseuille's law predicts blood flow based on the vessel geometry and properties of blood.

$$\text{Blood Flow } (F) = \Delta P \times \pi r^4/8\eta\, l$$

blood flow is proportional to the pressure differences (ΔP), the vessel radius (r) to the fourth power, and is inversely proportional to the length of the vessel (l) and the

viscosity of the blood (η). Even small increases in vessel diameter lead to large changes in blood flow.

1.4 Cerebral blood flow control

Cerebral blood flow (CBF) is regulated at two levels, the control of the basal cerebral blood flow and the hyperemic response (Cipolla, 2009). Basal CBF includes both autoregulation and a tonic signal from the local environment that ensures the brain receives an adequate supply of blood (Peterson, Wang and Britz, 2011). There is also the rapid and reliable increase of cerebral blood flow in response to increases in brain activity, driven by mental and physical activity (Sato, Sato and Uchida, 2001). Local neural activity is thought to regulate blood flow by dilating neighboring arterioles and capillaries (Mishra *et al.*, 2016).

1.4.1 Cerebral autoregulation maintains constant cerebral perfusion

Cerebral autoregulation has a role in setting vessel tone and the basal state of the vasculature (Cipolla, 2009; K. J. Kim *et al.*, 2016). Autoregulation is an intrinsic property of vessels that allows the arterioles to dilate and constrict within a range of systemic perfusion pressure changes for continued blood flow at a sustainable level (Iddings *et al.*, 2015). Experimental manipulations of blood pressure within the cerebral blood vessels do not attenuate any sensory evoked responses (Sato, Sato and Uchida, 2001) because any changes in vessel diameter that are related to pressure changes happen at a very slow time scale (on the order of minutes).

The mediators of cerebral autoregulation are not entirely known, but myogenic and metabolic regulation are involved in the mechanisms of cerebral autoregulation (Ruland and Aiyagari, 2007).

1.4.1.1 Myogenic regulation of the vasculature

Myogenic regulation is the principal mechanism in maintaining vascular tone even with changes in the cerebral pressure or flow. Any pressure change influences the basal smooth muscle cell contractility, where intraluminal pressure increases cause vessel constriction and pressure decreases cause dilation to mitigate the passive dilation and constriction from changing blood pressures. Mechanoreceptors translate increases in pressure, wall tension, and shear force into ionotropic signals causing the smooth muscle cells to depolarize, leading to Ca^{2+} influx eliciting MLCK phosphorylation to promote vasoconstriction (Pohl *et al.*, 1991; Schubert, Lidington and Bolz, 2008). The signaling pathways mediating the response of mechanical sensors are still unclear, but it is known that arterial tone is controlled by the Ca^{2+}-dependent coordination between the smooth muscle and endothelial cell layers.

1.4.1.2 Negative feedback control of neurovascular coupling

The original hypothesis in the regulation of cerebral blood flow was that active neurons release metabolic signals, which produce increases in blood flow (Attwell *et al.*, 2010). There is a metabolic hypothesis as well, where the regulation of cerebral blood flow is driven by a negative feedback control signal related to metabolic demand and/or the oxygen supply (Ruland and Aiyagari, 2007). The negative-feedback hypothesis involves increased cellular activity leading to consumption of glucose, of O_2 (Hamilton, Atwell and Hall, 2010), the influence of the metabolic by-products from neural activity, and the production of CO_2 (affecting pH) (Astrup *et al.*, 1976; Attwell *et al.*, 2010). Many of these negative feedback mechanisms are vasoactive and could contribute to the regulation of cerebral blood flow. However,

the influx of nutrients from the hemodynamic response far surpasses consumption of glucose or oxygen as a result of increased cellular activity (Cauli and Hamel, 2010) and blood flow increases after sensory stimulation were not affected by the perturbation of likely metabolic signals (Powers, Hirsch and Cryer, 1996; Wolf *et al.*, 1997; Lindauer *et al.*, 2010).

In recent years, the metabolic hypothesis has been replaced by evidence that neurovascular coupling is primarily driven by feed-forward pathways increasing vasoactive messengers mediated by changes in neuronal activity (Uhlirova, Kılıç, *et al.*, 2016).

1.5 **Cellular control of cerebral blood flow control**

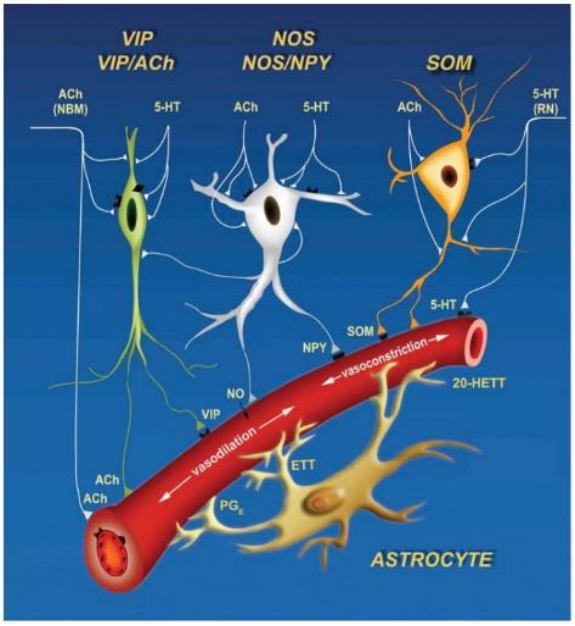

Figure 1.7 **Hypothesized signaling pathways for neurovascular coupling.**
Cartoon of hypothesized signaling pathways, including direct signaling from interneurons (VIP, NOS/NPY, SOM), indirect local signaling (astrocyte), and indirect global signaling (5HT and Ach). Adapted from "A guide to delineate the logic of neurovascular signaling in the brain." by Kleinfeld D, *Frontiers in Neuroenergetics*, 2011.

The feed-forward mechanism for the control of neurovascular coupling is defined by neural signaling either directly to vessels, or indirectly by activating astrocytes that signal to the vessels (Attwell *et al.*, 2010). During a sensory stimulus, glutamate released by thalamocortical afferents target glutamatergic excitatory neurons, GABAergic inhibitory interneurons, and astrocytes. Cerebral blood vessels lack NMDA and AMPA receptors, suggesting there is no direct action of glutamate on

smooth muscle cells to produce vasodilation (Faraci and Breese, 1993; Fergus and Kevin S. Lee, 1997). Glutamate release drives cellular changes in other cells, which leads to the release of vasoactive compounds eliciting increases in CBF (Faraci and Breese, 1993; Lecrux and Hamel, 2016).

Increases in neural activity elicits the changes in the concentrations of Na^+, K^+, Ca^{2+}, and neuromodulators. These changes can affect the vasculature through local astrocytes or neurons releasing vasoactive signals directly to vessels (Kim and Ogawa, 2012). Dissecting the signals to vessels is complex, as there are a wide variety of vasodilators (neurotransmitters, peptides, and small molecules) released by excitatory neurons, inhibitory neural populations, and astrocytes (Figure 1.7) (Stefanovic *et al.*, 2007). Additionally, there are multiple vasoactive factors that could be simultaneously involved in creating a push-pull balance, with concurrent signals that promote both vasoconstriction and vasodilation (Cauli *et al.*, 2004; Kleinfeld *et al.*, 2011).

1.5.1 **Regulation of neurovascular coupling by pyramidal cells**

Excitatory pyramidal neurons are the most abundant cortical neurons. As these neurons have such a large role in generating the local field potential and in the cerebral metabolism, they have been implicated as an important mediator of neurovascular coupling. In the pyramidal neurons of layers II/III, activation of the glutamate receptor NMDA causes increases in intracellular Ca^{2+}. The Ca^{2+} transients lead to activation of phospholipase A2 and the production of arachidonic acid (AA) (Alkayed *et al.*, 1996; Niwa *et al.*, 2000; Lecrux *et al.*, 2011). The COX-2 enzyme metabolizes AA to epoxyeicosatrienoic acids (EETs). COX-2 is not present in

astrocytes, and pyramidal neurons are the primary source of dilatory COX-2 derived prostanoids (Niwa *et al.*, 2000; Lecrux *et al.*, 2011). The released EETs are vasoactive, and dilate vessels through prostaglandin EP2 receptors on endothelial cells by enhancing K^+ currents in smooth muscle cells (Alkayed *et al.*, 1996). The action through the COX-2 pathway has been shown to account for 50% of the evoked hemodynamic response (Niwa *et al.*, 2000; Cauli and Hamel, 2010; Lacroix *et al.*, 2015).

Pyramidal neurons could also regulate the vasculature indirectly via astrocytes. The release of glutamate from pyramidal neurons will activate ionotropic (NMDA and AMPA) and metabotropic (mGluR) receptors that are expressed by neurons and astrocytes (Lecrux and Hamel, 2016). The binding of glutamate to mGluR1 in astrocytes induces increased Ca^{2+} in astrocytic endfeet which downstream leads to the release of vasoactive compounds (Alkayed *et al.*, 1996). See *1.5.6 Astrocyte mediated neurovascular coupling* for more details.

1.5.2 **Inhibitory neuron role in neurovascular coupling**

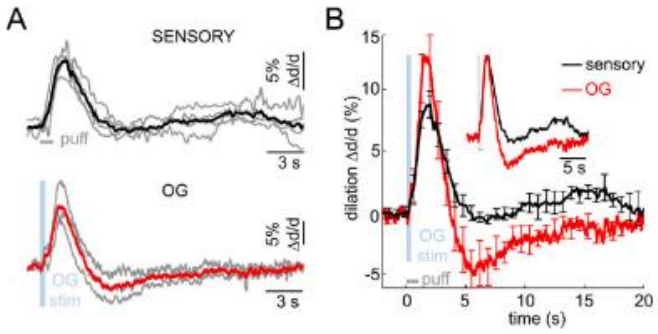

Figure 1.8 **Dilation of vessels by interneurons.** Optogenetic stimulation of interneurons (*red*, VGAT-ChR2) lead to a dilation response similar to a sensory induced (*black*). Adapted from "Cell type specificity of neurovascular coupling in cerebral cortex" by Uhlirova H, *eLife*, 2016

While not as numerous as excitatory neurons, inhibitory interneurons are important for cortical processing. Though they are less numerous and have a small metabolic load when compared to excitatory neurons (Vazquez, Fukuda and Kim,

2018), inhibitory interneuron activity has been associated with synchronizing cortical activity and the signaling to neighboring vasculature (Cauli and Hamel, 2010).

The selective optogenetic stimulation of interneurons (using VGAT-ChR2 mice, where channelrhodopson is expressed only in GABAergic neurons, *Vesicular GABA Transporter*) leads to a suppression of the LFP and spiking activity. GABA release drives the hyperpolarization of neurons, decreasing neural activity. Despite the decrease in neural activity, VGAT optogenetic stimulation produces a dilation response similar to a sensory induced response (Anenberg *et al.*, 2015; Uhlirova, Kılıç, *et al.*, 2016; Vazquez, Fukuda and Kim, 2018) (Figure 1.8). Light-evoked, interneuron-mediated hemodynamic responses remained even with the application of glutamatergic antagonists (Scott and Murphy, 2012; Anenberg *et al.*, 2015). These results suggest that depolarization of interneurons is sufficient to evoke vasodilation independent of excitatory neuronal networks.

While the previous experiments highlight the importance of GABAergic interneurons in neurovascular coupling, the inhibitory neurons of cortex are a heterogeneous population. Inhibitory interneurons co-express various inhibitory neuron markers and release many vasoactive compounds (Kawaguchi and Kubota, 1997; Kawaguchi, 2001; Pfeffer *et al.*, 2013). The neural sub-types also have

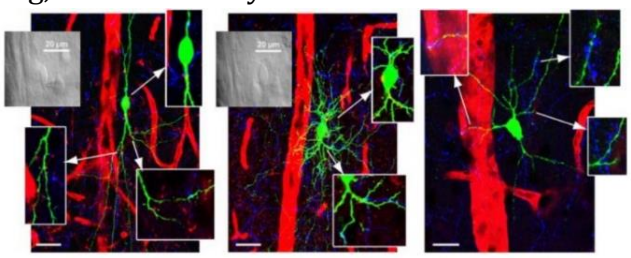

Figure 1.9 **GABA interneurons are next to vessels.** GABA interneurons are particularly well situated next to vessels (within 50um). GABA interneurons associate with microvessels and receive ACh (*red*) and 5HT (*blue*) afferents. *Green* biocytin in neurons, *red* local blood vessels. *Left* VIP; *middle* NOS/NPY; *right* NPY/SOM. Adapted from "Cortical GABA Interneurons in Neurovascular Coupling: Relays for Subcortical Vasoactive Pathways" Cauli B, *J Neuroscience*, 2004

varying anatomic connections to the vasculature (Figure 1.9) (Anenberg *et al.*, 2015).

1.5.3 **Inhibitory neural subtypes**

Cortical inhibitory neurons have an integrating role by contacting each other to form a network of inhibitory synaptic connections (Figure 1.10) (Bacci, Huguenard and Prince, 2005; Pfeffer *et al.*, 2013). GABAergic interneurons are a diverse population that are classified by anatomy, electrophysiology and expression of proteins or neuropeptides. There are three main subtypes of GABA interneurons, parvalbumin (PV+), somatostatin (SOM or SST), and vasoactive intestinal peptide (VIP). PV+ neurons are fast-spiking basket and chandelier cells (Bacci, Huguenard and Prince, 2005). PV+ neurons do not express SOM, nitric oxide synthase (NOS), or VIP. PV+ neurons have a limited vasoactive role. Though the stimulation of VIP neurons has been shown to cause vasodilation and VIP neurons are in close proximity to vessels (Figure 1.9 *left*) (Yaksh, Wang and Go, 1987), VIP does not have direct effects on the vasculature (Lecrux *et al.*, 2011; Lee *et al.*, 2013; Lecrux and Hamel, 2016). Indirect vascular effects of VIP activity could originate from their role in inhibiting PV+ and SOM interneurons, along with the disinhibition of pyramidal cells (Lecrux and Hamel, 2016).

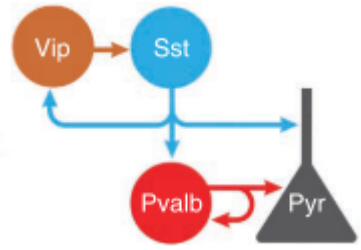

Figure 1.10 **Schematic of the inhibitory connections.** Local GABA interneurons have an integrating role. Mapped interneuron connectivity of PV+, SST+ (or SOM+), and VIP + neurons present in layers II/III and V. PV+ neurons inhibit one another and pyramidal neurons. SST/SOM+ neurons avoid one another but inhibit other interneurons. Adapted from "Inhibition of inhibition in visual cortex: the logic of connections between molecularly distinct interneurons" by Pfeffer C. *Nature Neuro*, 2013.

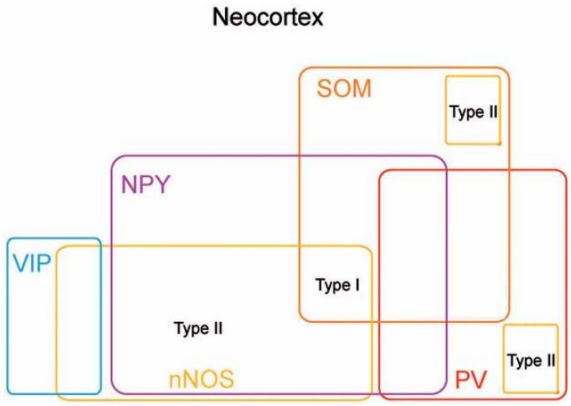

Figure 1.11 **nNOS expressing interneurons in cortex and hippocampus.**
Scheme summarizing the molecular profiles of neocortical nNOS+ interneurons. Adapted from "Neuronal nitric oxide synthase expressing neurons: a journey from birth to neuronal circuits" by Tricoire L. *Frontiers in Neural Circuits.* 2013.

SOM+ interneurons are associated with the release of the vasoactive NO and vasoconstrictive SOM (Cauli *et al.*, 2004) (Figure 1.9 *right*). NOS+ interneurons are a subpopulation of both SOM and VIP interneurons (Figure 1.11), and also co-express the marker for neuropeptide Y (NPY) (Tricoire and Vitalis, 2012). NPY+ neurons release neuropeptide Y, which causes the constriction of vessels through NPY-Y1 receptors on the vasculature (Cauli *et al.*, 2004) (Figure 1.9 *middle* and *right*).

1.5.3.1 GABA as a vasodilator

The neurons of cerebral cortex express ionotropic $GABA_A$ receptors that are localized to dendrites, primarily targets by SOM martinotti cells, cell soma, targeted by PV+ basket cells and the axon initial segment, targeted by PV+ chandelier cells. The release of GABA by interneurons decreases neural activity by hyperpolarizing postsynaptic neurons by increasing intracellular chloride concentrations (de Blas, Vitorica and Friedrich, 1988; Vanlandewijck *et al.*, 2018). Some early experiments with neurovascular coupling have implicated GABA, through $GABA_A$ receptors on the vasculature (Fergus and Kevin S Lee, 1997), as a mediator of vasodilation in cortex. There was speculation that GABA is released directly onto the cerebrovasculature from projections of the basal forebrain and local inhibitory neurons (Edvinsson, Larsson and Skarby, 1980; Vaucher *et al.*, 2000; Kocharyan *et al.*, 2008; Attwell *et al.*,

2010). While GABA would be a convenient mediator of neurovascular coupling, more convincing data has shown GABA has no direct effects on the vessels (Lecrux and Hamel, 2016) and that there are in fact no GABA receptors on the vasculature (de Blas, Vitorica and Friedrich, 1988; Vanlandewijck *et al.*, 2018).

1.5.4 The role of nNOS neurons and subcortical input on neurovascular coupling

Neuropeptides and neuromodulators released by interneurons are capable of signaling to the vessels. There is a great amount of evidence for nitric oxide (NO), a potent vasodilator, being the principal neuronally-derived regulator of the cerebral vasculature (Cauli *et al.*, 2004). Nitric oxide synthase (NOS+) neurons are closely associated with the local vasculature, with about 60% of NOS cells contacting blood vessels directly (Figure 1.9 *middle*) (Bredt, Hwang and Snyder, 1990; Estrada, Mengual and Gonzalez, 1993; Iadecola, 1993; Regidor, Edvinsson and Divac, 1993; Vaucher, Linville and Hamel, 1997; Sato, Sato and Uchida, 2001; Cauli *et al.*, 2004).

1.5.4.1 Nitric oxide synthase and guanalyl cyclase

Nitric oxide synthase (NOS) is a membrane associating enzyme that catalyzes the conversion of L-arginine to L-citrulline and nitric oxide (NO) (Yousef *et al.*, 2004; Stefanovic *et al.*, 2007; Chen, Pittman and Popel, 2008; Hall and Garthwaite, 2009). There are three different isoforms of NOS that all have a similar structure: NOS1 (nNOS), NOS2 (iNOS), and NOS3 (eNOS). The action of NOS1 and NOS3 are Ca^{2+} dependent (Mitrovic and Schachner, 1996). NOS1 is primarily found in the dense axonal terminals of neurons, usually near cerebral microvessels (Iadecola, 1993; Regidor, Edvinsson and Divac, 1993; Stefanovic *et al.*, 2007). The nNOS-positive

neurons are most numerous in deeper layers (layers V and VI), but there is also significant nNOS present in the neuropil (Montague *et al.*, 1994; Mitrovic and Schachner, 1996; Tomioka *et al.*, 2005).

There are a small number of nNOS+ neurons (known as Type 1 nNOS neurons see *1.5.4.2 Nitric oxide from nNOS neurons as a vascular relaxing agent*), mainly in the deeper layers, that have long-distance ipsilateral and contralateral projections not typical of GABA neurons (Tomioka *et al.*, 2005; Tomioka and Rockland, 2007; Williams, Black, *et al.*, 2018; Williams, Vazquez-derose, *et al.*, 2018). The distant projections allow for these nNOS neurons to have a widespread influence on cortex. The dense axons of nNOS neurons extend 200-300um from the soma and span horizontally and vertically through layers (Perrenoud *et al.*, 2012; Endo, Yanagawa and Komatsu, 2016a).

NOS2 (iNOS "inducible"/"immune"), is a Ca^{2+}-independent source of NO where there is increased NO production during inflammatory brain diseases (Necchi *et al.*, 2002). iNOS is not normally present in the healthy brain, and thus does not play a major role in regulating vascular relaxation or neurovascular coupling.

Endothelial cells express eNOS or NOS3. Like nNOS, the generation NO by eNOS is Ca^{2+}-dependent (Necchi *et al.*, 2002; Yousef *et al.*, 2004). eNOS is present in the endothelial cells that are immediately adjacent to smooth muscle, so past work has considered the endothelium as the major producers of NO for regulating vascular tone and tissue oxygen (Kavdia, Tsoukias and Popel, 2002; Chen, Pittman and Popel, 2008). eNOS regulates vascular relaxation by shear-mediated increases of NO levels in response to flow changes. The NO diffuses to the smooth muscle cell to produce

vasodilation and could diffuse into the lumen to react with hemoglobin. The release of endothelial NO and subsequent relaxation of vessel diameters evolve over minutes, not seconds (K. J. Kim *et al.*, 2016), so this pathway is not rapid enough to regulate the sensory-evoked hemodynamic response.

NO signals are catalyzed by NOS enzymes and activate soluble guanalyl cyclase (sGC), which is the major NO receptor (Kavdia, Tsoukias and Popel, 2002; Hall and Garthwaite, 2009; Pigott, Bartus and Garthwaite, 2013). sGC receptors are very sensitive to NO (down to concentrations of ~1nM), so even a small change in NO can evoke an effect (Hall and Garthwaite, 2009). NO is a gas that can readily diffuse and is soluble in both aqueous solutions and lipids (Stefanovic *et al.*, 2007). NO has been implicated as a messenger in the regulation of nerve tissue, the control of cell death, plastic changes of synaptic transmission, and a vascular relaxing agent (Estrada, Mengual and Gonzalez, 1993; Montague *et al.*, 1994; Yousef *et al.*, 2004). Within the vasculature, NO is reactive with hemoglobin, O_2, nitrogen species, and sGCs (Chen, Pittman and Popel, 2008). The rates of NO consumption in the blood plasma increase when there is cell-free hemoglobin in the plasma (up to 1000-fold increase in the degradation rate) (Kavdia, Tsoukias and Popel, 2002; Reiter *et al.*, 2002; Gramaglia *et al.*, 2006), which is relevant in the transfusion of hemoglobin-based oxygen carriers (HBOCs).

Though NO has many potential targets and functions, the intrinsic properties of NO make it hard to model and to measure concentrations (Figure 1.12). In the field, there has been a wide range of measured NO concentrations in brain tissue, from 2 to 390nM (Hall and Garthwaite, 2009).

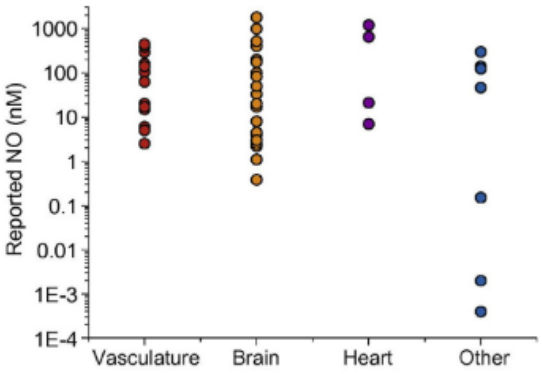

Figure 1.12 **NO is hard to model and measure concentrations.**
NO concentrations reported for different tissues. Adapted from "What is the real physiological NO concentration in vivo?" Hall C., *Nitric Oxide*, 2009.

High concentrations of nitric oxide can be neurotoxic, where excess production of NO in the brain leads to the potential for functional impairment (Necchi *et al.*, 2002), elicited by the conversion of NO into the neurotoxic compound, ONOO (Montague *et al.*, 1994), .

While there are various subtypes of NOS enzymes, the most common inhibitors of NOS isoforms have relatively little selectivity from each other (Poulos and Li, 2017). For example, 7-Nitroindazole (7NI) is thought to be specific to nNOS, but it has only modest selectivity for NOS subtypes (Bland-Ward and Moore, 1995). *In vivo,* 7-NI not only inhibits the activity of nNOS, but also targets eNOS (Reiner and Zagvazdin, 1998; Engelhardt *et al.*, 2006).

1.5.4.2 Nitric oxide from nNOS neurons as a vascular relaxing agent

NO is a rapidly produced and diffusible vasodilator which may act as a signaling molecule in neurovascular coupling (Buerk *et al.*, 2003; Cauli and Hamel, 2010) by stimulating sGC in the local smooth muscle cells (Montague *et al.*, 1994) and catalyzing the conversion of GTP to cGMP to relax the vessel (Alonso-Galicia *et al.*,

1999; Kavdia, Tsoukias and Popel, 2002). The pharmacological inhibition of NOS shows NO may influence cerebrovascular tone and the coupling between neural activity and blood flow changes (Montague *et al.*, 1994).

The release of glutamate activates NMDA receptors on neurons, causing Ca^{2+} entry and nNOS activation (Busija *et al.*, 2007). Neuronally-derived NO release has been found to dilate vessels in brain slice and *in vivo* (Iadecola, 1993; Stefanovic *et al.*, 2007).

Inhibiting nNOS activity reduces blood flow in the somatosensory cortex, but the addition of NO donors restores the dilation response (Lindauer *et al.*, 1999). NO donors supply a constant NO concentration, demonstrating that NO may not mediate the neurovascular signaling but may rather modulate the action of dilation and constriction of blood vessels. The NO signaling from neurons are responsible for at least 50% of the cerebral blood response(Lindauer *et al.*, 1999).

1.5.4.3 Role of type 1 nNOS neurons in cerebral perfusion

Neurons that express nNOS are present in motor and somatosensory cortex, where they are distributed across all cortical layers. The density of nNOS neurons vary by layer (Necchi *et al.*, 2002) dependent on if the neuron is type 1 vs type 2 nNOS neurons.

Type 2 nNOS neurons are typically neurogliaform-like in shape and are primarily located in layers II/III. They are about seven times more numerous than type 1 nNOS neurons (Smiley, McGinnis and Javitt, 2000; Perrenoud *et al.*, 2012; Endo, Yanagawa and Komatsu, 2016a). Type 2 neurons have a smaller somata, and have less

intense staining for nNOS (Perrenoud *et al.*, 2012; Williams, Black, *et al.*, 2018; Williams, Vazquez-derose, *et al.*, 2018).

In contrast to type 2 nNOS cells, type 1 nNOS neurons co-express neurokinin 1 receptors (NK1R) (Figure 1.13). 93% of NOS1 are NK1R-positive and 95% of NK1R

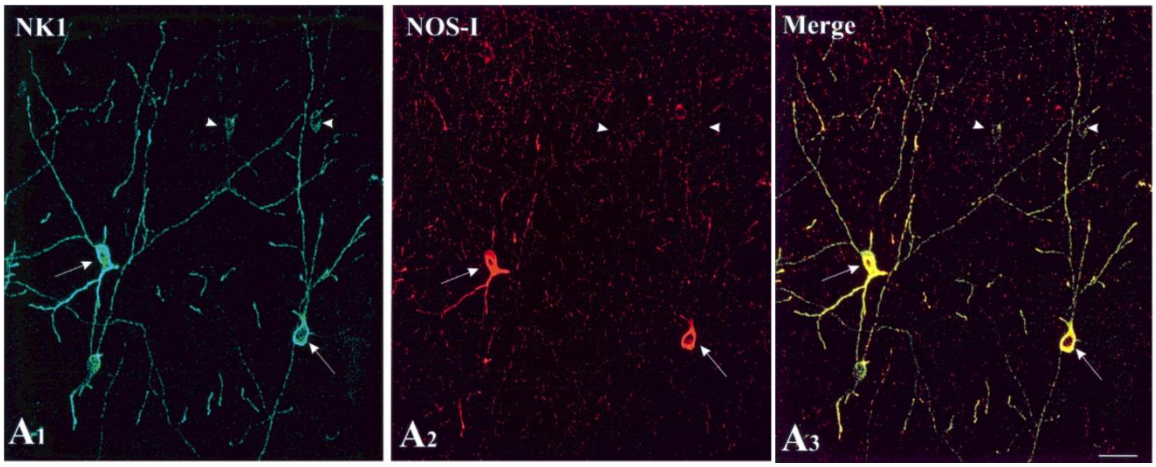

Figure 1.13 **Colocalization of NK1 with NOS-I.**
A1: NK1- immunoreactive, A2: NOS1- immunoreactive
Merge: Intensely NK1- immunoreactive neurons also stained for NOS-I (arrows). Adapted from "Substance P and nitric oxide signaling in cerebral cortex: Anatomical evidence for reciprocal signaling between two classes of interneurons" by Vruwink M, *Journal of Comparative Neurology*, 2001

are NOS1-positive. These neurons span layers V-VI (Perrenoud *et al.*, 2012; Endo, Yanagawa and Komatsu, 2016a; Williams, Black, *et al.*, 2018; Williams, Vazquez-derose, *et al.*, 2018), but are also sparsely present in layers II/III. They are the rarest cortical interneuron subtype (Smiley, McGinnis and Javitt, 2000; Vruwink *et al.*, 2001; Kubota *et al.*, 2011; Dittrich *et al.*, 2012; Perrenoud *et al.*, 2012; Williams, Black, *et al.*, 2018; Williams, Vazquez-derose, *et al.*, 2018). Along with NK1R and GABA, type 1 nNOS neurons co-express SOM and NPY (Montague *et al.*, 1994; Tomioka *et al.*, 2005), but rarely express PV or VIP (Kaneko *et al.*, 1994; Kubota *et al.*, 2011).

Substance P activates NK1R on type 1 nNOS neurons and induces a Ca^{2+} influx through non-selective cation channels (Endo, Yanagawa and Komatsu, 2016a). Substance P is classically known for its role as a neuromodulator and

neurotransmitter in nociception, but more recently is known to be related to stress and addiction (Nakaya *et al.*, 1994; Dittrich *et al.*, 2012). Substance P is released from cholinergic axons and PV interneurons, and binds to NK1R for cortical modulatory effects (Vruwink *et al.*, 2001). Type 1 nNOS neurons also receive neuromodulatory hypocretin/orexin inputs and have the Hrctr1 receptor (Estabrooke *et al.*, 2018; Williams, Black, *et al.*, 2018).

The basal forebrain cholinergic neurons project to type 1 nNOS neurons and become active during wakefulness and REM sleep (Vaucher, Linville and Hamel, 1997; Eggermann *et al.*, 2014; Williams, Vazquez-derose, *et al.*, 2018). When the basal forebrain is stimulated there is increased activity in nNOS neurons (Kocharyan *et al.*, 2008; Williams, Vazquez-derose, *et al.*, 2018) (see *1.5.5.1 Cholinergic projections to nNOS neurons*).

1.5.5 **Neuromodulatory sub-cortical input to the cortex**

In addition to vasoactive mediators that are released by local cells, sub-cortical neurons could influence the vasculature through projections to local interneurons, arterioles, capillaries or astrocytes. These neuromodulators enhance cortical information transfer by changing the excitability of cortical interneurons (Owen *et al.*, 2013).

Cortical interneurons receive inputs from the basal forebrain (acetylcholine, ACh releasing projections), the locus coeruleus (norepinephrine, NE releasing), and the raphe nucleus (serotonin, 5-HT releasing) (Hamel, 2004; Iadecola, 2004; Jones, 2008). Subcortical modulatory control by ACh, NE, and 5HT influences cortical state and thus neurovascular coupling (Sato, Sato and Uchida, 2001; Jones, 2008) because

the interneurons that receive subcortical input are associated with cortical microvessels (Vaucher *et al.*, 2000; Cauli *et al.*, 2004).

Noradrenergic projections from the locus coeruleus to the cortex receives is involved in arousal, attention, and memory (Lecrux and Hamel, 2016). The stimulation of neurons in the locus coeruleus enhances cortical response after a stimulus and increases intracellular Ca^{2+} of astrocytes. Norepinephrine projections also contact cortical microvessels directly (Bekar, Wei and Nedergaard, 2012). *In vivo* application of norepinephrine causes vasoconstriction and reduced cerebral blood flow (J.-H. Kim *et al.*, 2016).

Serotononergic projections from the raphe nucleus and cholinergic projections from the basal forebrain innervate cortical GABAergic neurons (Lee *et al.*, 2010) and microvessels (Vaucher, Linville and Hamel, 1997; Cauli *et al.*, 2004). Stimulation of cholinergic projections have a vasodilative effect, while stimulation of serotonergic projections drives vasoconstriction.

1.5.5.1 Cholinergic projections to nNOS neurons

Cholinergic neurons in the basal forebrain send long-range projections to sensory cortex and modulate cortical neural activity by ACh release (J.-H. Kim *et al.*, 2016; Lecrux and Hamel, 2016; Williams, Vazquez-derose, *et al.*, 2018) (Figure 1.14 and Figure 1.15). ACh projections from the basal forebrain are most active during wakefulness and REM sleep (Lee *et al.*, 2005), but silent during non-REM sleep (Harrison *et al.*, 2016). Electrical stimulation of the basal forebrain or selective

activation of basal forebrain cholinergic neurons induces cortical activation (Vaucher, Linville and Hamel, 1997; Vaucher *et al.*, 2000; Pinto *et al.*, 2013; Harrison *et al.*, 2016; Lecrux and Hamel, 2016) and causes CBF increases (Vaucher, Linville and Hamel, 1997; Vaucher *et al.*, 2000; Lecrux and Hamel, 2016). Conversely, the suppression of these neurons or blocking cholinergic transmission to cortex reduces cortical activity (Pinto *et al.*, 2013; Eggermann *et al.*, 2014; Harrison *et al.*, 2016).

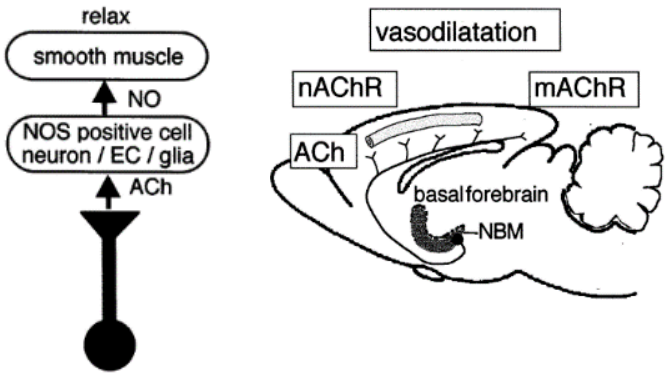

Figure 1.14 **ACh and NO are involved in the vasodilative system.**
Left, Schematic diagram of involvements of muscarinic and nicotinic cholinergic receptors in the cholinergic vasodilative system in the cerebral cortex. **Right**, Schematic diagram of involvements of ACh and NO in the cholinergic vasodilative system in the cerebral cortex. (EC, endothelial cell). Adapted from "Regulation of regional cerebral blood flow by cholinergic fibers originating in the basal forebrain" by Sato A, *Int J of Developmental Neuroscience*, 2001.

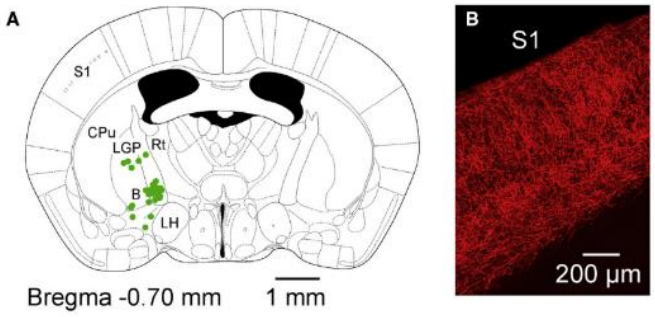

Figure 1.15 **Prominent cholinergic axonal innervation of S1.**
A. Soma locations of cholinergic neurons projecting to S1 in a section retrogradely labeled by the injection into the C2 barrel column.
B. Cholinergic axons in S1, labeled by injection of tdTomato virus into basal forebrain of a ChAT-Cre mouse. Adapted from "Cholinergic Signals in Mouse Barrel Cortex during Active Whisker Sensing" Eggerman E, *Cell Reports*, 2014

The cortical ACh release from basal forebrain projections promotes arousal (Williams, Vazquez-derose, *et al.*, 2018) through desynchronization of cortical activity (Goard and Dan, 2009; Kalinchuk *et al.*, 2012; Pinto *et al.*, 2013; Eggermann *et al.*, 2014; J.-H. Kim *et al.*, 2016).

The alterations in local neural activity caused by modulatory input enhances the cortical response to sensory stimulus (Pinto *et al.*, 2013).

Most of the neurons that project from the basal forebrain to cortex are ACh projections (about 80-90%) (Sato, Sato and Uchida, 2001; J.-H. Kim *et al.*, 2016), but there are also GABAergic and glutamatergic projections (Gritti, Mainville and Jones, 1993; Henny and Jones, 2008; Harrison *et al.*, 2016). GABAergic neurons project from the basal forebrain onto cortical neurons and directly to the cortical vessels (Vaucher *et al.*, 2000), but more recent evidence shows GABA has no direct effects on the vasculature (Lecrux and Hamel, 2016) (see also 1.5.3.1 GABA as a vasodilator).

Cholinergic neurons in the basal forebrain are consistently excited during movements (Harrison *et al.*, 2016). These ACh projections primarily extend directly to cortical vessels (Bacci, Huguenard and Prince, 2005) and to layer V interneurons (Vaucher, Linville and Hamel, 1997; Sato, Sato and Uchida, 2001). A subset of these interneurons are nNOS/SOM positive neurons that have mACh receptors (Hamel, 2004; Kalinchuk *et al.*, 2012; J.-H. Kim *et al.*, 2016; Williams, Black, *et al.*, 2018).

Through the recruitment of the interneurons, the basal forebrain projections modulate the local neural activity and the hemodynamics in cortex (Williams, Vazquez-derose, *et al.*, 2018). The nNOS/SOM interneurons project to the dendrites of pyramidal cells increasing cortical GABAergic inhibition and also release vasoactive peptides onto the vasculature (Lee *et al.*, 2010). The increases in cerebral blood flow after the stimulation of basal forebrain is attenuated with an NOS inhibitor, which shows the ACh signaling to the vasculature works through NO (Sato, Sato and Uchida, 2001; Hamel, 2004). Cortical vasodilation initiating from basal forebrain

projections occurs without changes in astrocytic Ca^{2+} (Takata *et al.*, 2013; Lecrux and Hamel, 2016), so there is no role for indirect signaling through astrocytes in the basal forebrain-NO signaling to the vessels in cortex.

The basal forebrain includes several nuclei with cholinergic projections to cortex (Mesulam *et al.*, 1983; Harrison *et al.*, 2016). Most basal forebrain projections that innervate cortex originate in the nucleus basalis of Meynert (NBM) (J.-H. Kim *et al.*, 2016) (Figure 1.14). The stimulation of NBM increases cortical ACh and also cortical cerebral blood flow (Sato, Sato and Uchida, 2001; Hamel, 2004). These increases in blood flow are specific to stimulation in the NBM, as the largest hemodynamic response occurs when the electrode is within NBM and declines as the electrode is moved away (Biesold *et al.*, 1989). There is a high degree of regional specificity and organization to afferent systems and cerebral blood flow response. Each cortical area is innervated by a subset of NBM neurons, and these projections are always in close association with the descending fibers from the same cortical areas they innervate (Saper, 1984). This means there are clear distinctions between neurons projecting to different sensory cortices, as there are few cholinergic neurons projecting simultaneously to two sensory cortices (J.-H. Kim *et al.*, 2016).

Though the stimulation of NBM increases the activity of inhibitory neurons, the metabolic rate for glucose is unaltered in cortex after this stimulation (Kimura, Sato and Takano, 1990). This can be explained because the cholinergic projections primarily target inhibitory neurons, which do not have a high metabolic load (Vazquez, Fukuda and Kim, 2018).

Degeneration of cholinergic basal forebrain nuclei is associated with early signs of dementia and Alzheimer's disease (Grothe *et al.*, 2014). Reduced levels of cholinergic markers in patients correlate with the degree of dementia and the partial lesion of the basal forebrain mimics perfusion deficits in cortex (Miettinen *et al.*, 1993; Sato, Sato and Uchida, 2001; Hamel, 2004; Harrison *et al.*, 2016; Lecrux and Hamel, 2016).

1.5.6 **Astrocyte mediated neurovascular coupling**

The model of how neural activity triggers an increase in blood flow has shifted from the activity of neurons generating metabolic signals that cause vasodilation (Roy and Sherrington, 1890) to a neurotransmitter-mediated feed-forward signal. This feed-forward system plays a significant role in setting the cerebral blood flow, but the signaling to blood vessels could be either directly from neurons or is mediated by astrocytes.

Astrocytes have receptors that allow for them to 'sense' local metabolic changes in neural activity and glutamate availability (Zonta *et al.*, 2002; Peng *et al.*, 2004; Rosenegger, Ha, *et al.*, 2015). The astrocyte processes are well-positioned to be mediators in indirect signaling to the vessels as they are in close contact with both neuronal synapses and arterioles (Figure 1.16) (Kacem *et al.*, 1998; Attwell *et al.*, 2010). Astrocytic endfeet ensheath blood vessels, and may supply vasoactive signals to smooth muscle cells. Both the presence of the sensing receptors and the convenient location make astrocytes an attractive option for mediating indirect signaling from the neurons to the arterioles.

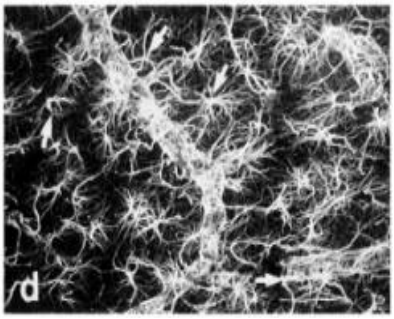

Figure 1.16 **Astrocyte processes are in close contact with the vasculature.**
Astrocytes surround vessels using Anti-GFAP monoclonal and polyclonal antibodies. Adapted from "Structural Organization of the Perivascular Astrocyte Endfeet and Their Relationship with the Endothelial Glucose Transporter" by Kacem, *Glia*, 1998

Active neurons release glutamate that activate astrocytic metabotropic glutamate receptors (mGluRs) leading to increases in intracellular Ca^{2+} in astrocytes (Porter and McCarthy, 1996; Zonta *et al.*, 2002). This activation leads to the Ca^{2+}-dependent synthesis of vasodilators and constrictors (Nizar *et al.*, 2013), initiated by the volume conduction of glutamate. On the astrocytic endfeet, transient receptor potential vanilloid 4 (TRPV4) channels respond to increases in EETs and are mechanosensitive (K. J. Kim *et al.*, 2016). Both mGluR and TRPV4 receptors have the potential to elicit Ca^{2+} transients in astrocytes in response to neural activity.

Inositol 1,4,5-triphos receptors (IP3R) are necessary for Ca^{2+} fluxes in astrocytes. Similar to COX-2 enzymes in neurons, COX-1 enzymes on astrocytes metabolize AA derivatives into EETs in response to the Ca^{2+} transients. EETs are vasodilatory messengers that could facilitate the astrocyte mediated regulation of resting blood flow (Zonta *et al.*, 2002; Peng *et al.*, 2004; Liu *et al.*, 2008; Cauli and Hamel, 2010; Rosenegger, Ha, *et al.*, 2015).

Some speculate increases in astrocytic Ca^{2+} cause the release of vasoactive components that mediate changes in neurovascular coupling (Takano *et al.*, 2006), but there are many lines of evidence that make the role of astrocytes controversial. First, in the somatosensory cortex, sensory evoked calcium events in neurons precede the Ca^{2+} transients in astrocytes by a few seconds (Schummers, Yu and Sur, 2008).

The astrocytic Ca^{2+} changes are delayed (by approximately three seconds) and are not consistently seen *in vivo* (Nizar *et al.*, 2013; Gu *et al.*, 2018). In the case of a sensory stimulus, the onset of neural activity precedes the onset of arteriole dilations. On this time scale, it is plausible that neuron-derived vasoactive messengers could explain the quick dilation response, while astrocytes seem to lack a temporally precise response (Zonta *et al.*, 2002; Rosenegger, Ha, *et al.*, 2015). Some claim there is a small population of astrocytes (5%) that can exhibit fast calcium responses (Winship, Plaa and Murphy, 2007). Second, when the IP3R are knocked-out (blocking increases in astrocytic calcium), stimulation-induced vasodilation remains intact (Nizar *et al.*, 2013). Also, COX-1 knockout mice show reduced baseline blood flow, with no effect on the responses to sensory stimulation (Rosenegger, Ha, *et al.*, 2015). This indicates that astrocytic calcium transients are not required for neurovascular coupling. Still, there is evidence that astrocytic calcium is necessary for capillary dilations (Biesecker *et al.*, 2016), and that these capillary dilations are regulated differently from arteriole dilations (Lourenço *et al.*, 2014; Mishra *et al.*, 2016).

1.5.7 **Potassium mediated neurovascular coupling**

Neurovascular coupling in cortex may also be mediated by K^+ release directly onto blood vessels. Active neurons and astrocytes release K^+ into the extracellular space, and this K^+ release leads to increased conductance of inward rectifying potassium (Kir) channels on endothelial cells (Longden *et al.*, 2017). Activation of the channels results in rapid hyperpolarization and relaxation of smooth muscle cells. Ba^{2+}, which is a selective pore-blocker of Kir2.1 (Harnett *et al.*, 2013), causes

significant constriction of arteries (Sonkusare *et al.*, 2016), meaning K^+ signaling could regulate a portion of neurovascular coupling.

Along with these Kir channels, endothelial cells on arteries (not on capillary endothelial cells) possess small and intermediate-conductance potassium (SK and IK, respectively) channels activated by Ca^{2+}. These channels transduce changes in intracellular Ca^{2+} to membrane hyperpolarization through K^+ transients (Longden *et al.*, 2017). Increases in endothelial cell Ca^{2+} activates SK and IK channels, causing hyperpolarization and endothelial dependent vasodilation (Sonkusare *et al.*, 2016). This form of vasodilation regulates vasculature changes by NO and phospholipase A2 (AA derivatives).

1.5.8 **Blood flow changes are tightly related to neural activity changes**

The temporal and spatial control of cerebral blood flow involves tight coupling between changes in blood vessels and neurons. This tight coupling is the basis of modern functional neuroimaging techniques (fMRI, PET). Understanding the underlying cellular mechanism will enable us to improve the translation of signals measured from those neuroimaging techniques.

1.6 **Cerebral hemodynamics are used for functionally brain mapping**

1.6.1 **The basis of fMRI**

Functional brain imaging has become an essential tool for basic research in the understanding of brain activity and neurological disorders (Raichle and Mintun, 2006). Functional magnetic resonance imaging (fMRI) provides a noninvasive measurement, but with relatively low spatial and temporal resolution (Logothetis,

2008). Spatial resolution has become higher with the development of technology increasing the magnetic field strength (Barth and Poser, 2011).

Deoxyhemoglobin is paramagnetic and sensitive to the magnetic fields that are pulsed during fMRI (Ogawa A *et al.*, 1990; Kim and Ogawa, 2012). Variations in the deoxyhemoglobin leads to faster magnetic relaxation of water protons, which appears as fluctuations in the MRI signal strength (Mateo *et al.*, 2017). Under normal oxygen conditions, arterial blood is fully oxygenated and does not contribute to blood-oxygen-level dependent (BOLD fMRI) (Ogawa A *et al.*, 1990). While the MRI-BOLD is most sensitive to the deoxyhemoglobin in veins, arterial dilation responses strongly correlate with the venous blood flow (Hillman *et al.*, 2007).

Since the development of functional imaging techniques there has been an interest in the relationship between the neural activity and local blood energy signals because hemodynamic signals are used as the basis for many of these neuroimaging techniques. BOLD fMRI assumes increased neuronal spiking and local metabolism eliciting regional increases in blood volume and oxygen from the cerebral vasculature (Fox and Raichle, 1986). Cerebral blood flow and BOLD fMRI signals evoked by neural activity relate to afferent input function, or local field potential (LFP) (Logothetis *et al.*, 2001; Lauritzen and Gold, 2003) (*1.6.2 Sensory evoked hemodynamics are tightly correlated to gamma-band power*). Neural activity changes are closely followed by rapid changes in cerebral blood flow (Iadecola, 1993), meaning that positive fMRI signals are usually correlated with neuronal activation (Shih *et al.*, 2009). There is the assumption that the BOLD signal reflects the population response averaged over a local region in space and time. In most cases the local neural activity is well predicted

by evoked hemodynamics (Boynton, 2011), but there is a complex relationship between the translation of these signals to infer basic neurophysiology (Lauritzen and Gold, 2003; Hillman *et al.*, 2007).

The disadvantage of this imaging technique is that it measures a surrogate signal that might not relate directly or linearly to neural activity. This means that understanding the cellular origin is crucial for interpreting neuroimaging data (Lecrux *et al.*, 2011). Hemodynamic signals underlying functional brain imaging are assumed to reflect metabolic demand by local neural activity, which means increases in hemodynamics translate to increases in local neural activity (Sirotin and Das, 2009). These assumptions can become problematic in studies where neural processes are non-linear, so using neuroimaging to decode neural activity becomes complicated (Kay, David, *et al.*, 2008; Kay, Naselaris, *et al.*, 2008).

1.6.2 Sensory evoked hemodynamics are tightly correlated to gamma-band power

The LFP and multi-unit activity (MUA) both correlate with cerebral blood flow and BOLD fMRI responses (Shmuel and Leopold, 2008), but the gamma band of the LFP is the most reliable predictor of hemodynamic responses (Logothetis *et al.*, 2001; Lauritzen and Gold, 2003; Iadecola, 2004; Goense and Nikos K Logothetis, 2008; Logothetis, 2008). The LFP is generated by synaptic input, and reflects the "incoming" neural signals to a region, while the MUA reflects spiking activity, effectively the output of a brain region (Figure 1.17) (Logothetis *et al.*, 2001; Goense and Nikos K. Logothetis, 2008).

The LFP signal follows the evoked stimulus within milliseconds, while the CBF is usually a delayed, low-pass filtered version of the LFP (Lauritzen and Gold, 2003). There is a non-linear relationship between synaptic activity and cerebral blood flow changes, as the blood flow response reaches a plateau in response to a prolonged stimulus (Lauritzen and Gold, 2003).

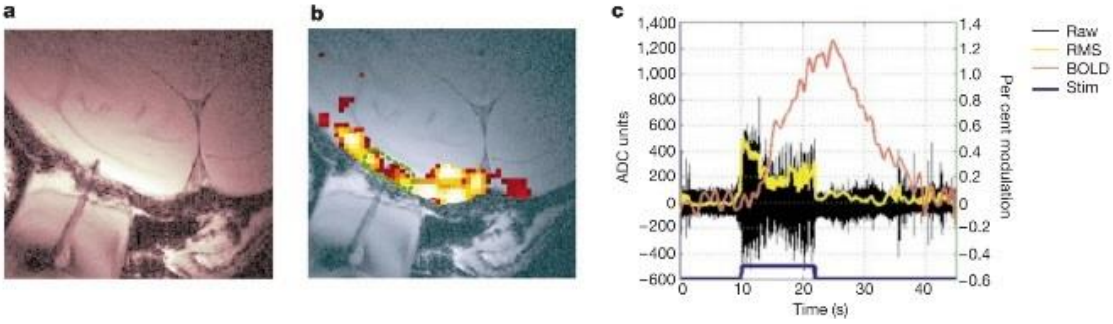

Figure 1.17 **Neural and BOLD responses to pulse stimuli.**
A. Location of the electrode tip in primary visual cortex. B. BOLD response to rotating chequerboard patterns in striate cortex. C. Hemodynamic response (red) superimposed on the de-noised raw neural signal (black). Adapted from "Neurophysiological investigation of the basis of the fMRI signal" by Logothetis, *Nature*, 2001.

1.6.3 **Resting-state fMRI and basal cerebral perfusion**

Initially most neuroimaging research focused on an evoked, activity dependent change, but a large proportion of the brain's energy is used under resting conditions (Raichle, 2009; Attwell *et al.*, 2010). There is ongoing and spontaneous background neural activity and vascular fluctuations, even without an experimenter-imposed stimulus. This is consistent, as the brain does not become inactive when there is no obvious cognitive or sensory stimuli (Raichle and Mintun, 2006; Scholvinck *et al.*, 2010). Resting state fMRI patterns are similar to those seen during sensory activation. These patterns brought a lot of attention to using fMRI for spatial correlation maps and functional connectivity of the brain. Functionally connected brain regions are identified using synchronous slow oscillations (0.1 Hz) in blood O_2, seen in resting-state BOLD imaging (Fox and Raichle, 2007; Nir *et al.*, 2009).

Oftentimes, these fluctuations are correlated across distant regions (Bharat Biswal *et al.*, 1995; Fox and Raichle, 2007; Mateo *et al.*, 2017) and from these correlations we can create maps of 'functionally connected' brain regions. The increased use of fMRI comes with the necessity to understand the underlying mechanisms of neurovascular coupling.

In the case of evoked responses, there are feed-forward Ca^{2+}-dependent pathways that causes the release of diffusible messengers to control arteriole diameter. For resting blood flow control, local feed-forward mechanisms are still unknown, but there must be a tonic and constant signal to the vasculature to ensure healthy cerebral perfusion.

The slow oscillation patterns measured in the resting-state BOLD fMRI signal could be attributed to either intrinsic properties of vessels or to spontaneous neural activity. Hemodynamic signals at rest are shown to be correlated with spontaneous neural activity (Scholvinck *et al.*, 2010; Ma *et al.*, 2016), but there is a portion of the hemodynamic signal that has non-neural origins (Winder *et al.*, 2017). In fact, in resting state hemodynamics only about 10% of variance can be explained by neural activity (Scholvinck *et al.*, 2010; Ma *et al.*, 2016; Winder *et al.*, 2017). One possible intrinsic property of vessels that could be involved in resting state BOLD fMRI signals is vasomotion. Vasomotion is the natural collective oscillation of contractile tone in smooth muscle cells (Intaglietta, 1990).

Ongoing spontaneous cortical activity and changes in brain state strongly affects sensory processing (Crochet and Petersen, 2009). Surprisingly, the basal condition is an important consideration in both the resting-state and stimulus-evoked response, as they are highly sensitive to arousal, attention, and memory (Logothetis, 2008; Chang *et al.*, 2016). Different basal conditions potentially change the magnitude and dynamics of the stimulus evoked response (Cohen, Ugurbil and Kim, 2002) (Figure 1.18). The sensory evoked response is additive to global CBF conditions that affect basal conditions, so a raised baseline will cause a normalized evoked response to seem lower. Alternatively, if the basal BOLD signal is lowered, the evoked response would be interpreted as being larger after normalization. The sensory evoked BOLD signal is dependent on the ratio of the change in blood flow to the baseline, so the basal conditions are important.

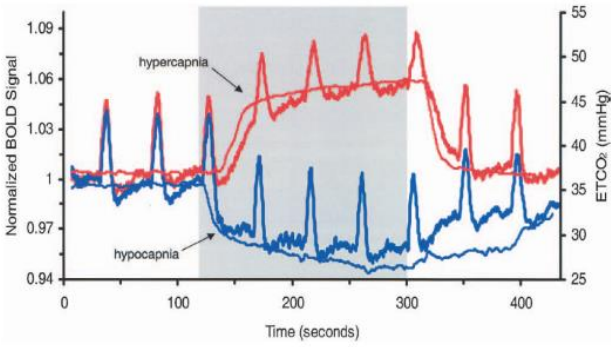

Figure 1.18 **Basal conditions will change the magnitude and dynamics of the stimulus evoked response.**
Averaged blood oxygenation level–dependent (BOLD) time courses (thick lines) and averaged end-tidal CO_2 level (thin lines) during hypercapnia (red lines) and hypocapnia (blue lines). Hypercapnia or hypocapnia are indicated by the shaded portion of the graph.
Adapted from "Effect of Basal Conditions on the Magnitude and Dynamics of the Blood Oxygenation Level–Dependent fMRI Response" by Cohen E, *Journal of Cerebral Blood Flow and Metabolism*, 2002

1.6.4 **Uncoupling of neural activity and hemodynamic responses**

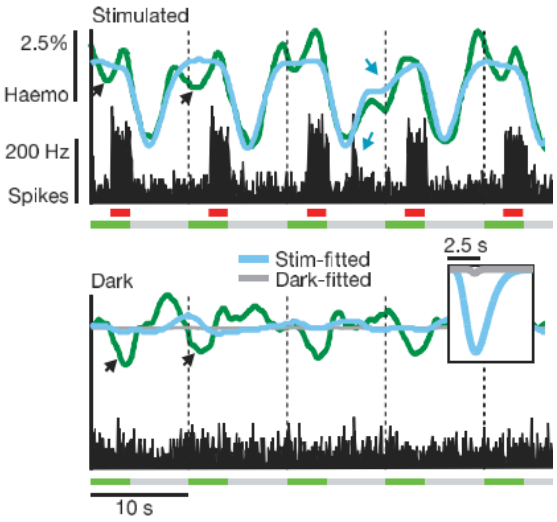

Figure 1.19 **Hemodynamics are not uniformly related to neural activity.**
Comparing measured hemodynamics (*green*) with optimal predictions from concurrent spiking (*Blue*, *grey*: using kernels (inset) obtained by fitting stimulated or dark-room signals respectively).
Black arrows: trial-related activity not predicted in either the stimulated or dark-room trials. Blue arrows: random bursts of neuronal activity generate matching deflections in the predicted and observed trace.
Top: visually driven MUA and hi-LFP predicted hemodynamic signals very well. Bottom: dark-room MUA and hi-LFP poorly predicted signals
Adapted from "Anticipatory haemodynamic signals in sensory cortex not predicted by local neuronal activity" by Sirotin Y, *Nature Letters*, 2009

There have been cases where the causal relationship between neural activity and hemodynamics breaks down or is inverted (Shih *et al.*, 2009). Functional hyperemia and BOLD fMRI signals are not an equivalent read out of local neural activation under all brain states and task-evoked brain activity. In some instances, there could be an uncoupling between neuroimaging signals and the activity of nearby neurons.

The fMRI BOLD signal is modeled as a linear convolution of neural activity with a hemodynamic response function that relies on spiking after a stimulus (Cardoso *et al.*, 2012). Modulatory input could affect alertness, leading to a mismatch between neural activity and hemodynamic signals (Figure 1.19).

There are also cases of uncoupling where there are decreases in blood volume in response to increases in local neural activity (Huo, Smith and Drew, 2014). Locomotion induces reliable increases of neural activity in somatosensory and frontal cortex, but there are blood flow decreases in the frontal cortex. If only hemodynamic

signals are recorded, decreases in the blood volume of the frontal cortex would be interpreted as decreased neural activity.

In the primary sensory cortex, during natural behaviors and passive sensory stimulation, there is a widely observed linkage between vasodilation and gamma band power (Goense and Nikos K Logothetis, 2008; Scholvinck *et al.*, 2010; Winder *et al.*, 2017), but there could be a small population of interneurons whose activity is not detectable in the local field potential (Buzsáki, Anastassiou and Koch, 2012) or in single unit recordings that contribute to control of the vasculature. In some cases, stimuli or modulatory conditions cause the activity of these neurons to become uncorrelated from the activity of pyramidal neurons. This would drive neurovascular *de*coupling, as has been observed in many studies (Sirotin and Das, 2009; Huo, Smith and Drew, 2014).

1.6.5 The role of cerebral perfusion in neurological disorders

Knowing how cerebral blood flow is controlled is crucial for understanding the dysfunction in neurological disorders, as an inadequate supply of glucose and oxygen to the brain leads to the death of neurons and glia (Attwell *et al.*, 2010). Dysregulation of blood oxygenation

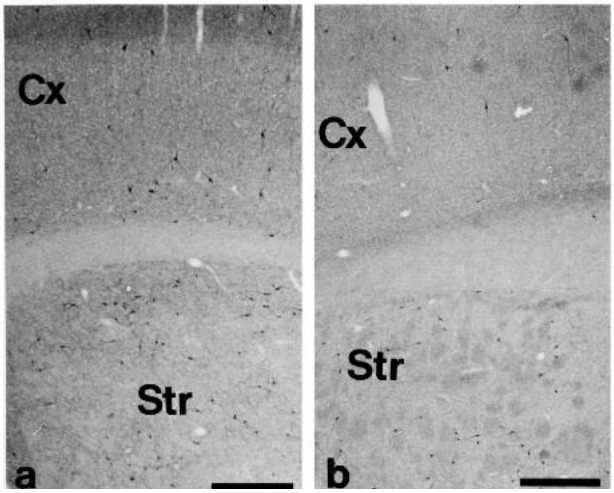

Figure 1.20 **Aged rats have fewer NADPHd-reactive (NOS) cells.**
Microphotographs of neocortex (Cx) and striatum (Str) in adult (a) and aged (b) rats after NADPHd activity staining. The number of NADPHd-reactive cells is decreased in aged animals. Scale bar: 1 mm
Adapted from "Regional alterations of the NO/NOS system in the aging brain: a biochemical, histochemical and immunochemical study in the rat" by Necchi D, *Brain Research*, 2002

and flow are implicated in vascular dysfunction (Kövari *et al.*, 2007), and decreased cerebral perfusion is linked to Alzheimer's disease and dementia (F. J. Wolters *et al.*, 2017). Cerebral perfusion is lowered with increased age, and a lower cerebral perfusion at baseline is associated with higher risks of dementia. These decreases in perfusion are correlated with degeneration of basal forebrain neurons (Lecrux and Hamel, 2016), and the SOM neurons in cortex they project to (Miettinen *et al.*, 1993). There is also a 30-50% decrease in the number of nNOS neurons in the cortex of aged rats when compared to young adults (Figure 1.20), along with decreased synthesis of the NOS enzyme and reduced effect for NO functions (Cha *et al.*, 1998; Necchi *et al.*, 2002).

1.7 **Motivation**

Understanding neurovascular coupling is important for dissecting the basis of cerebral perfusion and neuroimaging (Logothetis, 2008; Attwell *et al.*, 2010). There are still many unknowns in the control of the vasculature (Logothetis *et al.*, 2001; Raichle and Mintun, 2006; Lecrux and Hamel, 2016). Vasoactive signals cause smooth muscle cells to relax or constrict in response to Ca^{2+} transients (Duvernoy, Delon and Vannson, 1981; Emerson and Segal, 2000; Wölfle *et al.*, 2011; Huo, Greene and Drew, 2015). The structure of arteries makes them an attractive target for vasodilatory signaling from neurons (Cauli *et al.*, 2004; Hillman *et al.*, 2007).

Regardless of where on the vasculature the changes in blood flow initiate, we know that in response to a sensory stimulus there is a reliable increase in neural activity that correlates with arteriole dilation in the somatosensory cortex. The arteriole dilation leads to increases in local blood volume, blood flow, and

oxygenation. These oxygenation increases are easy to measure in humans using BOLD fMRI. The hemodynamic measurements are assumed to be linearly related to neural activity, so they are used as a proxy for brain activity (Sirotin and Das, 2009).

These neuroimaging techniques provide a powerful tool for indirect observations of neural activity in both the healthy and diseased brain, but a problem for the scientific community using these techniques is there is not a complete understanding of the signaling linking neural activity and vascular changes. The principal goal of my dissertation is to understand which cells exert the greatest influence over cortical blood volume and what signaling methods are used in the process of neurovascular coupling.

There are multiple pathways implicated in neurovascular coupling. Past work has shown either interneurons (Anenberg *et al.*, 2015; Uhlirova, Kılıc, *et al.*, 2016) or pyramidal neurons (Lacroix *et al.*, 2015; Ma *et al.*, 2016) could be involved in the control of cerebral blood flow. In *Chapter 3 The neural basis of neurovascular coupling*, I try to answer the question: Which neurons control blood flow in the cortex?

One key question that has been difficult to explore, but is essential for understanding both resting-state and the stimulus-evoked BOLD fMRI, is if resting and evoked neurovascular coupling are regulated through the same pathways. The state and control of the resting vasculature is important because it sets basal perfusion (Raichle and Mintun, 2006; Rosenegger, Tran, *et al.*, 2015; K. J. Kim *et al.*, 2016). Decreased cerebral perfusion correlates with increased risk of dementia and Alzheimer's disease (F. Wolters *et al.*, 2017).

Understanding the control of the vasculature in the basal state is also important because the basal state determines the magnitude and timing of an evoked hemodynamic response (Cohen, Ugurbil and Kim, 2002). The basal conditions are essential for the interpretation of vascular signals for modalities that normalize by a baseline value. A change in the baseline would lead to differences in the sensory response. In the past, experimental design has made it difficult to probe the control of both basal conditions and sensory evoked responses. In Chapter 4 Basal perfusion and ratiometric imaging, I examine the mechanisms controlling basal arteriole diameter and if the mechanisms that regulate basal diameter are similar or different than those that control the evoked response.

Associated with identifying signaling from various neural subtypes, previous researchers have also implicated astrocytes and other indirect signaling in mediating hemodynamics. These signals have been associated with the regulation of basal cerebral perfusion and setting the vascular tone (Zonta *et al.*, 2002; Peng *et al.*, 2004; Rosenegger, Ha, *et al.*, 2015). Some have observed that the Ca^{2+} changes in astrocytes are too slow to regulate the dynamics of a sensory vascular response (Zonta *et al.*, 2002; Rosenegger, Ha, *et al.*, 2015), but astrocytes have endfeet near vessels (Kacem *et al.*, 1998; Attwell *et al.*, 2010) and have receptors that sense neural activity changes (Zonta *et al.*, 2002; K. J. Kim *et al.*, 2016). In Chapter 5 *Role of astrocytes and potassium signaling in neurovascular coupling*, I test the role of astrocytes and potassium signaling as mediators of the basal conditions and in sensory responses.

Our experimental design allowed us to test both baseline as well as experimental conditions in single animals over multiple behavioral states. We were

able to manipulate vasoactive signaling pathways in the cortex using multiple chemogenetic and pharmacological modalities and measured changes in vessel diameter, red blood cell velocity, cerebral blood volume and neural activity to understand how each signaling pathway influences arterial diameter and subsequently cortical blood volume and tissue oxygenation during both quiescent and active behavioral states in mouse somatosensory cortex.

Chapter 2 | Experimental Methods

2 General Experimental Methods

2.1 Rodent Model

All procedures were performed in accordance with protocols approved by the Institutional Animal Care and Use Committee (IACUC) of Pennsylvania State University. Data were acquired from mice (for 2PLSM imaging, electrophysiology, intrinsic optical imaging, and immunohistochemistry – see Table 1: AAV-injected mice and Table 2: Infused mice) C57-BL6J mice (Jackson Laboratory), Aldh1l1-cre/ERT2, and cre-nNOS mice (B6.129-*Nos1*$^{tm1(cre)Mgmj}$/J) between 3-8 months of age. Mice were given food and water ad libitum and maintained on 12-hour light/dark cycles in isolated cages during the period of experiments. All *in vivo* experiments were performed in the morning.

2.2 Surgery

2.2.1 Viral Injections

All viruses were obtained from UNC Vector Core or Addgene (see Table 1: AAV-injected mice). For viral injections, mice were anaesthetized with isoflurane (5% induction, 2% maintenance) and placed in a stereotaxic apparatus. A small craniotomy was made over the FL/HL representation of the somatosensory cortex (0.75 mm caudal, 2.5 mm lateral from bregma). Using a pulled glass micropipette (30-50µm tip diameter) and infusion pump (Harvard Apparatus, Holliston, MA), we microinjected 500 nanoliters (at a rate of 100nl/min) of the adeno-associated viral

(AAV) vectors (see Table 1) ~300μm below the cortex. After the viral injections were completed, the glass micropipette was kept in place for 10 minutes before removal. The skin was sutured, and mice were returned to their home cage. Four weeks after AAV injections, I performed surgeries for electrode or window implantation, or perfusion for immunohistochemistry.

Table 1: AAV-injected mice	# mice (vessels) for 2PLSM	Electrophysiology	Immuno-histochemistry	IOS
C57-BL6J: AAV5-CMV-TurboRFP-WPRE-rBG (UNC Vector Core)	12 mice (56 vessels)	4 mice	3 mice	7 mice
C57-BL6J: AAV8-hSYN-HA-hM3D(Gq)-mCherry (Addgene #50474-AAV8)	7 mice (37 vessels)	3 mice	3 mice	6 mice
C57-BL6J: AAV5-hSYN-HA-hM4D(Gi)- mCherry (UNC Vector Core)	7 mice (45 vessels)	3 mice	2 mice	4 mice
C57-BL6J: AAV5-CaMKIIa-hM3D(Gq)- mCherry (Addgene # 50476-AAV5)	6 mice (41 vessels)	4 mice	2 mice	
C57-BL6J: AAV5-CaMKIIa-hM4D(Gi)- mCherry (UNC Vector Core)	7 mice (38 vessels)	5 mice	2 mice	
B6.129-*Nos1*$^{tm1(cre)Mgmj}$/J: AAV8-hSyn-DIO-hM3D(Gq)-mCherry in nNOS-cre mice (Addgene #44361-AAV8)	6 mice (32 vessels)	4 mice	2 mice	
B6.129-*Nos1*$^{tm1(cre)Mgmj}$/J: AAV8-hSyn-DIO-hM4D(Gi)-mCherry in nNOS-cre mice (Addgene #44362-AAV8)	9 mice (49 vessels)	5 mice	2 mice	
B6;FVB-Tg$^{(Aldh1l1\text{-}cre/ERT2)1Khakh}$/J: AAV8-hSyn-DIO-hM3D(Gq)-mCherry in Aldh1l1-cre mice (Addgene #44361-AAV8)	7 mice (31 vessels)	4 mice	2 mice	
B6;FVB-Tg$^{(Aldh1l1\text{-}cre/ERT2)1Khakh}$/J: AAV8-hSyn-DIO-hM4D(Gi)-mCherry in Aldh1l1-cre mice (Addgene #44362-AAV8)	5 mice (24 vessels)	3 mice	2 mice	

The Aldh1l1-cre/ERT2 mice received tamoxifen (Sigma-Aldrich, CAS # 10540-29-1) doses 75mg/kg intraperitoneal (i.p.) for 5 consecutive days three weeks after

AAV injections. This allows for the control of gene expression over time and space. The tamoxifen was dissolved in corn oil (Sigma-Aldrich, CAS #C8267).

2.2.1.1 Designer Receptors Exclusively Activated by Designer Drugs (DREADDs)

Chemogenetics were used to bi-directionally and selectively manipulate the activity in a cell-type specific manner (Urban and Roth, 2015). DREADDs are a mutated muscarinic receptor (mAChR) that is selectivity activated by the clozapine analog clozapine-n-oxide (CNO). The mutated mAChR is unresponsive to the endogenous ligand ACh.

The combination of CNO and the G(q) DREADDs has a similar effect as the natural M3 muscarinic receptors activated by ACh (Urban and Roth, 2015). Past work has shown that activation of G(q)-coupled DREADDs increases the excitability of neurons (Rogan and Roth, 2011) and can cause increased Ca^{2+} transients in astrocytes (Agulhon *et al.*, 2013).

The G(i)-coupled DREADDs is a mutation of the M4 mAChRs, where GPCR signaling activates a G-protein inwardly rectifying K^+ channel (GIRK) (Urban and Roth, 2015). This signaling reduces neuronal excitability, by inducing hyperpolarization and suppressing spontaneous firing (Rogan and Roth, 2011). The receptors have no other active ligand and CNO has no other active receptor.

Because chemogenetic manipulations of excitability work via endogenous G-protein-coupled ion channels, there will be some variability in the amplitude of the DREADD modulation of excitability from cell-type to cell-type depending on the compliment of ion channels present. It is also well-established that increasing and

decreasing the activity of a neuron type does not have symmetric effects on network activity due to interactions within the cortical network (Phillips and Hasenstaub, 2016).

2.2.2 Polished and Reinforced Thin Skull Windows (PoRTs)

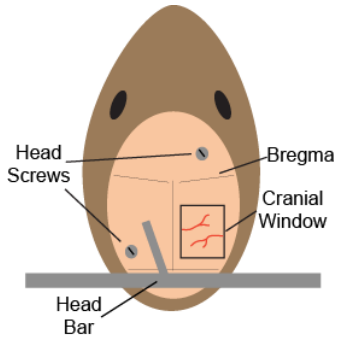

Figure 2.1 **Surgical method schematic.** Thinned cranial window with two head screws and head bar. All are attached with cyanoacrylate cement and dental cement.

Mice were anesthetized with isoflurane and the scalp was resected. A custom-made titanium bar was fixed to the skull with cyanoacrylate glue (Vibra-Tite, 32402) just posterior to the lambda cranial suture. A 4-8 mm^2 area polished and reinforced thinned-skull window (Figure 2.2) was created over the forepaw/hindpaw representation of somatosensory cortex on the right hemisphere, as described previously (Gao and Drew, 2016; Winder *et al.*, 2017). The thinned area was polished with size 3F grit (Covington Engineering, Step Three 3F-400) and reinforced with a fitted #0 glass coverslip (Electrode Microscopy Sciences, #72198). Self-tapping screws (#000, 3/32", JI-Morris, Southbridge, MA) were placed into the contralateral parietal and ipsilateral frontal bone to stabilize the skull (Figure 2.1). The titanium bar and screws were secured with black dental acrylic resin. The animals were allowed 2-3 days to recover before habituation.

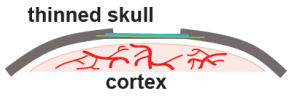

Figure 2.2 **PoRTs window schematic.** The thinned and polished skull is protected with a cover glass attached with cyanoacrylate cement. Dental cement is used to seal the edge of the cover glass.

2.2.3 Stereotrode and Cannula Implants

For electrode or cannula implantation, small (<0.5mm diameter) craniotomies were made to insert the

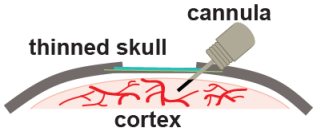

Figure 2.3 **PoRTs window with cannula implant.**

stereotrode or cannula (Plastics One, C315DCS, C315GS-4) into the upper layers of cortex near the FL/HL representation. The cannula was attached to the skull and headbar with cyanoacrylate glue and dental acrylic (Figure 2.3). Implanted cannulas do not alter the hemodynamic response (Winder *et al.*, 2017).

2.3 **Experiments**

2.3.1 **Habituation**

Mice were habituated to head-fixation on the spherical treadmill (60 mm diameter) over three days before all physiological measurements. Mice were habituated for 15 minutes of acclimation on the first day. On successive days, the time was increased to up to two hours. During habituation the mice were monitored for any signs of distress during habituation.

2.3.2 **Intraperitoneal injections**

CNO (2.5 mg/kg in 2% DMSO in saline) or vehicle (DMSO in saline) were injected intraperitoneal 20 minutes before imaging began. Electrophysiological experiments showed that the neural effects of DREADDs begin within 20 minutes of injection. CNO and vehicle were injected in a counterbalanced order.

2.3.3 **Intracortical infusions of pharmacologic agents**

For the intracortical infusions, mice were first head-fixed on the spherical treadmill. The dummy cannula was then slowly removed and replaced with an infusion cannula (Plastics One, C315IS-4). The interface between the infusion cannula and the guide cannula was sealed with Kwik-Cast (World Precision Instruments). All infusions were done at a rate of 25 nL/min for a total volume of 500 nL. Animals were kept in place for 20 min after the end of the infusion and then moved to the imaging

apparatus. The infusion cannulas were kept in place for the duration of the imaging session. Pharmacological treatments and aCSF were infused in a counterbalanced order.

Table 2: Infused mice	# mice (vessels) for 2PLSM	electrophysiology
C57-BL6J: Muscimol (10mM)	6 mice (26 vessels)	3 mice
C57-BL6J: L-Arginine (10μM)	5 mice (24 vessels)	3 mice
C57-BL6J: L-NAME (1mM)	6 mice (36 vessels)	5 mice
C57-BL6J: Substance P (1μM)	7 mice (30 vessels)	4 mice
C57-BL6J: CP-99994 (8mM)	7 mice (28 vessels)	4 mice
C57-BL6J: ML-133 (10μM)	5 mice (36 vessels)	4 mice
C57-BL6J: $BaCl_2$ (100μM)	5 mice (24 vessels)	3 mice

2.3.4 **Two-photon Laser Scanning Microscopy (2PLSM)**

Prior to imaging, mice were briefly anesthetized with isoflurane, and retro-orbitally injected with 50 μL 5% (weight/volume) fluorescein conjugated dextran (FITC-dextran 70 kDa; Sigma-Aldrich) in the plasma to label blood vessels (Patrick J. Drew *et al.*, 2010; Gao and Drew, 2016) then head-fixed upon a spherical treadmill. The treadmill was coated with anti-slip tape and attached to an optical rotary encoder (US Digital, E7PD-720-118) to monitor rotational velocity (Figure 2.4). Velocity changes were used to distinguish between periods of rest and locomotion. Imaging was done on a Sutter Movable Objective Microscope with a 16x 0.8NA objective (Nikon). A MaiTai HP laser tuned to 800 nm was used to excite the FITC. The power exiting the objective was 10-15 mW for imaging surface arteries. For vessel diameter measurements, movies of individual arteries were taken at a nominal frame rate of 8 Hz for 5 minutes. For red blood cell

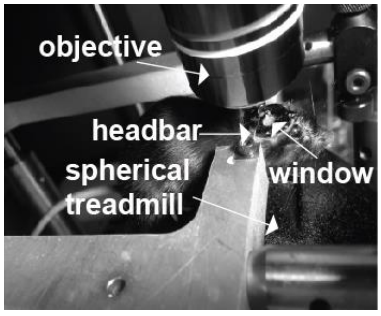

Figure 2.4 **Experimental setup of an awake, head fixed mouse.** Vessel diameter and locomotion behavior were measured in awake, head-fixed mice. Vessel diameter was measured optically using the two-photon microscope. Locomotion was monitored using a spherical treadmill and rotary encoder.

(RBC) velocity measurements, line-scans were made along the long axis of the capillary lumen (Patrick J Drew *et al.*, 2010). The same vessel segments were imaged after both the treatment (intraperitoneal CNO injection or local drug infusion) and vehicle controls (intraperitoneal vehicle injection or intracranial vehicle infusion). Treatments and vehicle condition were imaged in a counterbalanced order on separate days.

For each mouse, bright field and fluorescent images of the PoRTs window were taken before imaging on the 2-photon in order to determine the position of imaged vessels in the window. For imaging experiments with DREADDs manipulations the imaged vessels were chosen if they were within the region that expressed fluorescence, indicating DREADD expression. For infusion experiments, the vessels were imaged if they were within 1.5mm of the cannula. For repeated imaging of the same vessel, three-dimensional image stacks of the regions were made, and the position of nearby vessels were used to return to the same imaging plane on subsequent imaging sessions. Only vessels anatomically identified to be in the FL/HL representation were used in locomotion-triggered averages.

2.3.5 **Electrophysiology**

Neural activity was recorded differentially between the two leads of Teflon-insulated tungsten micro-wires (A-M Systems, #795500)(Huo, Smith and Drew, 2014; Mateo *et al.*, 2017; Winder *et al.*, 2017). Differential recordings between two closely spaced electrodes to avoid the volume conduction of remote signals (Parabucki and Lampl, 2017). To construct the stereotrodes, micro-wires with an inter-electrode spacing of ~100μm were threaded through polyimide tubing (A-M

Systems, #822200). Electrode impedances were between 70-120 kΩ at 1 kHz. The electrodes were implanted in the upper layers of cortex (~400 μm depth). The acquired signals were amplified (World Precision Instruments, DAM80), band-pass filtered between 0.1 and 10 kHz (Brownlee Precision, Model 440) during acquisition, then digitized at 20 kHz.

2.3.6 **Intrinsic Optical Imaging (IOS)**

Intrinsic optical signal imaging was performed on a subset of virus-injected mice to measure changes in cerebral blood volume. Mice (n=17) were fixed upon a spherical treadmill using the attached titanium head bar. Blood volume changes were measured by illuminating the cranial window (Figure 2.5) with three filtered 530±5 nm LEDs (Thor Labs, FB530-10, M530L2). At this wavelength, decreased reflectance from the cranial window corresponds to increased absorption by hemoglobin due to increased CBV (Sirotin and Das, 2009; Huo, Gao and Drew, 2015). The reflected light was measured using a Dalsa 1M60 Pantera CCD camera (Phase One, Cambridge MA) positioned directly above the cranial window. Light entering the camera was filtered using a mounted green filter (Edmund Optics, Barrington NJ, #46540). Images (256x256 pixels, 15 μm per pixel, 12-bit resolution) were acquired at 30 Hz. The data was then temporally filtered to remove heart-rate

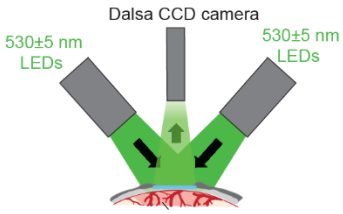

Figure 2.5 **Schematic of IOS.** CBV was measured optically using the light absorbance of hemoglobin at 530 nm, so that decreases in the measured light intensity (ΔR/R) correspond to increases in CBV

related fluctuations (Butterworth, order=4, low-pass frequency cutoff=3 Hz, MATLAB function: filtfilt).

2.3.7 **Histology**

2.3.7.1 Cytochrome oxidase staining

At the end of the experiment, mice were deeply anesthetized with 5% isoflurane, and then transcardially perfused with heparinized saline followed by 4% paraformaldehyde. The brain was removed from the skull and sunk in 30% sucrose/4% PFA. For cytochrome oxidase histochemistry, the cortex was then flattened and 60μm tangential sections were cut on a freezing microtome. The cytochrome oxidase in the sections was stained, and the location of the FL/HL representation in somatosensory cortex was reconstructed relative to the vasculature visible through the cranial window (Adams *et al.*, 2018).

2.3.7.2 Immunohistochemistry

For immunohistochemistry labeling, the brains were immersed in a 4%PFA/30% sucrose solution for 1 day. Tissues were sectioned coronally to a 90μm thickness and then washed in PBS twice. For heat-induced antigen retrieval, the slices were boiled in 10mM sodium citrate for 10 minutes. The sections were then incubated with primary antibodies on slides at a 1:200 dilution for two days at 4℃ (Mouse monoclonal GAD-65 Antibody (A-3): sc-377145 Santa Cruz Biotechnology, Mouse monoclonal CaMKII Antibody (G-1): sc-5306 Santa Cruz Biotechnology, Rabbit polyclonal to GFAP: ab7260 abcam). The brain sections were washed twice and incubated for one hour with secondary antibodies (Abcam Alexa Fluor® 488 Goat Anti-Mouse IgG H& L and Goat Anti-Rabbit IgG H& L). The brain sections were washed

twice, and cover-slipped with DAPI fluoroshield mounting media (Abcam ab104139). The sections were imaged on an Olympus FV10i Confocal.

2.4 Data Analysis

2.4.1 2PLSM data

2.4.1.1 Vessel diameter

Data analysis was performed in MATLAB (MathWorks). 2PLSM images were aligned in the x–y plane using a rigid-body registration algorithm (Drew, Shih and Kleinfeld, 2011; Gao, Greene and Drew, 2015). Each movie was manually reviewed to ensure that z-axis motion during locomotion was minimal. A rectangular box was manually drawn around a segment of the vessel. For surface arteries, the fluorescence intensity of a short segment (1-3 micrometers in length) was averaged along the long axis of the vessel, and the diameter was calculated from the full-width at half-maximum (Drew, Shih and Kleinfeld, 2011). For penetrating arteries, the Thresholding in Radon Space (TiRS) method (Gao and Drew, 2014) was used as it effectively performs a full-width at half maximum measurement along every angle of the penetrating artery (https://github.com/DrewLab/Thresholding_in_Radon_Space). For diameters of penetrating vessels, using the TiRS method is important, as penetrating vessels are not circular and the cross sectional shape will change during dilation, making single-axis diameter measurements inaccurate (Greensmith and Duling, 1984; Steelman *et al.*, 2010; Gao and Drew, 2014). A square region of interest (ROI) enclosing the penetrating arteriole of interest was manually drawn. The images were transformed into Radon space, thresholded, and then transformed back to image space, where the

vessel cross-sectional area was quantified after a second thresholding. In order to facilitate comparison with pial vessels, diameters (D) of penetrating vessels were taken to be: $D=2\sqrt{A/\pi}$, where A was the cross-sectional area calculated using the TiRS method. Frames in which the temporal derivative of diameter changed by >16 μm/s were tagged as motion artifacts and replaced with the linear interpolation between the proceeding and subsequent points. The diameter was filtered with a five-point median filter (MATLAB function: medfilt1; filter order = 5). Example images of individual vessels were 3D median filtered in ImageJ (ImageJ: 3D Median, radius=2) and then the max intensity projection was taken for 40 frames with or without locomotion.

2.4.1.2 Linescans for red blood cell velocity

Red blood cell velocity in capillaries was calculated using the Radon transform (Patrick J. Drew *et al.*, 2010) (https://github.com/DrewLab/MCS_Linescan).

2.4.2 Electrophysiology data

2.4.2.1 LFP and MUA

Power was calculated after digitally band-pass filtering the raw neural signal (MATLAB function: butter, filtfilt; filter order = 4). The local field potential (LFP) was calculated by digitally band-pass filtering the raw neural signal between 10-100 Hz (Goense and Nikos K Logothetis, 2008) (MATLAB function: butter, filtfilt; filter order = 4) and using a notch filter to remove 60 Hz noise (MATLAB function: iirnotch). The basal power was computed by calculating the log power during periods of recording with no locomotion. The locomotion power was computed by calculating the log power during periods of recording with locomotion. Gamma-band power was

quantified by averaging the 40-100 Hz band of the LFP after using a notch filter to remove 60 Hz noise.

2.4.3 **Locomotion events and rest**

To detect locomotion events, the signal from the rotational encoder on the spherical treadmill was low-pass filtered (10 Hz, fifth-order Butterworth), and then the absolute value of the acceleration was binarized with a 10^{-5} cm/s^2 threshold (Huo, Smith and Drew, 2014; Gao and Drew, 2016). Stationary periods were defined as times when the mouse was still, with a 2s buffer after the end of any preceding locomotion event and a 1s buffer before the start of the next locomotion event. Onset time was calculated with a linear regression between 20% and 80% to the peak dilation (Nizar *et al.*, 2013). The change in basal diameter under each treatment was normalized by the basal diameter of the same vessel under the vehicle control.

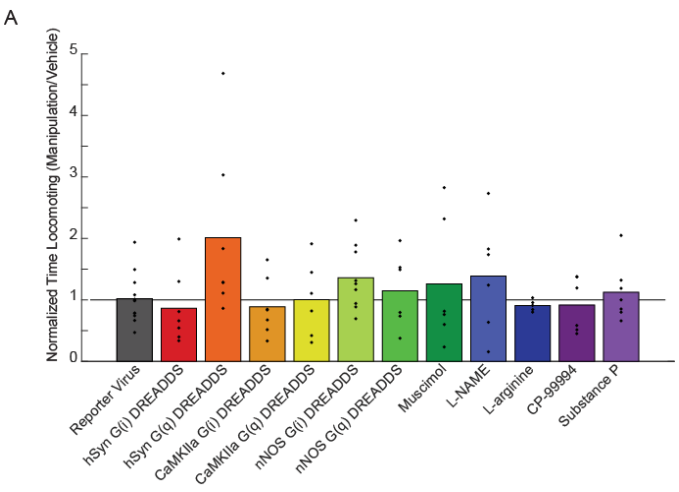

Figure 2.6 **Effects of chemogenetic and pharmacological manipulation on locomotion.** Plot showing the amount of time locomoting for each manipulation normalized by the amount of time locomoting with the vehicle. No manipulation resulted in a significant change in the behavior (LME, all p-values were Bonferroni corrected by the number of different viruses used or by the number of different drugs infused: *Reporter Virus* p=1 n=12 mice; *muscimol* p=1 n=6 mice; *hSyn-G(i) DREADDs* p=1 n=7 mice; *hSyn-G(q) DREADDs* p=0.3 n=7 mice; *CaMKIIa-G(i) DREADDs* p=1 n=7 mice; *CaMKIIa-G(q) DREADDs* p=1 n=6 mice; *nNOS-G(i) DREADDs* p=0.2 n=9 mice; *nNOS-G(q) DREADDs* p=1 n=6 mice; *L-NAME* p=1 n=6 mice; *L-arginine* p=1 n=5 mice; *CP-99994* p=1 n=7 mice; *Substance P* p=1 n=7 mice).

For the vessels that were histologically identified as being within the FL/HL representation, locomotion-triggered averages (LTA) were calculated by taking the

average of any locomotion event >5 seconds in duration with at least 2 seconds of no locomotion before the event. These averages were normalized by the average basal diameter of the same vessel under vehicle control conditions. Mice continued to spontaneously locomote after all manipulations of neural activity (Figure 2.6).

2.4.4 **IOS data**

For IOS, the reflectance from the regions of the cranial window that were histologically identified as being within the FL/HL representation, were used to calculate the locomotion-triggered averages (LTA). This was done by calculating the average of any locomotion event >5 seconds in duration with at least 2 seconds of no locomotion before the event. These averages were normalized by the average basal diameter of the same vessel under vehicle control conditions.

2.4.5 **Statistical analysis**

Statistical analysis was performed using MATLAB (R2018, MathWorks). All summary data were reported as mean ± standard deviation. For comparisons of vehicle vs. treatment conditions, where multiple measurements of different vessel diameters were taken from the same mouse, we used the linear mixed effects (LME) model (MATLAB function: fitlme). For each manipulation (e.g. CNO vs. vehicle in DREADD-expressing mice) we fit a linear mixed effects model given by:

$$\Delta D_{n,a} = \gamma + \beta_a$$

where $\Delta D_{n,a}$ is the diameter differences between the vehicle and manipulation condition, a is the identifier of the animal group, and n is the identifier of the vessel. The γ term is the (fixed) effect of the manipulation, and β_a is the within animal (random) effect that accounts for the within animal correlations (Aarts *et al.*, 2014).

To determine if any of the manipulations caused a significant change in the vessel diameter, we calculated if the γ term differed from 0, after a Bonferroni correction for the number of groups of DREADD-expressing mice (7 groups) or the number of infusions (7 groups). A difference was determined to be statistically significant if $p<0.05$ after Bonferroni correction. For plotting the relationship of the basal diameter in the control condition versus the manipulation in the figures, we fit a linear mixed effects model given by:

$$\Delta D_{n,a} = \gamma + \beta_a + \alpha_n D_n$$

where D_n is the diameter of vessel n in the control condition, and α_n is a vector of (fixed) coefficients.

For comparisons of vehicle vs. treatment conditions of the gamma-band (averaged power from 40-100Hz after removing 60 Hz noise), we used the paired t-test (MATLAB function: ttest).

Chapter 3 |
Neural basis of neurovascular coupling

3 The neural basis of neurovascular coupling

3.1 Introduction

The brain is an energetically demanding organ, and understanding the mechanisms by which neural activity regulates local blood flow is a fundamental issue in neuroscience. Changes in neural activity are coupled to blood flow via neurovascular coupling, where neural activity drives the dilation of arterioles and other vessels (Drew, Shih and Kleinfeld, 2011; Hill *et al.*, 2015; Mishra *et al.*, 2016; Rungta *et al.*, 2018). Typically, increases in the gamma-band power of the LFP, a reliable indicator of overall neural activity, are correlated with vasodilation in the awake animal (Goense and Nikos K Logothetis, 2008; Logothetis, 2008; Mateo *et al.*, 2017; Winder *et al.*, 2017). However, under some conditions, neural activity (as measured with electrophysiological recordings) and hemodynamic signals are decoupled (Shih *et al.*, 2009; Sirotin and Das, 2009; Boynton, 2011; Winder *et al.*, 2017). There are multiple signaling pathways implicated in linking neural activity, both directly and indirectly, to arteriole dilations (Attwell *et al.*, 2010; Cauli and Hamel, 2010). Whether these dilations are controlled by the activity of excitatory pyramidal neurons (Lecrux *et al.*, 2011; Vazquez *et al.*, 2014; Ma *et al.*, 2016) or interneurons (Cauli *et al.*, 2004; Anenberg *et al.*, 2015; Uhlirova, Kılıç, *et al.*, 2016) remains unresolved. Elucidating which neuronal types control arterial dilation (Uhlirova, Kılıc, *et al.*, 2016) is important for interpreting and decoding neural activity

(Kay, David, *et al.*, 2008; Kay, Naselaris, *et al.*, 2008) from hemodynamic imaging signals such as those used by fMRI (Logothetis, 2008; Kim and Ogawa, 2012). Moreover, the regulation of *basal* arterial diameter, important in controlling baseline blood flow, remains poorly understood. Changes in baseline flow can radically alter the sign and magnitude of evoked BOLD fMRI signals (Cohen, Ugurbil and Kim, 2002), which depend on the ratio of the change in blood flow to the baseline. Additionally, decreases in basal cerebral blood flow occur with aging, and the amplitude of these decreases predicts the onset of neurodegeneration (F. Wolters *et al.*, 2017), which implies adequate basal blood flow is important for a healthy brain. Thus, understanding the neural control of both basal and evoked changes in arterial diameter is essential for interpreting functional imaging and understanding the pathophysiology of disease. Here, we show that the activity of a small group of neurons that express nNOS and the substance P receptor (NK1R) are the predominant regulators of cortical hemodynamic signals, whose activity is invisible to traditional extracellular recordings of neural activity.

3.2 **Materials and Methods**

We used two-photon microscopy (Shih *et al.*, 2012) to chronically image pial and penetrating arterioles in the somatosensory cortex of awake, head-fixed mice (Figure 3.1A and B) (Gao and Drew, 2016; Mateo *et al.*, 2017) through polished and reinforced thinned-skull (PoRTs) windows (Patrick J Drew *et al.*, 2010). Because we were able to repeatedly image from the same vessels (Figure 3.1C), we were able to make quantitative comparisons of the responses of individual vessels to experimental modulations in neural activity. As we measured multiple vessels from each mouse,

we used linear mixed-effect models (see Chapter 2) (Aarts *et al.*, 2014) to account for within-animal correlations (Winder *et al.*, 2017; Adams *et al.*, 2018) that make methods such as ANOVA inappropriate (Aarts *et al.*, 2014). Using cytochrome oxidase histochemistry, we reconstructed the locations of individual arterioles relative to the forelimb representation in somatosensory cortex (purple and green shaded regions Figure 3.1B, top) that is strongly activated by locomotion. We measured arteriole diameter dynamics driven by locomotion, as behavior is the primary driver of hemodynamic signals in the awake brain (Figure 3.1D) (Gao and Drew, 2016; Winder *et al.*, 2017), and because sensory stimulation in awake animals invariably elicits movement (Cooke *et al.*, 2015; Drew, Winder and Zhang, 2018). During bouts of voluntary locomotion, neural activity increased substantially in the forelimb/hindlimb (FL/HL) representation in somatosensory cortex, as measured by changes in firing rate or power in the gamma-band of the LFP (Huo, Smith and Drew, 2014). In response to this increase in neural activity, both pial and penetrating arterioles in the FL/HL representation dilated (Huo, Gao and Drew, 2015; Gao and Drew, 2016) (Figure 3.1D) with short latency (onset time: 0.59±0.31 seconds in the FL/HL region).

3.2.1 **Surgery**

3.2.1.1 Electrode, cannula, and window implantation procedure for two-photon microscopy imaging experiments

Mice were anesthetized with 2% isoflurane (in oxygen). Head bars were attached, then windows, cannula, and electrodes were implanted as described in Chapter 2.

The animals were allowed to recover for 2-3 days before habituation.

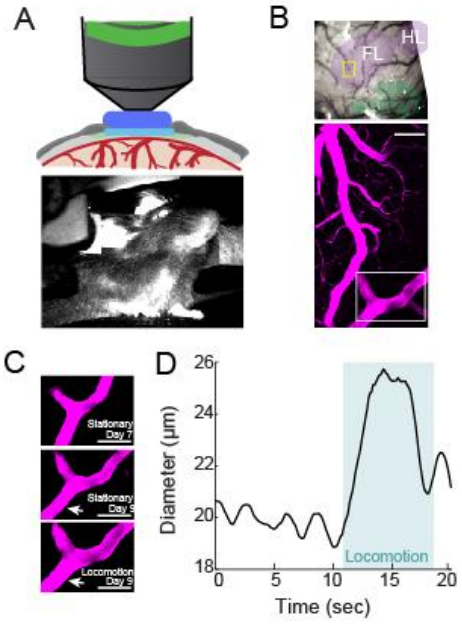

Figure 3.1 **Two-photon imaging of arteriole dynamics.**
A. Top, schematic of imaging window. Bottom, photo of mouse on spherical treadmill.
B. Top, photo of the pial vasculature of the somatosensory cortex through the PoRTs window. Cytochrome oxidase processing was used to localize the forelimb/hindlimb (FL/HL, purple) and vibrissae cortex (green). Bottom, a maximum projection of two-photon images of vasculature (scale bar 50µm) within the yellow box in the top image.
C. Top and middle, two-photon images (from white box in Bottom B) of the same arteriole 7 and 9 days after window implantation (scale bars 50µm), both taken when mouse was stationary. The bottom image shows an example image 9 days after implantation during locomotion (scale bar 50µm).
D. Locomotion induces rapid dilation in pial arterioles. Diameter (region marked by white arrow in **C**) was plotted versus time. Blue shading denotes period of locomotion

3.2.2 **Physiological Measurements**

All habituation to the apparatus and data acquisition for the experiments in this chapter were described in detail in Chapter 2. Briefly, vessel diameter measurements were recorded from mice using the two-photon microscope (2.3.4 Two-photon Laser Scanning Microscopy (2PLSM)) and neural recordings were taken using stereotrodes. Electrophysiology was measured as the differential potential between the leads of a stereotrode implanted in the imaged region of the window. The physiological measurements were taken simultaneously as behavior measurements to ensure mice were alert.

3.2.2.1 **Habituation, Imaging, Chemogenetics and Infusions**

Habituation for experiments was carried out as described in Chapter 2. For this chapter, we used both G(q) and G(i) DREADDs viruses with each of the following promoters/mice: hSyn/C57-BL6, CaMKIIa/C57-BL6, and hSyn-DIO/nNOS-cre.

For this chapter, we also did a number of pharmacological intracortical infusions through a cannula. We used muscimol ($GABA_A$ agonist, 10mM), L-Arginine (precursor of NO, 10μM), L-NAME (inhibitor of NOS activity, 1mM), Substance P (NK1R agonist, 1μM), and CP-99994 (NK1R antagonist, 8mM). We infused each of these at a rate of 25 nL/minute for a total volume of 500 nL. Pharmacological treatments and aCSF were each infused in a counter-balanced order. All mice received both infusions of drugs and an aCSF control, so no randomization was needed.

3.2.3 **Data Analysis**

All analyses were conducted using custom-written code (see Chapter 2) in MATLAB.

3.3 **Outcomes**

3.3.1 **Basal arterial diameter and evoked dilation are controlled by local neural activity**

We first determined the role of overall local neural activity in maintaining baseline arterial diameter and for mediating hemodynamic changes during locomotion. We suppressed the activity of all neurons via intracranial infusions of muscimol (a $GABA_A$ receptor agonist) (Figure 3.2A), and compared the changes in neural activity and arterial diameter dynamics to artificial cerebrospinal fluid (aCSF) infusions in the same mouse. Infusions of muscimol substantially decrease neural activity ~1.5mm from the cannula (Winder *et al.*, 2017), and so will suppress activity in all cortical layers, unlike topical administration of drugs which only affect the supragranular layers (Ferezou, Bolea and Petersen, 2006). Cannula implantations do not alter hemodynamic responses (Winder *et al.*, 2017).

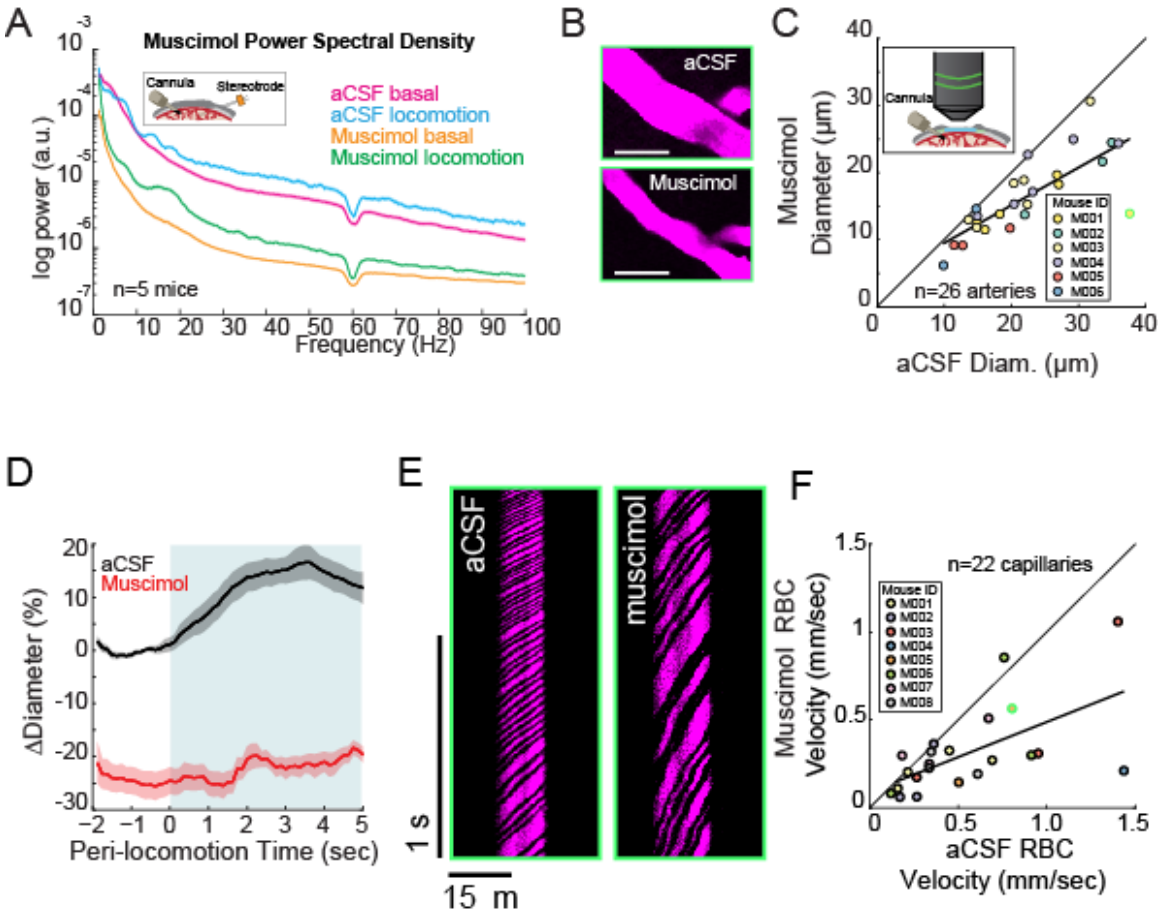

Figure 3.2 **Local neural activity controls basal and evoked arteriole diameter.**
A. LFP power spectra during stationary periods (basal) and locomotion after muscimol infusion, normalized to vehicle infusion in the same animal. Muscimol caused a substantial decrease in gamma band power (basal, -60.9±13.3%, paired t-test $p=2.8x10^{-3}$; locomotion, -52.7±5.3%, paired t-test p=0.01, n=3 mice). Inset, schematic of electrode-cannula preparation
B. Representative images of a pial arteriole during times of no locomotion after vehicle infusion (top) and after muscimol infusion (bottom). Arteriole diameter decreased after muscimol infusion (scale bar 50μm)
C. Basal arteriole diameter following vehicle infusion plotted versus basal diameter after muscimol infusion. Each point is a single vessel, and the mouse identity is represented by the color. The black line shows the linear regression of aCSF vs. muscimol diameter, and muscimol caused a significant decrease in diameter (-25.4±2.3%, LME $p=3.3x10^{-4}$, n=6 mice, 26 vessels). Insets show schematic of PoRTs window-cannula preparation and mouse ID color code. The point outlined in green is representative image from B.
D. Population locomotion-triggered averages following aCSF (black) and muscimol (red) infusions (n=6 mice, 12 arterioles in FL/HL representation). For both cases, the individual diameters are normalized by the average basal diameter of the vessel after vehicle infusion. Note the rapid rise to peak in the control, and the lack of dilation in muscimol-infused mice, showing the locomotion-triggered response is under local neural control. Shading represents mean ± standard deviation.
E. Representative space-time image of linescans of the same capillary after aCSF or muscimol infusion.
F. Basal red blood cell (RBC) velocity plotted after vehicle infusion (x-axis) vs after muscimol infusion (y-axis). Muscimol caused a significant decrease in the RBC velocity (-44±27%, LME p=0.03, n=5

We found that after the infusion of muscimol, there was a 60.9±1.0% decrease

in baseline gamma-band power (Figure 3.2A, line, paired t-test $p=2.8x10^{-3}$) and 52.7±5.3% decrease in the gamma-band power during locomotion relative to aCSF infusions (Figure 3.2A, paired t-test p=0.01). We found that muscimol infusions led to a substantial decrease in the basal arterial diameter (-25.4±2.3%, Figure 3.2B-C, LME $p=3.3x10^{-4}$). We refer to the diameter of the vessel during periods lacking locomotion (see Methods) as the "basal" diameter. Note that the locomotion-triggered averages calculated using vessels histologically identified to be in the FL/HL representation, while the changes in basal diameters were calculated using all vessels imaged in the somatosensory cortex. The effects of muscimol infusions were not due to direct actions on the cerebral vasculature, which lack $GABA_A$ receptors (de Blas, Vitorica and Friedrich, 1988; Vanlandewijck *et al.*, 2018), but rather by the removal of tonic vasodilatory signals released by neurons. The locomotion-evoked response was nearly completely blocked by local silencing of neurons, showing that these arterial dilations were not due to non-specific cardiovascular responses (Huo, Greene and Drew, 2015) or modulatory input from other brain regions directly onto the vessels (Drew *et al.*, 2008), but rather controlled by local activity. Suppressing neural activity with muscimol did not abolish spontaneous fluctuations in arterial diameter, consistent with previous reports of autonomous oscillations in arterioles (Winder *et*

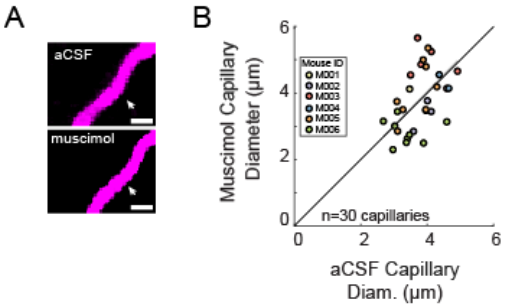

Figure 3.3 **Muscimol infusion does not significantly affect capillary diameter.**
A. Representative images of the same capillary after vehicle infusion (left) and after muscimol infusion (right). There was no significant change seen after muscimol infusion (scale bar 5µm).
B. Capillary diameter measured after vehicle infusion (x-axis) vs. after muscimol infusion (y-axis) showed no significant changes (0.12±1.1µm LME p=0.66, n=3 mice, 5 capillaries).

al., 2017). To determine if this decrease in arterial basal diameter drove a decrease in blood flow, we then measured red blood cell (RBC) velocity in the capillaries (Patrick J. Drew *et al.*, 2010) (Figure 3.2E and F). Capillary RBC velocity was decreased in muscimol-infused mice relative to aCSF infusions (-44±27%, n=13 capillaries, LME p=0.03, Figure 3.2F). We observed no significant change in the diameter of the capillaries following the infusion of muscimol (0.12±1.1μm, LME p=0.66, Figure 3.3). Taken together, these results show that baseline levels of neural activity have a tonic vasodilatory effect on cerebral arteries, and decreasing neural activity causes a corresponding decrease in arterial diameter and blood flow.

3.3.2 Bi-directional chemogenetic manipulation of local neural activity controls basal arterial diameter

We then asked if we could bi-directionally manipulate arterial diameters using chemogenetic techniques to drive changes in overall neural activity. We expressed either hM4D-G(i) or hM3D-G(q)-coupled DREADDs (Urban and Roth, 2015) pan-neuronally under a synapsin promoter in C57-BL6J mice. We targeted the deeper cortical layers, as there is evidence that hemodynamic responses initiate there (Rungta *et al.*, 2018). We imaged arterioles in the DREADD-expressing region of cortex (identified by mCherry expression seen in vivo, Figure 3.6A, and histologically, Figure 3.6B).

Control mice infected with an AAV expressing only a fluorescent reporter protein did not show significant changes in neural activity or basal arterial diameter after the injection of CNO (Figure 3.4B-D), showing CNO has minimal off-target effects in our system.

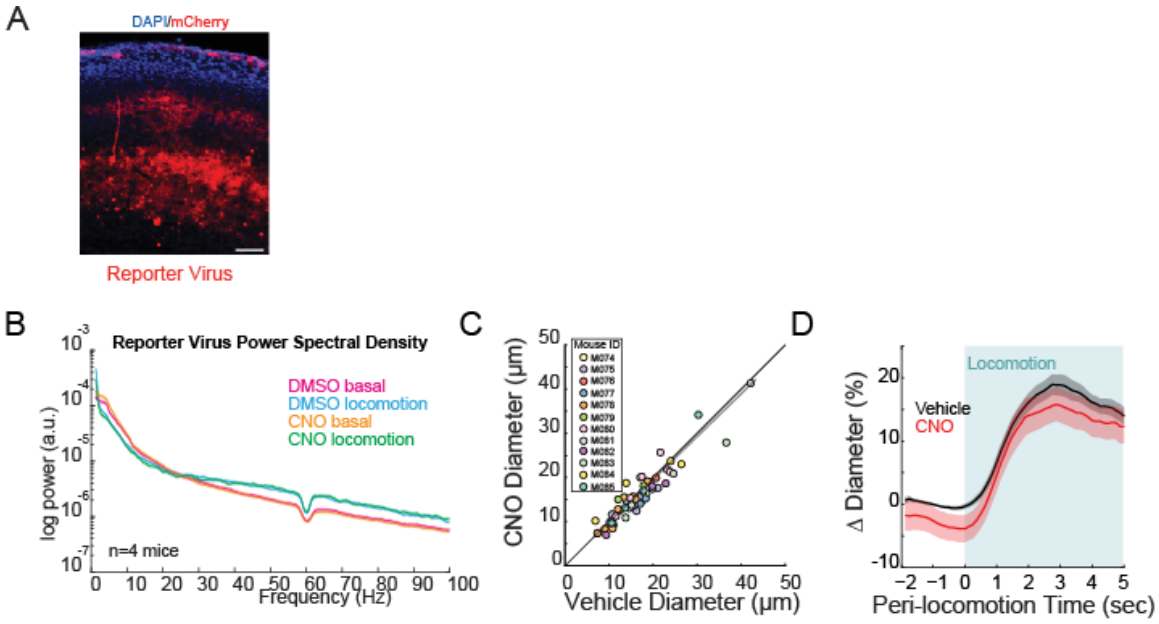

Figure 3.4 **No significant effect of CNO on basal vessel diameter or neural activity.**
A. Representative 90µm thick coronal section of the cortical region infected with the reporter virus showing mCherry expressing neurons (red) and cell nuclei (DAPI, blue). Scale bar is 100µm.

Data in **B-D** are from mice injected with AAV-CMV-TurboRFP-WPRE-rBG (fluorescent reporter virus)
B. LFP power spectra during stationary periods (basal) and locomotion after CNO injection, normalized to vehicle injection in the same mouse. The fluorescent reporter virus does not significantly change neural activity in the gamma band (basal, -9.7±10.6%, paired t-test p=0.17; locomotion, 5.4±8.8 %, paired t-test p=0.29, n=4). Shading denotes mean ± standard deviation.
C. Plot of basal arteriole diameter after vehicle injection (x-axis) versus CNO injection (y-axis). There were no significant changes in basal diameter (-3.2±14.5%, LME p=0.46 Bonferroni corrected, n= 12 mice, 56 vessels).
D. Locomotion-triggered averages after vehicle (black) and CNO (red) injections (n= 12 mice, 39 arterioles in FL/HL representation). For both cases, the diameters were normalized by the average basal diameter of the vessel after vehicle injection.

Injections of CNO in mice with pan-neuronal expression of hM4D-G(i) DREADDs resulted in a decrease in gamma-band power relative to vehicle injections (CNO gamma-band power -8.7±3.9% relative to vehicle, paired t-test p= 0.18 for basal periods, Figure 3.6C). Consistent with the results of pharmacological infusions of muscimol, the decreases in overall neural activity drove a decrease in basal arterial diameter (7.1±7.0%, Figure 3.6D, LME p=0.02) and in the locomotion-evoked response (Figure 3.6E). In contrast, mice expressing hM3D-G(q) DREADDs, which increases excitability pan-neuronally, showed increases in gamma-band power

(+8.46±7.6%, paired t-test p= $2.7x10^{-3}$ for basal periods, Figure 3.6F) with CNO injection relative to vehicle. The hM4D-G(i) DREADDs did not uniformly lower neural activity, as we observed bursting activity every few seconds (Figure 3.5A), and corresponding dilations of arteries at similar intervals (Figure 3.5B). The basal arterial diameter was also increased when the excitability of all neurons was significantly increased (+18.8±5.6%, LME p=0.03, Figure 3.6G). The increase in basal arteriole diameter by hM3D-G(q) DREADD activation was large enough to almost completely occlude the locomotion-evoked response (Figure 3.6H). These results demonstrate that neurons, or a subset of neurons, tonically release vasodilator(s), and that the manipulation of this population of neurons up or down increases or decreases the basal arteriole diameter correspondingly.

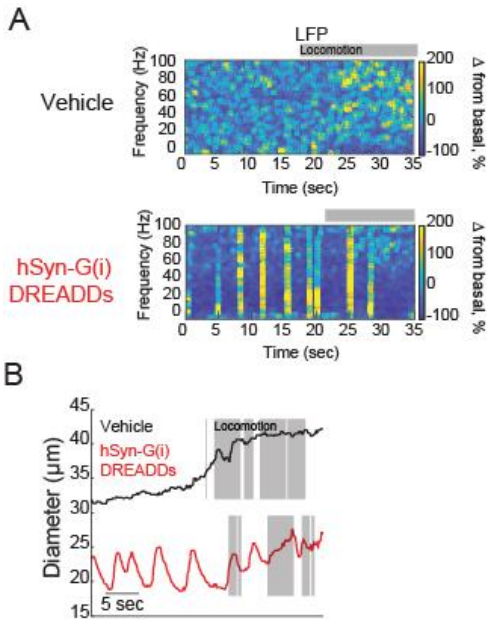

Figure 3.5 **hM4D-G(i) DREADDs did not uniformly lower neural activity**

A. Representative trial after vehicle (top) or CNO (bottom) injection in hSyn-G(i) DREADDs mice. The gamma band power of the local field potential (LFP) showed that the CNO in hSyn-G(i) mice induced bursting activity every few seconds

B. Plot of basal arteriole diameter after vehicle injection (x-axis) versus CNO injection (y-axis). CNO caused corresponding dilations of arteries at similar intervals as seen in the LFP (**A**)

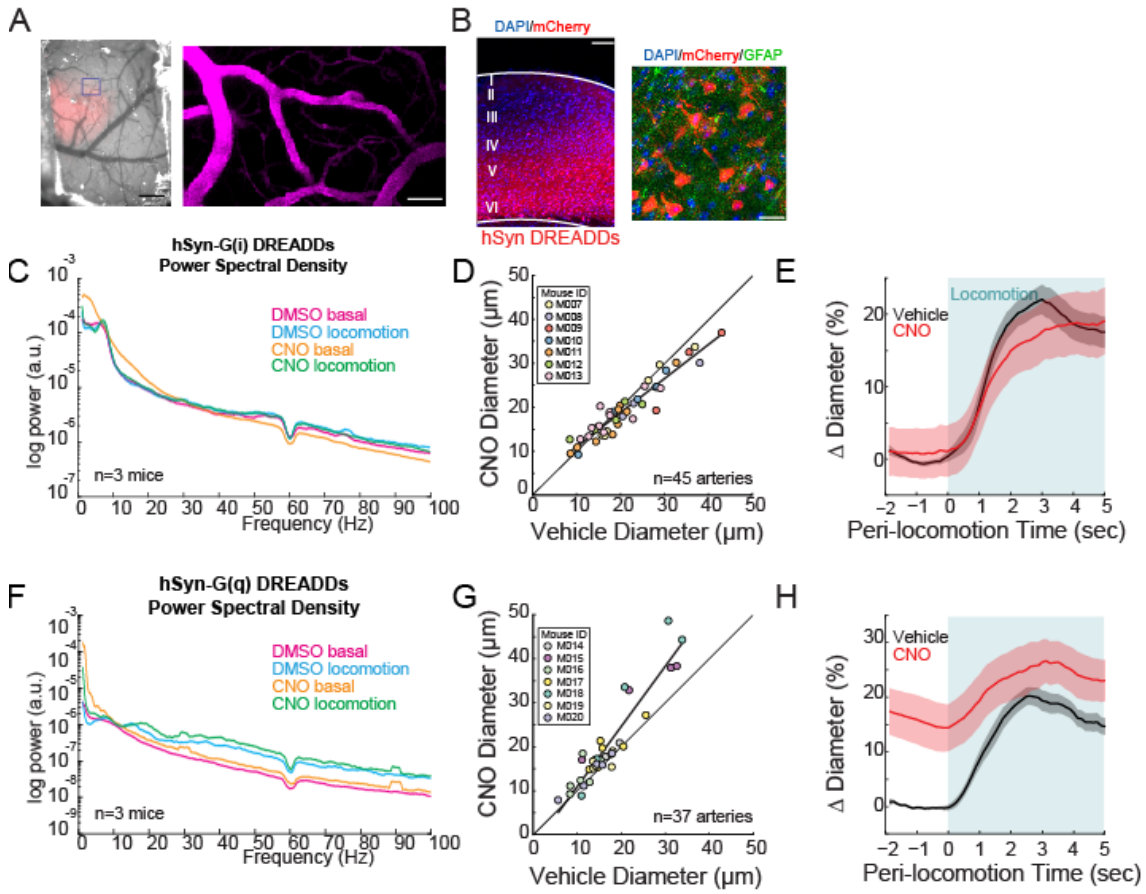

Figure 3.6 **Neural activity bidirectionally controls basal arteriole diameter.**
A. Left, image through the polished and reinforced thinned-skull window showing AAV expression (red) in the somatosensory cortex (scale bar 1 mm). Right, two-photon image of vasculature (scale bar 50μm) taken from the purple box on left. **B.** Representative image of AAV-hSYN-HA-hM3D(Gq)-mCherry infected cortex. Left image is wide field image of hSyn-mCherry DREADDs virus (red) in cortex with DAPI (blue) staining (scale bar 100μm). Right is magnified image of hSyn-mCherry DREADDs virus (red) in cortex with DAPI (blue) and GFAP (green) staining (scale bar 30μm), showing the virus was not expressed in astrocytes. Tissues sectioned to a 90μm thickness
Data in **C-E** are from mice injected with AAV-hSYN-HA-hM4D(Gi)-mCherry, data in **F-H** is from mice injected with AAV-hSYN-HA-hM3D(Gq)-mCherry.
C. LFP power spectra during stationary periods (basal) and locomotion after CNO injection in hSyn G(i) DREADDs mice, normalized to vehicle injection in the same animal. Pan-neuronal expression of G(i) DREADDs reduces neural activity in the gamma band (basal, -8.7±3.9%, paired t-test p= 0.18; locomotion, -29.1±37 %, paired t-test p=0.38, n=3). Shading denotes mean ± standard deviation.
D. Plot of basal arteriole diameter after vehicle injection (x-axis) versus CNO injection (y-axis). CNO caused a significant decrease in arterial diameter (-7.1±7.0%, LME p=0.02 Bonferroni corrected, n=7 mice, 45 vessels).
E. Population locomotion-triggered averages after vehicle (black) and CNO (red) injections (n=7 mice, 33 arterioles in FL/HL representation).
F. LFP power spectra during stationary periods (basal) and locomotion after CNO injection in hSyn G(q) DREADDs mice, normalized to vehicle injection of the same mouse. Pan-neuronal expression of G(q) DREADDs increases neural activity in the gamma band (basal, 8.46±7.6%, paired t-test p= 2.7×10^{-3}; locomotion, +0.2±10.3 %, paired t-test p=0.21, n= 3).

G. Plot of basal arteriole diameter after vehicle injection (x-axis) versus CNO injection (y-axis). CNO caused a significant increase in arterial diameter (+18.8±5.6%, LME p=0.03 Bonferroni corrected, n= 7 mice, 37 vessels).
H. Population locomotion-triggered averages in response to locomotion after vehicle (black) and CNO (red) injections (n= 7 mice, 25 arterioles in FL/HL representation). Increasing neural activity caused a basal arterial dilation that nearly completely occluded the locomotion-triggered response.

3.3.3 Pyramidal neural activity drives large population neural activity changes without corresponding changes in arterial diameter

The importance of local neural activity on the regulation of the vasculature raises the question of which sub-population(s) of neurons are involved in the signaling. We sought to manipulate the activity of pyramidal neurons by injecting AAVs encoding hM3D(q) and hM4D(i) DREADDs under a CaMKIIa promoter, restricting the expression of the DREADDs to pyramidal cells (Lopez *et al.*, 2016). CaMKIIa-DREADDs labeled cells colocalized with CaMKIIa expression and are primarily localized to layer 5 (Figure 3.7A). Previous work has shown that optogenetic stimulation of layer 5 pyramidal neurons drives increases in neural activity in all layers, similar to what is seen with sensory stimulation (Vazquez *et al.*, 2014; Vazquez, Fukuda and Kim, 2018). The dilatory signal in the deeper cortical layers is electrically conducted through the vasculature by gap junctions to the pial vessels. Expressing DREADDs in excitatory neurons produced large changes in overall neural activity as measured with extracellular electrophysiology. Activating hM4D(i) DREADDs expressed in excitatory neurons with CNO caused large decreases in basal gamma-band power (CNO gamma-band power -40.26±3.3% relative to vehicle, Figure 3.7B, paired t-test p=0.05). When hM3D(q) DREADD receptors in excitatory neurons were activated, a corresponding increase in basal gamma-band

power was observed (CNO gamma-band power increased by 41.23±18.7% relative to vehicle controls, Figure 3.7E, paired t-test p=0.03). Despite the large changes in neural activity, we did not see significant changes in the basal arterial diameters with manipulation of pyramidal neuron activity (-2.2±5.7%, LME p=1 for inhibition and +7.2±8.8%, LME p=0.66 for excitation) (Figure 3.7 C and F, respectively).

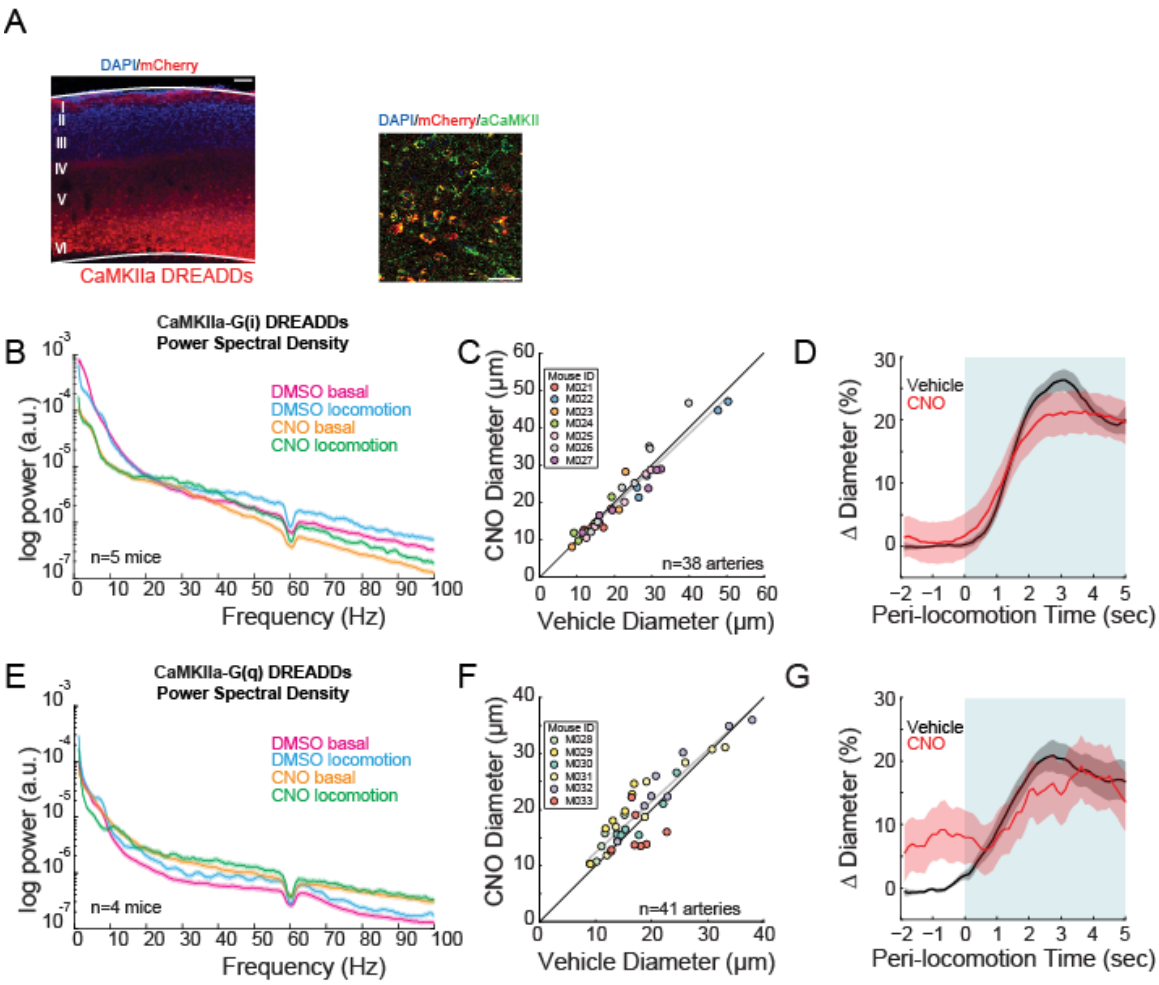

Figure 3.7 **Pyramidal neurons do not control basal arteriole diameter.**
A. Representative image of AAV-hSYN-HA-hM3D(Gq)-mCherry infected cortex. Left image is wide field image of hSyn-mCherry DREADDs virus (red) in cortex with DAPI (blue) staining (scale bar 100µm). Right is magnified image of hSyn-mCherry DREADDs virus (red) in cortex with DAPI (blue) and GFAP (green) staining (scale bar 30µm), showing the virus was not expressed in astrocytes. Tissues sectioned to a 90µm thickness
Data in **B-D** are from mice injected with AAV-CaMKIIa-hM4D(Gi)-mCherry, data in **E-G** is from mice injected with AAV-CaMKIIa-hM4D(Gq)-mCherry (expression in pyramidal neurons)
B. LFP power spectra during stationary periods (basal) and locomotion after CNO injection in CaMKIIa G(i) DREADDs mice, normalized to vehicle injection of the same mouse. Pyramidal neuron expression

of G(i) DREADDs reduces neural activity in the gamma band (basal, -40.26±3.3%, paired t-test p=0.05; locomotion, -30.9±18.1 %, paired t-test p=0.019, n=5).
C. Plot of basal arteriole diameter after vehicle injection (x-axis) versus CNO injection (y-axis). There was no significant change in the diameter (-2.2±5.7 %, LME p=1 Bonferroni corrected, n=7 mice, 38 arterioles).
D. Population locomotion-triggered averages after vehicle (black) and CNO (red) injections (n=7 mice, 33 arterioles in FL/HL representation). For both cases, the diameters were normalized by the average basal diameter of the vessel after vehicle injection.
E. LFP power spectra during stationary (basal) and locomotion periods after CNO injection in CaMKIIa G(q) DREADDs mice, normalized to vehicle injection of the same mouse. Pyramidal neuron expression of G(q) DREADDs increased neural activity in the gamma band (basal, +41.23±18.7%, paired t-test p=0.03; locomotion, +54.9±53.3 %, paired t-test $p=4.4x10^{-3}$, n=4).
F. Plot of basal arteriole diameter after vehicle injection (x-axis) versus CNO injection (y-axis). There was no significant change in diameter (+7.2±8.8%, LME p=0.66 Bonferroni corrected, n=6 mice, 41 vessels).
G. Population locomotion-triggered averages after vehicle (black) and CNO (red) injections (n=6 mice, 33 arterioles in FL/HL representation). For both cases, the diameters were normalized by the average basal diameter of the vessel after vehicle injection. Increasing pyramidal neural activity caused no change in basal arterial dilation.

Note that decreases in basal neural activity generated by activation G(i)-coupled DREADDs in pyramidal neurons were nearly as large as those elicited by muscimol (Figure 3.8A and Figure 3.3), and the increases in basal neural activity generated by activation G(q)-coupled DREADDs in pyramidal neurons were as large as those seen during locomotion (Figure 3.8B), yet in neither of these cases did we observe arterial diameter change of similar magnitude.

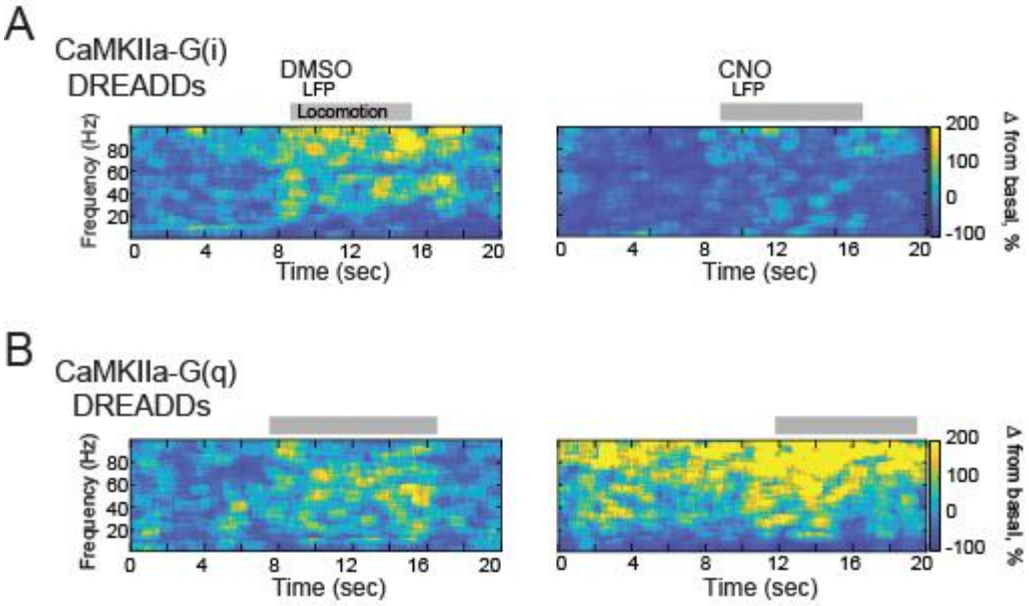

Figure 3.8 **Expressing DREADDs in excitatory neurons produced large changes in overall neural activity.**
A. Representative LFP spectrograms of CaMKIIa-G(i) DREADD infected mouse after DMSO (left) or CNO (right) injection. Locomotion events are denoted by shading. Note the large decrease in neural activity after CNO injection.
B. Representative LFP spectrograms of CaMKIIa-G(q) DREADD infected mouse (expression in pyramidal neurons) after DMSO (left) or CNO (right) injection. Locomotion events are denoted by shading. Note the large increase in neural activity after CNO injection.

These results show that arteriole diameter can be completely uncoupled with the standard measures of cortical neuronal activity, which largely reflects activity of excitatory neurons. It also suggests that the activity of the neurons that control local arterial diameter receive minimal input from local pyramidal neurons.

3.3.4 NO released by nNOS-expressing neurons controls arterial diameter independent of overall neural activity

Previous work has implicated neuronally-generated nitric oxide (NO) as a messenger coupling neural activity to arterial vasodilation (Mishra *et al.*, 2016), though it has also been proposed that NO only modulates the functional hyperemic response (Lindauer *et al.*, 1999). To test the role of neuronal nitric oxide synthase (nNOS) expressing neurons, we expressed hM3D(q) and hM4D(i) DREADDs in nNOS-

expressing neurons using flexed AAVs and cre-nNOS mice (B6.129-*Nos1*$^{tm1(cre)Mgmj}$/J, Jackson Laboratory #017526). The reporter protein was primarily expressed by a few inhibitory neurons in the deep, infragranular layers (Figure 3.9A). Neither suppressing (CNO gamma-band power, -0.80±2.1% relative to vehicle, paired t-test p=0.98, Figure 3.11B) nor increasing (CNO gamma-band power -20.17±3.2% relative to vehicle, paired t-test p=0.057, Figure 3.11E) the excitability of nNOS-expressing neurons resulted in a significant change in gamma-band power. However, while decreasing the excitability of nNOS neurons did not affect overall neural activity, there was a substantial decrease in basal arteriole diameter (-10.3±6.4% LME $p=1.2x10^{-4}$ Figure 3.11C) and a large blunting of the locomotion-induced dilation (Figure 3.11D). Elevating the excitability of nNOS expressing neurons significantly increased the basal arterial diameter (+5.8±6.6%, LME $p=2.8\ x10^{-4}$, n=8 mice, 52 vessels, Figure 3.11F), but did not increase the locomotion-evoked increase above the control (vehicle 17.4±1.8%, CNO 19.6±3.8%, LME p=1, n=8 mice, 25 arterioles in FL/HL representation). The decreases in evoked dilation were not just due to a shift in the baseline, showing that nNOS neurons play a role in evoked dilations in addition to basal diameter. The activity of nNOS-expressing neurons impacts both basal and evoked dilations, with minimal changes in overall neural activity.

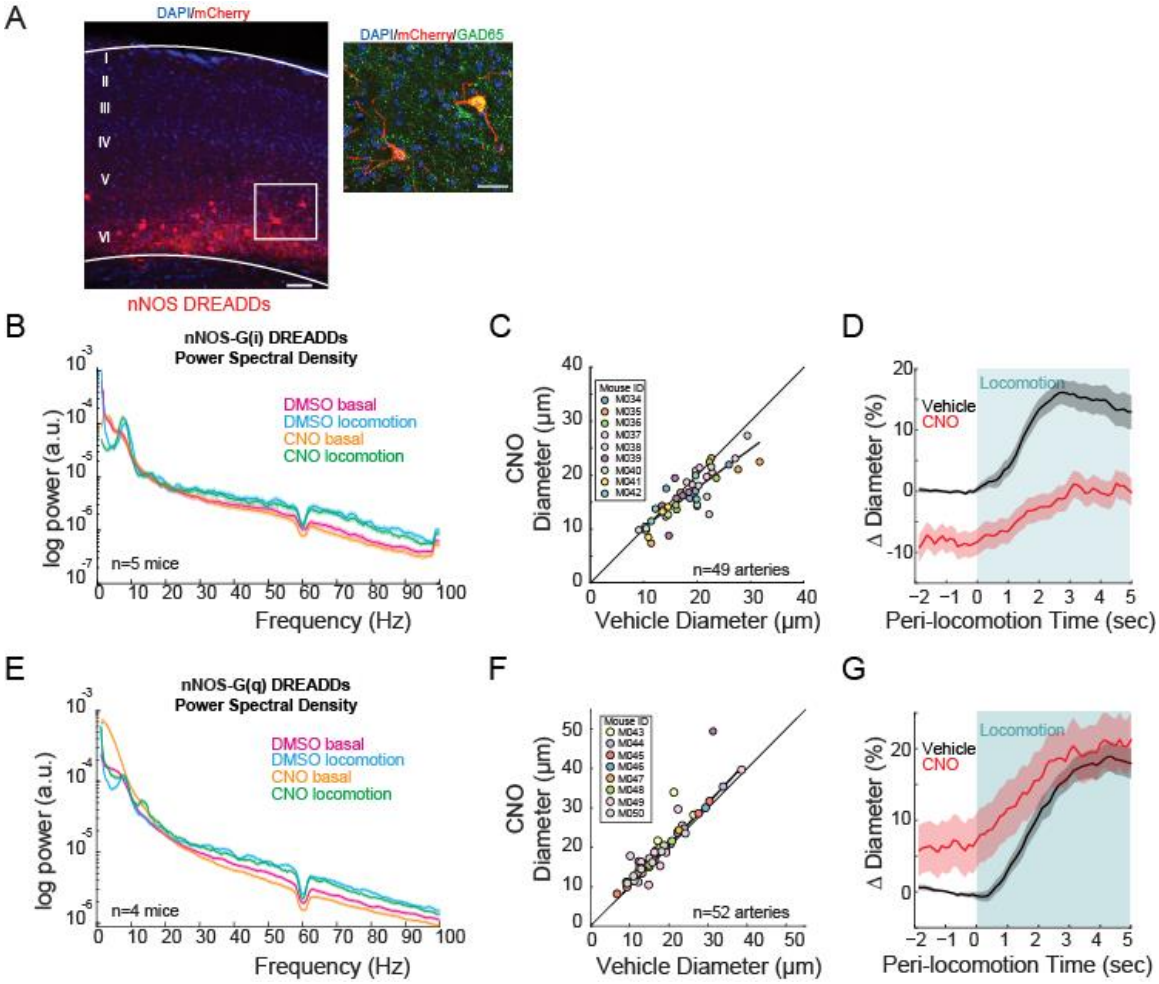

Figure 3.9 **nNOS expressing neurons controls arteriole diameter independent of overall neural activity.**

A. Representative image of cortex taken of AAV-hSyn-DIO-hM3D(Gq)-mCherry in nNOS-cre mice, where DREADDs expressed in nNOS$^+$ cells. Left image is wide field image of nNOS-mCherry DREADDs virus (red) in cortex with DAPI (blue) staining (scale bar 100µm). Right image is zoomed image of nNOS-mCherry DREADDs virus (red) in cortex with DAPI (blue) and GAD65 (green) staining (scale bar 30µm). Tissues sectioned to a 90µm thickness

Data in **B-D** are from nNOS-cre mice injected with AAV-hSyn-DIO-hM4D(Gi)-mCherry, data in **E-G** is from nNOS-cre injected with AAV-hSyn-DIO-hM4D(Gq)-mCherry.

B. LFP power spectra during stationary periods (basal) and locomotion after CNO injection in nNOS G(i) DREADDs mice, normalized to vehicle injection of the same mouse. nNOS+ expression of G(i) DREADDs did not change neural activity in the gamma band (basal, -0.80±2.1%, paired t-test p=0.98; locomotion, 13.8±8.2 %, paired t-test p=0.047, n=5). Shading denotes mean ± standard deviation.

C. Plot of basal arteriole diameter after vehicle injection (x-axis) versus CNO injection (y-axis). CNO caused a significant decrease in the arterial diameter (-10.3±6.4%, LME p=1.3x10^{-4} Bonferroni corrected, n=9 mice, 49 vessels).

D. Population locomotion-triggered averages after vehicle (black) and CNO (red) injections (n=6 mice, 22 arterioles in FL/HL representation). For both cases, the diameters were normalized by the average basal diameter of the vessel after vehicle injection. Decreasing nNOS+ neural activity reduced the locomotion-triggered dilation.

E. LFP power spectra during stationary periods (basal) and locomotion after CNO injection in nNOS G(q) DREADDs mice, normalized to vehicle injection of the same mouse. nNOS+ expression of G(q)

DREADDs reduced neural activity in the gamma band (basal, -20.17±3.2%, paired t-test p=0.057; locomotion, -14.9±8.9 %, paired t-test p= 5.2 $x10^{-3}$, n= 4).
F. Plot of basal arteriole diameter after vehicle injection (x-axis) versus CNO injection (y-axis). CNO did not cause a significant change in vessel diameters (+5.8±6.6 %, LME p=0.66 Bonferroni corrected, n=6 mice, 32 vessels).
G. Population locomotion-triggered averages after vehicle (black) and CNO (red) injections (n=6 mice, 18 arterioles in FL/HL representation). For both cases, the diameters were normalized by the average basal diameter of the vessel after vehicle injection.

We then tested whether the effects of nNOS-expressing neuron activity on arteriole diameter was mediated by NO, as these neurons also release vasoactive peptides (Cauli *et al.*, 2004). Previous studies with NOS inhibitors have shown conflicting effects (Lindauer *et al.*, 1999; Stefanovic *et al.*, 2007). Discrepancy in the literature likely results from differences in experimental methodology: topical application does not reach lower cortical layers (Ferezou, Bolea and Petersen, 2006) where most of the nNOS expressing neurons reside, and systemic administration impacts the cardiovascular system. To avoid these experimental confounds, we infused the water-soluble NO synthase inhibitor, Nω-nitro-L-arginine methyl ester (L-NAME). Note that previous work has shown that cortical neurons express eNOS (Yousef *et al.*, 2004; Lein *et al.*, 2007; Tasic *et al.*, 2016), endothelial cells on cerebral arterioles express nNOS (Vanlandewijck *et al.*, 2018), and that there are no truly specific pharmacological inhibitors of nNOS (Bland-Ward and Moore, 1995; Reiner and Zagvazdin, 1998; Engelhardt *et al.*, 2006; Pigott, Bartus and Garthwaite, 2013). Locomotion-evoked dilations are unlikely to be mediated by eNOS expressed in endothelial cells because shear-mediated increases in eNOS activity in response to flow-evoked changes in diameter evolve over minutes, not seconds (K. J. Kim *et al.*, 2016), too slow to account for the locomotion-evoked dilations. Blocking the production of NO caused no significant change in the basal gamma-band power

(+8.24±2.8%, paired t-test p=0.39, Figure 3.10A), but a strong decrease in the basal vessel diameter and locomotion-evoked dilation (-10.6±4.6%, LME $p=7.6x10^{-6}$, Figure 3.10B and -9.6±1.9%, paired t-test $p=5.2x10^{-4}$, Figure 3.10C). Comparisons of the average constriction induced by L-NAME to the constriction induced by hM4D-G(i) DREADDs in nNOS-expressing neurons showed no significant difference (Figure 3.10D, t-test p=0.57), indicating that the NO regulating basal vessel diameter is primarily produced by nNOS in neurons, not eNOS from endothelial cells.

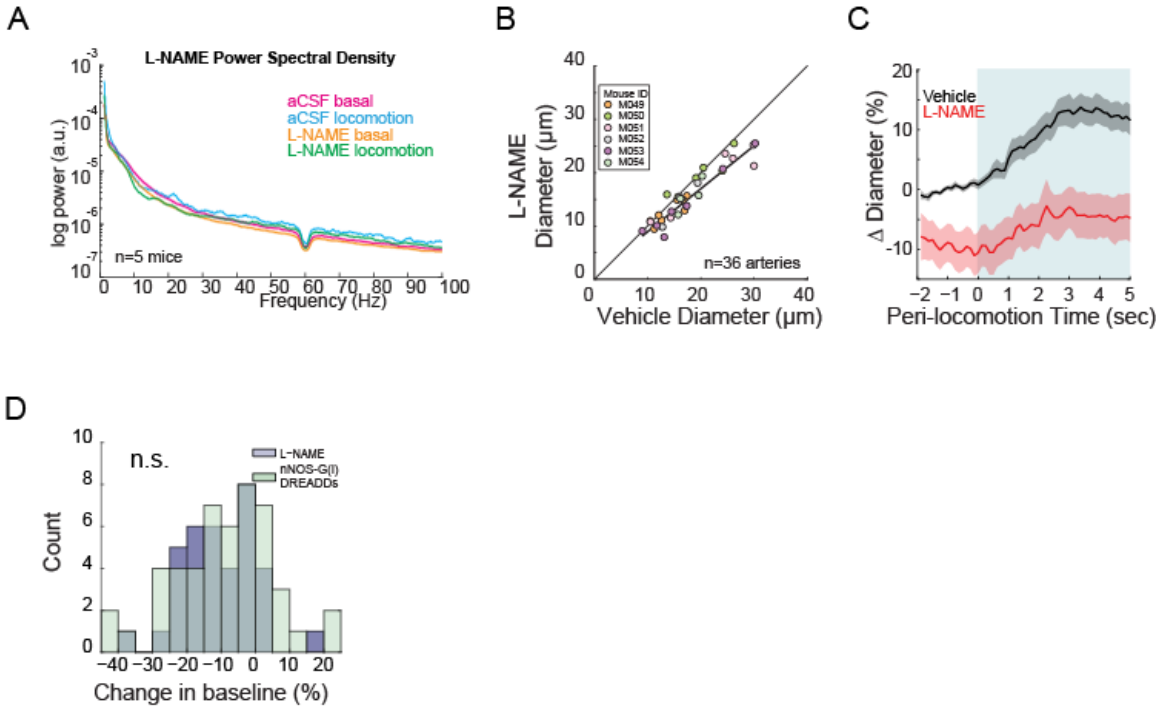

Figure 3.10 **NO released by nNOS expressing neurons controls arteriole diameter.**
Data in **A-C** are from mice after L-NAME infusions, data in **D-F** is from mice L-arginine infusions.
A. LFP power spectra during stationary (basal) and locomotion periods after L-NAME infusion, normalized to vehicle infusion in the same mouse. L-NAME has a small, non-significant change neural activity in the gamma band (basal, 8.24±2.8%, paired t-test p=0.39; locomotion, -4.3±10.7%, paired t-test p=0.67, n=5).
B. Plot of basal arteriole diameter after vehicle (x-axis) versus L-NAME infusion (y-axis). L-NAME caused a significant decrease in arterial diameter (-10.6±4.6, LME $p=7.6x10^{-6}$ Bonferroni corrected, n=6 mice, 36 vessels). **C.** Population locomotion-triggered average after vehicle (black) and L-NAME (red) infusions (n=6 mice, 26 arterioles in FL/HL representation). For both cases, the diameters are normalized by the average basal diameter of the vessel after vehicle infusion.
D. Comparison of the percent change in basal arteriole diameter after treatment with L-NAME (n=6 mice, 36 vessels) and nNOS-G(i) DREADDs (n=9, 49 vessels) relative to vehicle controls (aCSF infusions and DMSO injection, respectively). The percent changes to the basal vessel diameter are not

significantly different (LME p=0.57), showing the NO regulation of basal vessel diameter is primarily produced by nNOS in neurons, not eNOS from endothelial cells.

There are two varieties of nNOS–expressing neurons in the cortex, Type 1 and Type 2 (Perrenoud *et al.*, 2012). Type 2 nNOS neurons are a heterogeneous group of interneurons that are more numerous and located throughout the cortex. In contrast, Type 1 nNOS neurons are sparse, are located in deeper layers (similar to our viral expression, Figure 3.11A), and express nNOS at higher levels. While Type 1 nNOS neurons receive many different neuromodulatory inputs (Williams, Black, *et al.*, 2018; Williams, Vazquez-derose, *et al.*, 2018), nearly all of them express the Substance P (SP) receptor (NK1R), and they are the only cells in the cortex that do so (Vruwink *et al.*, 2001; Dittrich *et al.*, 2012; Endo, Yanagawa and Komatsu, 2016b). Type 1 nNOS neurons also have extensive, long-range projecting axonal arbors that well-position them to influence the vasculature. Substance P causes prolonged depolarization and spiking in Type 1 nNOS neurons (Dittrich *et al.*, 2012). As there are no NK1 receptors in vascular cells (Vanlandewijck *et al.*, 2018), we can pharmacologically manipulate the activity of Type 1 nNOS neurons independently of other neurons by infusing SP, or an antagonist for the SP receptor, CP-99994. Infusions of CP-99994 caused non-significant decreases in gamma-band power (-5.28±5.11%, paired t-test p=0.5 Figure 3.11A) and a non-significant decrease in basal arteriole diameter (-8.0±7.2%, LME p=1 Figure 3.11B). Infusions of SP caused non-significant decreases in gamma-band power (-24.42±3.8%, paired t-test p=0.19 Figure 3.11D), but a substantial increase in basal diameter (+13.4±4.4 %, LME $p=4.2x10^{-3}$ Figure 3.11E). Co-infusion of SP with muscimol produced no dilation (Figure 3.11G and H), consistent with the action of SP being mediated through local

neural excitation. These results show that NO released from a small subset of neurons, whose activity is not reported in measures of population activity, controls both the basal diameter of arterioles, and mediates a substantial portion of the hyperemic response.

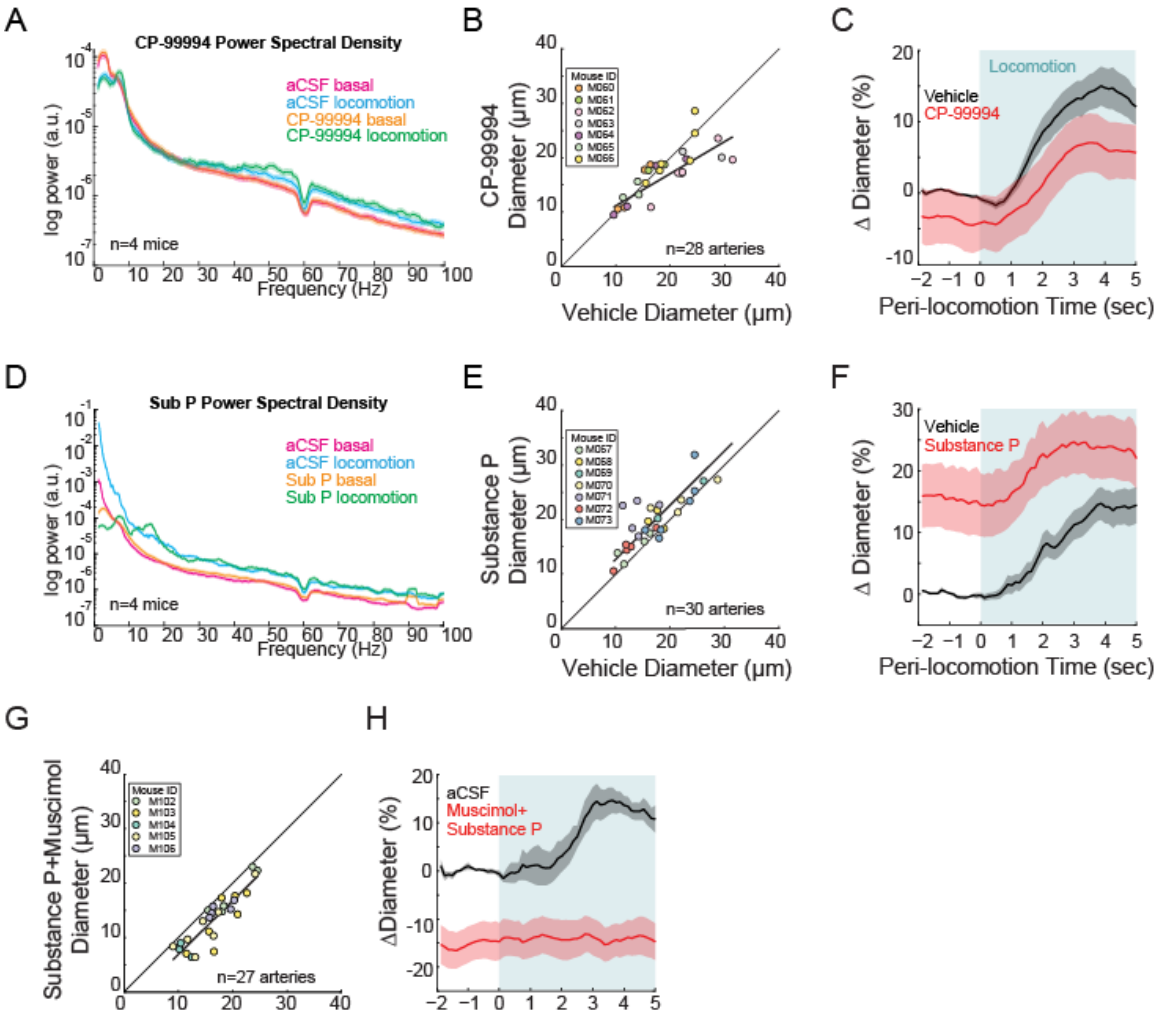

Figure 3.11 **Type I nNOS expressing neurons control basal arteriole diameter.**
Data in **A-C** are from mice after CP-99994 infusions, which will bock the excitatory Substance P input onto Type1 nNOS neurons, data in **D-E** is from mice after Substance P infusions, which will excite Type1 nNOS neurons.
A. LFP power spectra during stationary (basal) and locomotion periods after CP-99994 infusion, normalized to vehicle infusion in the same mouse. CP-99994 non-significantly reduced neural activity in the gamma band (basal, -5.28±5.11%, paired t-test p=0.5; locomotion, -6.8±52.3%, paired t-test p=0.69, n=4). Shading denotes mean ± standard deviation.
B. Plot of basal arteriole diameter after vehicle (x-axis) versus CP-99994 infusion (y-axis). CP-99994 caused a non-significant decrease in the basal arterial diameter (-8.0±7.2%, LME p=1, n=7 mice, 28 vessels).

C. Population locomotion-triggered averages after vehicle (black) and CP-99994 (red) infusions (n=7 mice, 14 arterioles in FL/HL representation). For both cases, the diameters were normalized by the average basal diameter of the vessel after vehicle infusion.
D. LFP power spectra during stationary (basal) and locomotion periods after Substance P infusion, normalized to vehicle infusion in the same mouse. Substance P causes a non-significant reduction of neural activity in the gamma band (basal, -24.42±3.8 %, paired t-test p=0.19; locomotion, -12.7±4.2 %, paired t-test p=0.67, n=4).
E. Plot of basal arteriole diameter after vehicle infusion (x-axis) versus Substance P infusion (y-axis). Substance P caused a significant increase in the basal arterial diameter (+13.4±4.4 %, LME $p=4.2x10^{-3}$ Bonferroni corrected, n=7 mice, 30 vessels).
F. Population locomotion-triggered averages after vehicle (black) and Substance P (red) infusions (n=7 mice, 16 arterioles in FL/HL representation). For both cases, the diameters were normalized by the average basal diameter of the vessel after vehicle infusion.
G. Plot of basal arteriole diameter after vehicle infusion (x-axis) versus muscimol and substance P infusion (y-axis). The co-infusion of muscimol and Substance P resulted in a significant decrease in basal arterial diameter (-20.0±14.9%, LME $p=4.0x10^{-7}$ Bonferroni corrected, n= 5 mice, 27 vessels).
H. Locomotion-triggered averages after vehicle (black) and muscimol and substance P (red) infusions (n=5 mice, 16 arterioles in FL/HL representation). For both cases, the diameters were normalized by the average basal diameter of the vessel after vehicle injection. Shading denotes mean ± standard deviation.

3.3.5 Relationship between neural activity and arterial diameter changes in the basal and evoked conditions

To better reveal the overall relationship between neural activity and arterial diameter, we plotted all the impacts of all of our perturbations (Figure 3.12A). If arterial diameter tracks neural activity, then we would expect all the points to lie in a straight line or along a curve. However, we see no one-to-one relationship between basal neural activity and basal arterial diameter. A similar lack of one-to-one relationship between neural activity and dilation is also seen during locomotion (Figure 3.12B). Perturbations of neural activity or NO production can drive large changes in arterial diameter that are incommensurate, or even opposing what one would expect from the neural activity. With the exception of muscimol, locomotion drives a similar increase in neural activity across all perturbations, though the amount of vasodilation is cut in half when the production of NO is blocked at the cellular (G(i) DREADDs, CP99994) or biochemical (L-NAME) level, an indication that

NO signaling from neurons drives approximately half of the functional hyperemic response (Lindauer *et al.*, 1999)l. Importantly, the manipulations of NO that lead to vessel dilation (G(q) DREADDs, L-arginine and Substance P) or down (G(i) DREADDs, L-NAME, CP-99994) using multiple orthogonal approaches results in very similar changes in neural activity and arterial diameter, suggesting that a small nexus (an 'oligarchy') of NO-producing Substance P-responsive neurons are the primary controllers of the cerebral vasculature, not the average activity of all neurons.

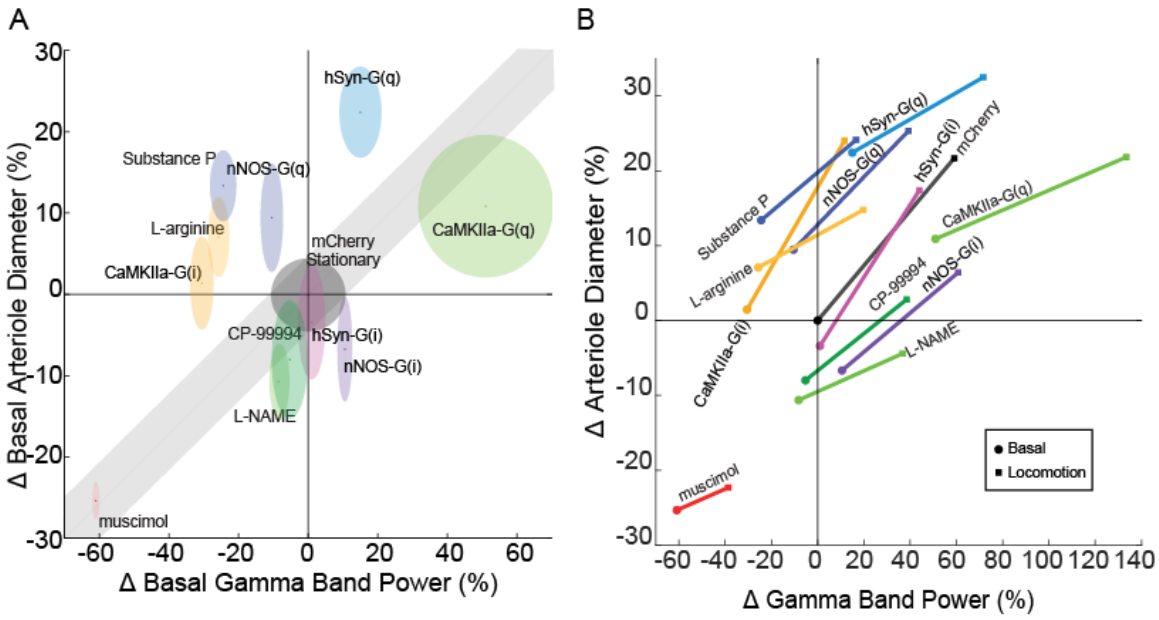

Figure 3.12 **Lack of one-to-one relationship between neural activity and arterial dilation.**
A. Summary figure outlining the change in basal gamma band power vs change in basal arteriole diameter under each condition outlined in this paper. Shading surrounding each point shows standard deviation from mean. The unity line represents where the points would lie if there was a linear relationship between neural activity and vasculature. For chemogenetic manipulations, neural activity and basal arterial dilation have been shifted so that the reporter virus expressing animals (mCherry) are centered at the origin.
B. Summary figure plotting the change in gamma band power vs in arteriole diameter during locomotion for the various manipulations performed. Note the lack of a one-to-one relationship between neural activity change and arterial dilation.

3.4 **Discussion**

Our results show that both basal and sensory-evoked changes in arterial diameter are controlled by local neural activity. Surprisingly, large alterations of the

activity of pyramidal neurons had little effect on either basal or evoked arterial diameter, even though the activity of these neurons dominates extracellular recordings of electrical signals and are the major energy consumers in cortex (Vazquez, Fukuda and Kim, 2018). Rather, cortical hemodynamic signals are controlled primarily by NO produced by the activity of nNOS-positive neurons. Our experiments with NOS-inhibitor infusion and suppression of nNOS-expressing neural activity with DREADDs showed that approximately half of the evoked arterial dilatory response, and half of the baseline artery diameter change seen with muscimol infusion, were caused by neuron-generated NO. Other neurovascular coupling mechanisms such as voltage-gated potassium channels of astrocytes (Longden *et al.*, 2017) and signaling from astrocytes (Rosenegger, Tran, *et al.*, 2015) likely underlie the remaining basal and evoked diameter changes (*see Chapter 4 Role of astrocytes and potassium signaling in neurovascular coupling*).

Hemodynamic signals have generally been interpreted as reporters of bulk neural activity (but see (Logothetis, 2008)), with increases in neural activity thought to be directly correlated with increases in vessel dilation and blood flow. Our results support an alternative model, where basal and evoked blood flow is controlled by a selected group of neurons independent of the bulk population activity. Rather than being a 'democracy', where the activity of all neurons contributes to increases in blood flow, vascular control in the cortex is an 'oligarchy', where a small group of neurons controls the flow nearly independent of the activity of their neighbors. This is apparent when we look at the relationship between gamma-band power and basal (Figure 3.12A) or evoked arteriole diameter (Figure 3.12B). We see no one-to-one

relationship between neural activity and the hemodynamic response, meaning neural activity cannot always be decoded from hemodynamic signals. We note that this problem is exacerbated when using BOLD imaging, as changes in baseline blood flow can change the magnitude or even the sign of the BOLD response without changes in the underlying neural activity (Cohen, Ugurbil and Kim, 2002; Kim and Ogawa, 2012).

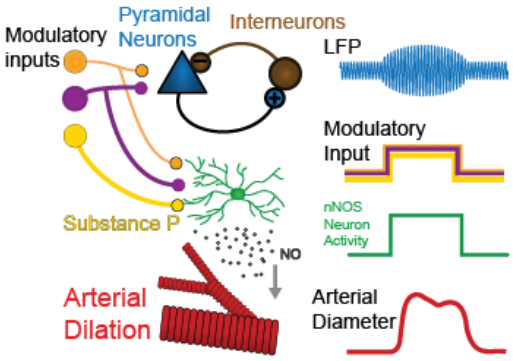

Figure 3.13 **Schematic showing neural circuit.**
Pyramidal and nNOS type 1 neurons are both driven by common modulatory drive, resulting in a correlation between gamma-band power increases and vasodilation during normal behavior.

Our data point to a way of resolving several troubling issues in the field of neurovascular coupling. This mismatch between neural activity and hemodynamic signals, seen in many studies (Sirotin and Das, 2009; Cardoso *et al.*, 2012), can be resolved if the hemodynamic signals are not controlled by the overall local neural activity, but by a small group of neurons primarily driven by modulatory signals that are engaged when a sensory stimulus is presented or by attention modulation of neural activity (Boynton, 2011) (Figure 3.13C). The lack of effect of changes in pyramidal neuron activity on arterial diameters suggests that these type 1 nNOS neurons receive minimal local recurrent excitatory input. At least in the primary sensory cortex, during natural behaviors and passive sensory stimulation, the activity of the nNOS-positive neurons and pyramidal neurons are correlated, generating the widely observed linkage between vasodilation and gamma band power (Goense and Nikos K Logothetis, 2008; Scholvinck *et al.*, 2010; Winder *et al.*, 2017), though because of the small size and number of Type 1 nNOS neurons (<1%

of all neurons) and their closed electrical fields, their activity will not be detectable in the local field potential (Buzsáki, Anastassiou and Koch, 2012) or in single unit recordings. Stimuli or modulatory conditions that cause the activity of nNOS-positive neurons to become uncorrelated from the activity pyramidal neurons will drive neurovascular decoupling, as has been observed in many studies (Shih *et al.*, 2009; Sirotin and Das, 2009; Huo, Smith and Drew, 2014). Type 1 nNOS neurons are hubs for modulation, as they receive orexinergic and substance P input, as well as cholinergic input from the basal forebrain (Bacci, Huguenard and Prince, 2005; Lee *et al.*, 2010; Owen *et al.*, 2013; Williams, Black, *et al.*, 2018). Stimulation of the basal forebrain is known to greatly increase basal cortical blood flow independent of metabolic changes (Sato, Sato and Uchida, 2001; Hamel, 2004), and the projections of basal forebrain neurons are topographically mapped (Saper, 1984; J.-H. Kim *et al.*, 2016), consistent with the spatially localized hemodynamic responses. Increases in the activity of cholinergic neurons in the basal forebrain and other modulatory regions occur during sensory stimulation (Eggermann *et al.*, 2014) and voluntary movement (Harrison *et al.*, 2016), consistent with the vasodilation accompanying these behaviors (Huo, Smith and Drew, 2014; Winder *et al.*, 2017). These neurons may also play a role in the large increases in cerebral blood flow seen during REM sleep (Gerashchenko *et al.*, 2008; Bergel *et al.*, 2018).

Chapter 4 | Basal perfusion and ratiometric imaging

4 Basal perfusion and ratiometric imaging

4.1 Introduction

In the brain, there is constant ongoing background neural activity, even when there is no overt stimulus (Raichle and Mintun, 2006; Scholvinck *et al.*, 2010). This spontaneous neural activity consumes a large amount of the brain's energy, yet it is unknown if the neural activity has a role in setting resting arteriole diameter and blood flow

The resting state blood flow has functional significance, as there must be a constant signal to the vasculature to ensure healthy cerebral perfusion and because basal blood flow impacts ratiometric signals.

Ongoing spontaneous cortical activity and brain state are known to impact sensory processing and alertness (Crochet and Petersen, 2009), both of which dictate the signals that are obtained during resting state fMRI imaging (Logothetis, 2008; Chang *et al.*, 2016). State dependent variations in basal blood flow can profoundly influence the sign and extent of the stimulus BOLD fMRI signals (Cohen, Ugurbil and Kim, 2002), because responses to stimuli are usually expressed as relative changes from baseline blood flow (Hoge *et al.*, 1999; Kastrup *et al.*, 1999; Li, Moseley and Glover, 1999; Corfield *et al.*, 2001; Zaldivar *et al.*, 2018). For example, if baseline cerebral blood flow is increased, the BOLD response to the same stimulus is lessened considerably. This sensitivity of the BOLD signal to basal state is relevant because with neuroimaging modalities, subjects may come in with altered baseline basal flows

that could make the BOLD responses different, even if the underlying neural response is similar.

Furthermore, decreases in basal cerebral blood flow occur with aging and correlate with the onset of neurodegeneration (F. Wolters *et al.*, 2017). This suggests that sufficient basal blood flow is essential for a healthy brain. Researchers have demonstrated that early metabolic changes in Alzheimer's disease coincide with resting state decreases in functional imaging studies (Reiman *et al.*, 1996). As a result, identifying the role of neurons in the control of basal arterial diameter is crucial for translating neuroimaging and interpreting the pathophysiology of disease.

In this chapter, we looked at the impact of manipulating the activity of defined neural populations on basal perfusion and ratiometric imaging. Here, we show that understanding the neural control of basal blood flow is essential for interpreting the pathophysiology of diseases where there is decreased basal perfusion, especially for neuroimaging experiments using ratiometric signals.

4.2 **Materials and Methods**

4.2.1 **Surgery**

4.2.1.1 Window implantation procedure for Intrinsic Optical Imaging (IOS) experiments

Mice were anesthetized with 2% isoflurane (in oxygen). Head bars were attached, then windows were implanted as described in Chapter 2.

The animals were allowed to recover for 2-3 days before habituation.

4.2.2 **Physiological Measurements**

All habituation to the apparatus and data acquisition for the experiments in this chapter were described in detail in Chapter 2. Briefly, cerebral blood volume was recorded from mice using the intrinsic optical imaging apparatus (see 2.3.6 Intrinsic Optical Imaging (IOS)). The physiological measurements were taken simultaneously as behavior measurements to ensure mice were alert. Cerebral blood volume measurements were acquired by measuring the optical reflectance from the cortical surface. Decreases in the measured reflectance from the thinned-skull window indicates increased Cerebral blood volume.

4.2.2.1 **Habituation, Imaging, Chemogenetics, and Infusions**

Habituation for experiments was carried out as described in Chapter 2.

For this chapter, we used both G(q) and G(i) DREADDs virus with each of the following promoters/mice: reporter virus/C57, hSyn/C57 and hSyn-DIO/nNOS-cre. The same experiments were performed using a reporter virus to account for any effects the virus injection or CNO injections might have (Figure 4.1).

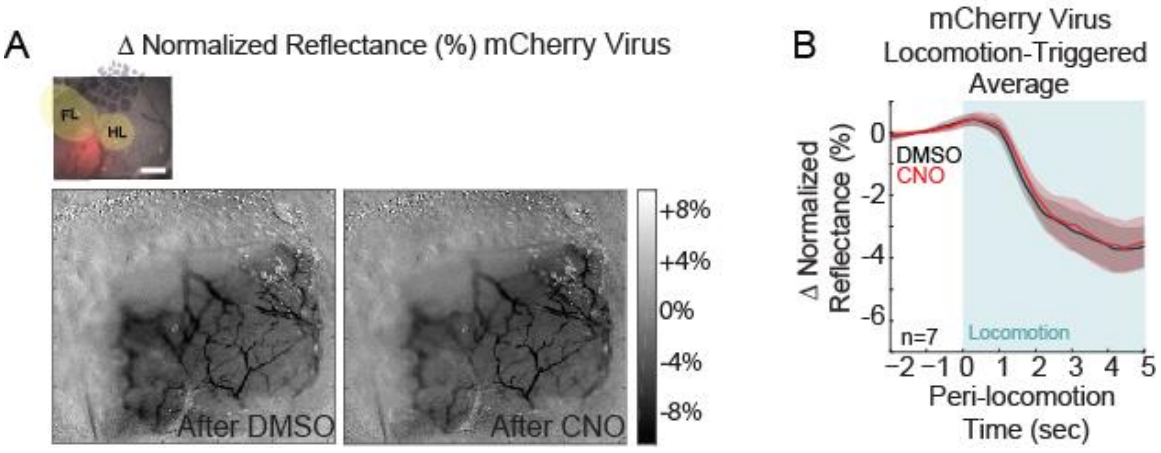

Figure 4.1 **No significant effect of CNO on intrinsic optical signal (IOS) measurements.**
CBV and locomotion behavior were measured in awake, head-fixed mice. 530nm LEDs illuminate the thinned skull window and the CBV was measured optically using the light absorbance of hemoglobin

at 530 nm. Decreases in the measured light intensity (ΔR/R) correspond to increases in CBV. The window was imaged with the Dalsa CCD camera positioned directly above the mouse.
A. Upper left inset, thinned skull window. Red fluorescent region shows the location of the control virus, AAV-CMV-TurboRFP-WPRE-rBG. (scale bar 1mm; shaded yellow FL is forelimb, HL is hindlimb, shaded black barrel cortex)
Images, For the control virus, the average pixel-wise CBV response to locomotion relative to the average pixel-wise CBV during no movement two seconds before the locomotion event. Left Image, after DMSO injection; Right Image, after CNO injection
B. The region of interest for these calculations are within the red fluorescent area seen in the PoRTs window of A. For the control virus, average ΔR/Ro in FL/HL area from -2 to 5 seconds of locomotion averaged over 7 mice. The locomotion triggered average is normalized to the time period 2 seconds before locomotion. The shaded area is the standard deviation from the mean across all animals.

4.2.3 **Data Analysis**

All analyses were conducted using custom-written code (see Chapter 2) in MATLAB.

4.3 **Outcomes**

4.3.1 **Baseline changes in arterial diameters confound ratiometric imaging**

In contrast to our quantitative, single-vessel measurements with 2PLSM, most hemodynamic imaging modalities use ratiometric signals (like BOLD fMRI(Cohen, Ugurbil and Kim, 2002)), looking at the percentage change in the signal from the baseline to infer neural activity changes. The hemodynamic signals are often measured ratiometrically, with the change in signal being normalized to a pre-stimulus baseline. These types of measurements would likely be affected by the sort of changes in basal arterial diameter presented in Chapter 3. It has been noted that

changes in baseline can confound ratiometric signals (Cohen, Ugurbil and Kim, 2002), so we performed intrinsic optical signal (IOS) imaging. Using IOS, increases in cerebral blood volume (vasodilation), causes decreases in reflected 530nm light (Drew, Shih and Kleinfeld, 2011; Huo, Gao and Drew, 2015). The measurements were from mice expressing either G(i) or G(q)-coupled DREADDs pan-neuronally.

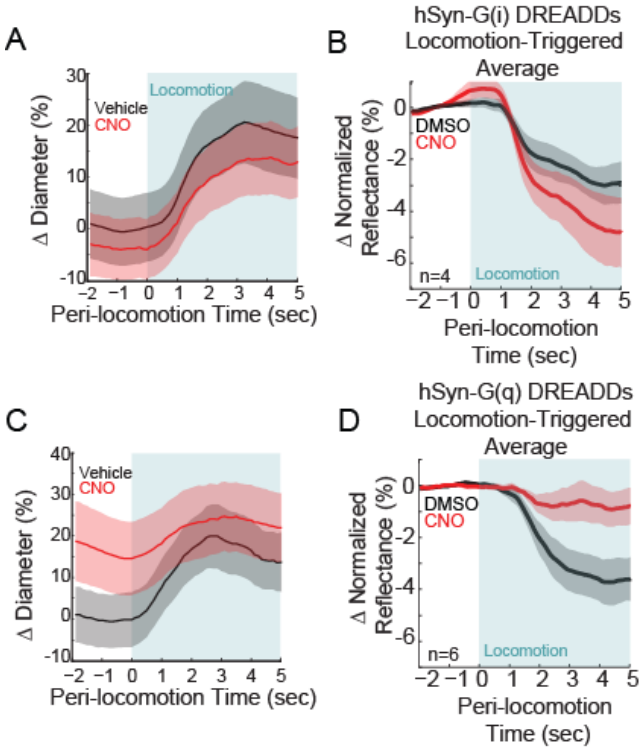

Figure 4.2 **Difficulty of ratiometric imaging**.
A. From Figure 3.6, population locomotion-triggered averages after vehicle (black) and CNO (red) injections for hSyn-G(i) DREADDs mice (n=7 mice, 33 arterioles in FL/HL representation).
B. For hSyn-G(i) DREADDs, average ΔR/Ro in FL/HL area from -2 to 5 seconds of locomotion. The locomotion triggered average is normalized to the time period 2 seconds before locomotion. The shaded area is the standard deviation from the mean across all animals. (n=4 mice)
C. From Figure 3.6, population locomotion-triggered averages in response to locomotion after vehicle (black) and CNO (red) injections for hSyn-G(q) DREADDs mice (n= 7 mice, 25 arterioles in FL/HL representation). Increasing neural activity caused a basal arterial dilation that nearly completely occluded the locomotion-triggered response.
D. For hSyn-G(q) DREADDs, average ΔR/Ro in FL/HL area (yellow from B inset) from -2 to 5 seconds of locomotion. The locomotion triggered average is normalized to the time period 2 seconds before locomotion. The shaded area is the standard deviation from the mean across all animals. (n=6 mice)

While CNO did not change the hemodynamic responses in reporter virus-injected mice (Figure 4.1), we found that basal constriction, after suppressing the neural activity pan-neuronally, potentiated the ratiometrically-measured locomotion-induced CBV increase (Figure 4.2B). A dilated baseline state in the arterioles, caused by increasing the local neural activity, greatly reduced the amplitude of the evoked response (Figure 4.2D). In ratiometric imaging, a decreased baseline diameter (shown from

time -2 to 0 sec in Figure 4.2A, *red line*), causes an increase in the normalized sensory-evoked response (Figure 4.1B, *red line*). This would lead to the erroneous interpretation that decreasing neural activity increases the sensory evoked response. The increased baseline diameter that is shown from time -2 to 0 sec (Figure 4.2C, *red line*) occludes any sensory response. If the effects of increasing neural activity were measured using IOS measurements alone, the sensory evoked response is interpreted as going away (Figure 4.2D, *red line)*.

Not accounting for changes in resting arterial diameter caused by differences in neural activity between a wild-type and knockout mouse, or between young and aged subjects, will lead to wrong inferences about underlying neural activity. Such differences could easily arise from changes in baseline neural activity.

4.3.2 The effects of chemogenetic and pharmacological infusions on normalized evoked arterial diameter changes

As baseline conditions can confound ratiometric signals, we also examined the effect of normalizing to the pre-stimulus baseline on our data (Figure 4.3). We found that manipulations that caused increases in baseline (such as pan-neuronal excitation) without changing the absolute locomotion-induced dilation appeared to block the evoked dilations. These results show that it is critical to perform quantitative, within vessel measurements when testing the role of specific signaling pathways.

The activity of different groups of neurons have the potential to contribute differentially to the basal and evoked arterial diameter. We calculated individual normalized locomotion evoked diameter responses to separate the contributions of

the different neural manipulations on the sensory evoked response. The locomotion evoked response is calculated by normalizing each locomotion-triggered average by the diameter of the vessel in each condition at rest (no locomotion). For example, the decreases in evoked dilation when the activity of nNOS neurons were suppressed or the NOS enzyme was inhibited with LNAME were not just due to a shift in the baseline (Figure 4.3F and H), showing that nNOS neurons through NO signaling play a role in evoked dilations in addition to basal diameter.

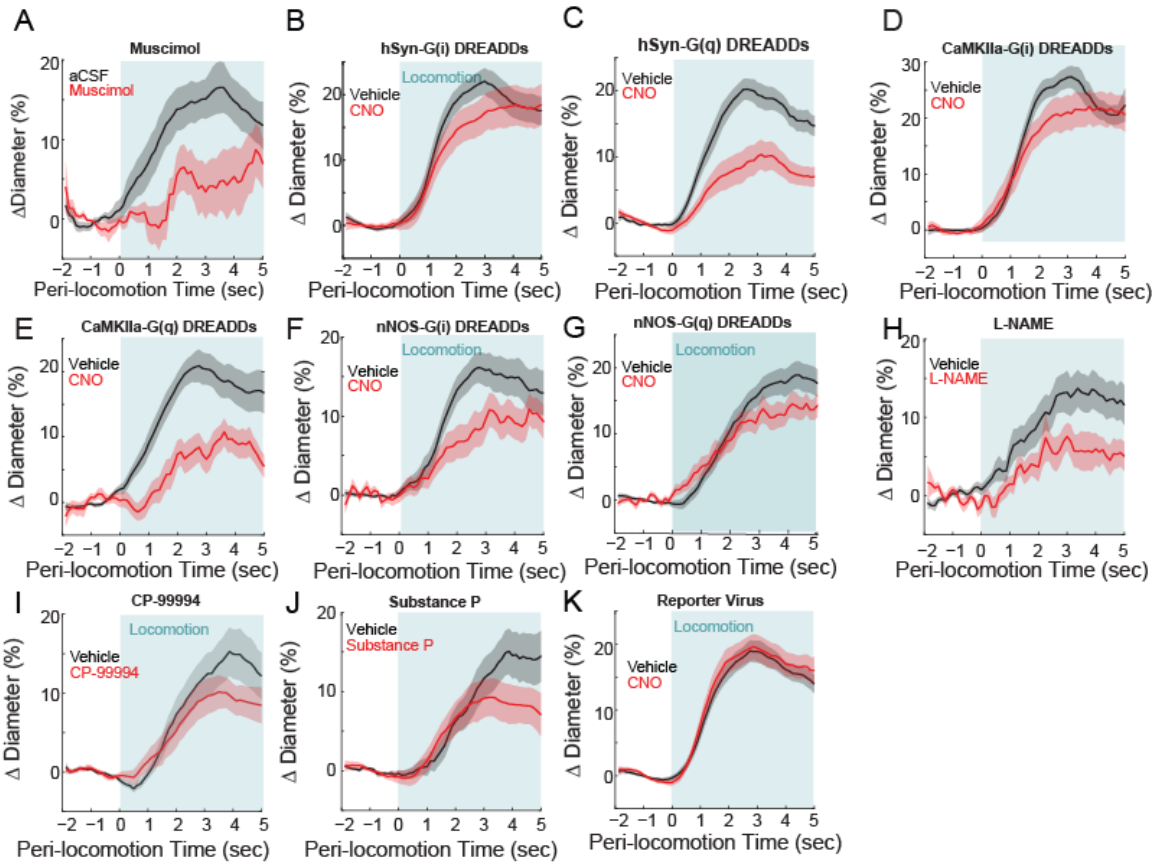

Figure 4.3 **The effects of chemogenetic and pharmacological infusions on normalized evoked arterial diameter changes.**
A. Population locomotion-triggered averages in response to locomotion after aCSF (black, 15.8±2.7%) and muscimol (red, 4.4±0.3%) infusions, LME p=0.04, n=6 mice
B. In hSyn-G(i) DREADDs mice population locomotion-triggered averages in response to locomotion after vehicle (black, 20.5±2.0%) and CNO (red, 17.8±2.8%) injections, LME p=1, n=7 mice
C. In hSyn-G(q) DREADDs mice population locomotion-triggered averages in response to locomotion after vehicle (black, 18.6±1.7%) and CNO (red, 9.7±2.1%) injections, LME $p=7.1x10^{-3}$, n=7 mice;
D. In CaMKIIa-G(i) DREADDs mice population locomotion-triggered averages in response to locomotion after vehicle (black, 25.3±1.9%) and CNO (red, 21.4±3.0%) injections, LME p=1, n=7 mice;
E. In CaMKIIa-G(q) DREADDs mice population locomotion-triggered averages in response to locomotion after vehicle (black, 19.1±2.3%) and CNO (red, 9.0±2.1%) injections, LME p=0.06, n=6 mice;
F. In nNOS-G(i) DREADDs mice population locomotion-triggered averages in response to locomotion after vehicle (black, 15.3±2.0%) and CNO (red, 9.8±2.1%) injections, LME p=0.26, n=9 mice;
G. In nNOS-G(q) DREADDs mice population locomotion-triggered averages in response to locomotion after vehicle (black, 17.4±1.8%) and CNO (red, 13.1±1.8%) injections, LME p=0.94, n=6 mice;
H. Population locomotion-triggered averages in response to locomotion after aCSF (black, 13.1±2.3%) and L-NAME (red, 6.1±2.2%) infusions, LME p=0.5, n=6 mice;
I. Population locomotion-triggered averages in response to locomotion after aCSF (black, 13.7±2.6%) and CP-99994 (red, 9.8±2.1%) infusions, LME p=1, n=7 mice;
J. Population locomotion-triggered averages in response to locomotion after aCSF (black, 13.0±2.2%) and Substance P (red, 8.7±2.3%) infusions, LME p=1, n=7 mice;
K. In reporter virus mice population locomotion-triggered averages in response to locomotion after vehicle (black, 17.7±1.5%) and CNO (red, 18.3±1.9%) injections, LME p=1, n=12 mice

4.4 **Discussion**

The activity of nNOS neurons can change basal arterial diameter independent of overall neural activity (see Chapter 3) so commonly used ratiometric imaging techniques of hemodynamic signals can give erroneous picture of neural activity and neurovascular coupling mechanisms. Importantly, changes in nNOS neuron activity can cause changes in basal diameter of arteries without changing population neural activity, which will greatly impact the magnitude ratiometric signals.

An important ramification for our work is that studies of blood flow in the brain should make quantitative measurements when comparing across populations

(e.g., transgenic versus wildtype mice, diseased versus control humans) as ratiometric changes will give misleading signals. There are many potential factors that could alter the baseline state of a patient during neuroimaging (anxiety, medications, sleepiness) and these could significantly alter both the resting state fMRI and the BOLD responses. Our results show that basal arterial diameter is controlled by local neural activity, and that this control has the potential to confound ratiometric imaging modalities.

Previous work where basal cerebral blood flow has been globally increased by hypercapnia, have shown that the stimulus-evoked response is additive. Most previous studies looking at the effect of varying baselines on the sensory-evoked response have changed basal vascular tone by inducing hypercapnia or hypocapnia (Hoge *et al.*, 1999; Li, Moseley and Glover, 1999; Corfield *et al.*, 2001). The advantage of our experimental paradigm is that we can modulate local neural activity using DREADDs to get at local influences on the basal arterial diameter. Cortical hemodynamic signals are regulated by NO released during the course of activity in nNOS-positive neurons, but if there is a raised baseline, the sensory evoked hemodynamic response is occluded. These results indicate that researchers using ratiometric imaging should account for changes in the resting state vasculature caused by changes in neural activity (*in vivo* this could be because of differences between a wild-type and knockout mouse, or between young and aged subjects).

Without accounting for baseline changes there will be inaccurate interpretation of the neural activity that lies beneath the hemodynamic signal. The effects of changing the baseline diameter (and thus flow) on responses using

metabolic hemodynamics signals, such as BOLD (Kim and Ogawa, 2012), will be even more severe than the cerebral blood volume-based measurement here (Buxton *et al.*, 2004). We have shown that changes in the basal cerebral blood flow can affect the BOLD response, but next we wanted to probe what mediates the basal state.

Chapter 5 | Role of astrocytes and potassium signaling in neurovascular coupling

5 Role of astrocytes and potassium signaling in neurovascular coupling

5.1 Introduction

As seen in Chapter 3, changes in neural activity are coupled to blood flow via neurovascular coupling, where neural activity drives the dilation of arterioles (Drew, Shih and Kleinfeld, 2011; Hill *et al.*, 2015; Mishra *et al.*, 2016; Rungta *et al.*, 2018). Additional neurovascular coupling mechanisms such as voltage-gated potassium channels (Longden *et al.*, 2017) and signaling from astrocytes (Rosenegger, Tran, *et al.*, 2015) potentially affect the basal and evoked diameter changes. Understanding the mechanisms by which neural activity regulates local blood flow includes distinguishing the role of astrocytes or other indirect signals.

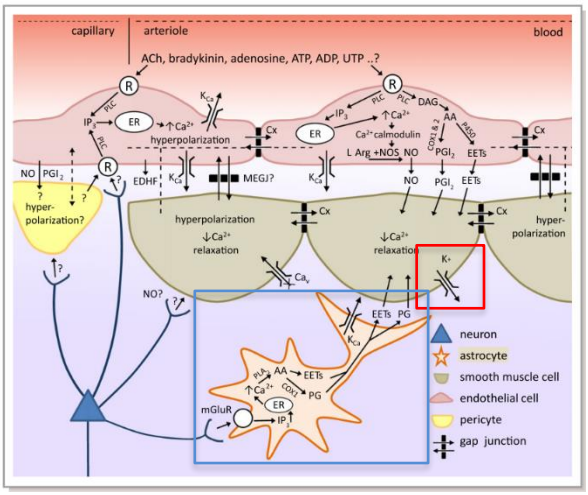

Figure 5.1 **Cartoon of proposed involvement of astrocytes in neurovascular coupling.** Incorporating the vascular endothelium into neurovascular coupling Astrocyte: hypothesized to sense glutamate through mGluR, increasing intracellular Ca^{2+} and generating AA which is converted by COX1 to prostaglandins and by P450 into EETs. Both PGs and EETs can relax smooth muscle cells. Endothelial cells can increase Ca^{2+} in response to receptor. Included in the cartoon is the possibility of signaling between astrocytes, pericytes and endothelial cells, or even direct neuronal signaling to the vascular endothelium at the capillary level.
Adapted from "A critical role for the vascular endothelium in functional neurovascular coupling in the brain" by Chen B., Journal of the American Heart Association, 2014.

Whether these dilations are mediated in part by increases in astrocytic Ca^{2+} causing the release of vasoactive components (Kacem *et al.*, 1998; Zonta *et al.*, 2002; Peng *et al.*, 2004; Stefanovic *et al.*, 2007; Nizar *et al.*, 2013; Rosenegger, Ha, *et al.*, 2015; Mishra *et al.*, 2016) or by local K^+ transients inducing smooth muscle relaxation (Harnett *et al.*, 2013; Sonkusare *et al.*, 2016; Longden *et al.*, 2017) remains unresolved.

Astrocytes are implicated as intermediates for vasoactive messengers (Zonta *et al.*, 2002; Peng *et al.*, 2004; Nizar *et al.*, 2013; Rosenegger, Ha, *et al.*, 2015) because astrocytes have endfoot processes enveloping blood vessels and surrounding neural synapses (Kacem *et al.*, 1998; Attwell *et al.*, 2010) and they are responsive to neural activity changes (Zonta *et al.*, 2002; K. J. Kim *et al.*, 2016).

In neurovascular coupling, it is hypothesized that astrocytes sense glutamate through metabotropic glutamate receptors (mGluR), which when activated increase intracellular Ca^{2+}. These Ca^{2+} transients lead to arachidonic acid (AA) conversion by COX1 to prostaglandins, and by P450 into EETs. Prostaglandins and EETs relax smooth muscle cells by increasing $[Ca^{2+}]$ in endothelial cells (blue box in Figure 5.1).

When active, astrocytes and neurons increase extracellular K^+, which can cause smooth muscle cell hyperpolarization through endothelial cell Kir channels (Attwell *et al.*, 2010). The increased K^+ conductance causes outward current flow. This leads to hyperpolarization and decreased smooth muscle cell Ca^{2+} influx. This smooth muscle cell relaxation through K^+ transients could contribute to a portion of the hemodynamic signals (Sonkusare *et al.*, 2016) (red box in Figure 5.1).

Here, we show that the activity of astrocytes, at least using DREADDs manipulations, is not necessary for the regulation of cortical hemodynamic signals. We also find that pharmacological blockers of voltage gated potassium channels also increase neural activity, which make it hard to resolve the role of K^+ sensing on the endothelial cells from effects caused by increased neural activity.

5.2 Materials and Methods

5.2.1 Surgery

5.2.1.1 Electrode, cannula, and window implantation procedure for two-photon microscopy imaging experiments

Mice were anesthetized with 2% isoflurane (in oxygen). Head bars were attached, then windows, cannula, and electrodes were implanted as described in Chapter 2. The animals were allowed to recover for 2-3 days before beginning habituation.

5.2.2 Physiological Measurements

All habituation to the apparatus and data acquisition for the experiments in this chapter were described in detail in Chapter 2. Briefly, vessel diameter measurements were recorded from mice using the two-photon microscope (2.3.4 Two-photon Laser Scanning Microscopy (2PLSM)) and neural recordings were taken using stereotrodes. Electrophysiology was measured as the differential potential between the leads of a stereotrode implanted in the imaged region of the window.

The physiological measurements were taken simultaneously as behavior measurements to ensure mice were alert.

5.2.2.1 Habituation, Imaging, Chemogenetics and Infusions

Habituation for experiments was carried out as described in Chapter 2.

For this chapter, we used both G(q) and G(i) DREADDs virus with hSyn-DIO/Aldh-1l1-cre. The Aldh1l1-cre/ERT2 mice had tamoxifen doses of 75mg/kg i.p. as described in Chapter 2. This allows for the control of gene expression over time and over space when coupled with viral infection.

For this chapter, we also used two pharmacological intracortical infusions through a cannula. We used ML-133 (Selective blocker of Kir2 potassium channels, 10μM) and $BaCl_2$ (Selective blocker of Kir potassium channels, 100μM). We infused each of these at a rate of 25 nL/minute for a total volume of 500 nL. Pharmacological treatments and aCSF were each infused in a counter-balanced order. All mice received both infusions of drugs and an aCSF control, so no randomization was needed.

5.2.3 Data Analysis

All analyses were conducted using custom-written code (see Chapter 2) in MATLAB.

5.3 Outcomes

5.3.1 Activation of inwardly-rectifying potassium channels drives large changes in population neural activity and arterial diameter

Previous reports have suggested that increases in extracellular K^+ arising from neural or astrocyte activity leads to the activation of inwardly-rectifying potassium channels that could mediate vasodilation (Longden *et al.*, 2017). To test the role of Kir2.1 channels, we performed experiments where we infused either $BaCl_2$ or ML-133, both blockers of Kir2.1 channels. Blocking Kir2 channels with $BaCl_2$ increased

basal arterial diameter (+12.49.1±17.2% LME $p=6.9x10^{-3}$, Figure 5.2C), but also increased neural activity and induced epileptic-like activity (Figure 5.2A), consistent with previous reports of $BaCl_2$ increasing neural excitability associated with the blockade of neural K^+ channels (Harnett *et al.*, 2013) .

We obtained similar results with the Kir blocker ML-133 (Sonkusare *et al.*, 2016), which drove elevations of basal neural activity and basal arterial diameter (+23.8±3.3%, paired t-test p=0.16 Figure 5.2E and +11.8±17.0% LME $p=1.3x10^{-3}$ Figure 5.2F, respectively) which occluded the sensory-evoked response (Figure 5.2G). Given the large effects of Kir-channel blockers on neural activity (see also (Harnett *et al.*, 2013)), it is hard to untangle the role of K^+ sensing on the endothelial or smooth muscle cells directly from any effects caused by increases in neural activity.

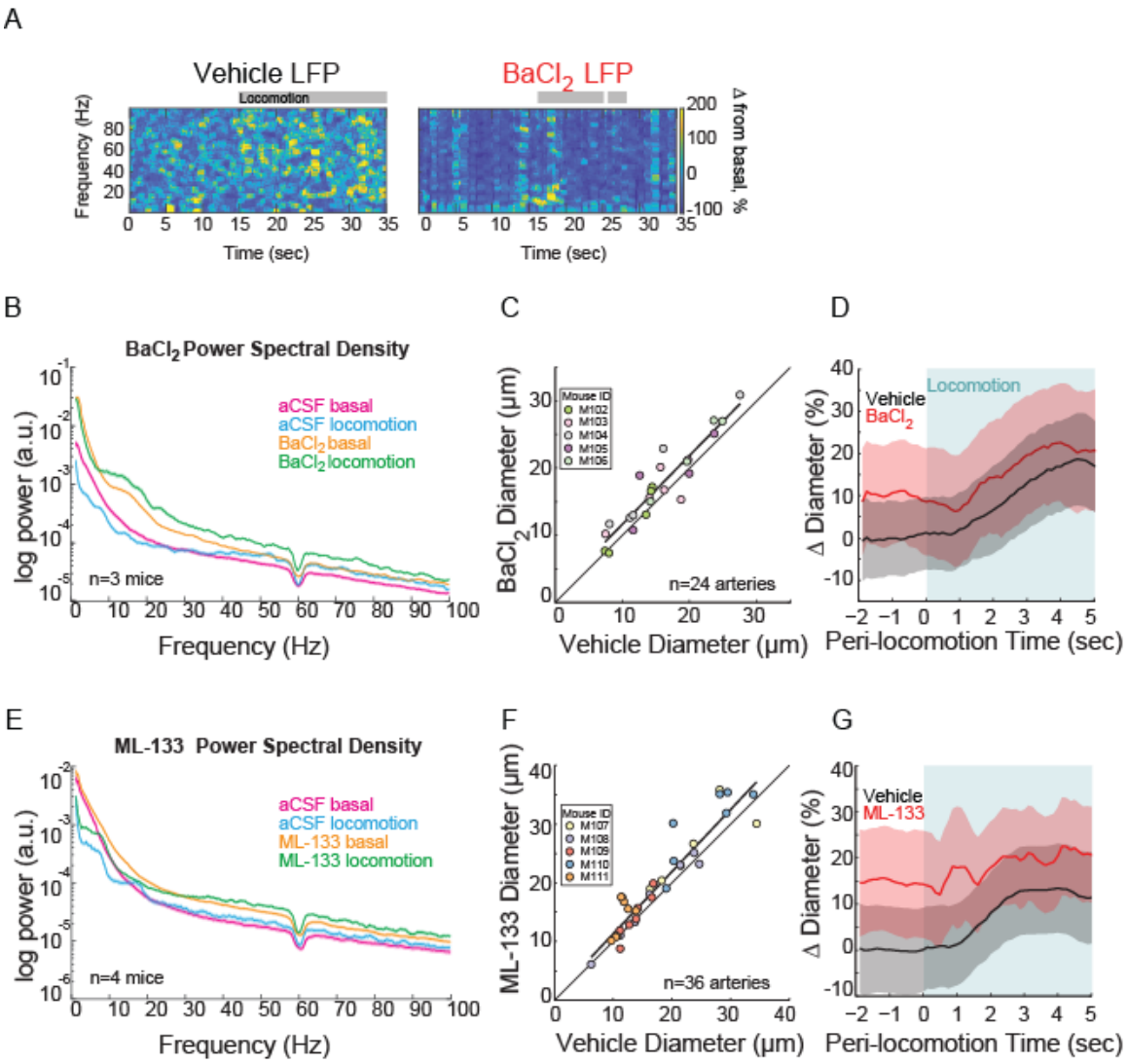

Figure 5.2 **Kir-channel blockers cause large increases in neural activity and basal arterial diameter.**

A. Spectrogram of the LFP in a mouse after infusion with vehicle (left) or $BaCl_2$ (right). The bursts across all frequency bands of the LFP indicate that the $BaCl_2$ infusion induced epileptic-like activity. Locomotion events are denoted with shading.

B. LFP power spectra during stationary periods (basal) and locomotion after $BaCl_2$ infusion, normalized to vehicle infusion in the same mouse. $BaCl_2$ infusion greatly increases neural activity in the gamma band (basal, +226±188%, paired t-test $p=1.1x10^{-2}$; locomotion, +290±180.1 %, paired t-test $p=4.6x10^{-2}$, n=3). Shading denotes mean ± standard deviation.

C. Plot of basal arteriole diameter after vehicle infusion (x-axis) versus $BaCl_2$ infusion (y-axis). $BaCl_2$ significantly increased arterial diameter (+12.4±17.2%, LME $p=6.9x10^{-3}$ Bonferroni corrected, n= 5 mice, 24 vessels)

D. Population locomotion-triggered average after vehicle (black) and $BaCl_2$ (red) infusions (n=5 mice, 16 arterioles in FL/HL representation). For both cases, the diameters were normalized by the average basal diameter of the vessel after vehicle infusion

E. LFP power spectra during stationary periods (basal) and locomotion after ML-133 infusion, normalized to vehicle infusion in the same mouse (basal, +23.8±3.3%, paired t-test p=0.16; locomotion, +8.7±11.3 %, paired t-test p=0.16, n=4).

F. Plot of basal arteriole diameter after vehicle infusion (x-axis) versus ML-133 infusion (y-axis). ML-133 significantly increased the basal arterial diameter (+11.8±17.0% LME $p=1.3x10^{-3}$ Bonferroni corrected, n= 5 mice, 36 vessels)
G. Locomotion-triggered averages after vehicle (black) and ML-133 (red) infusions (n=5 mice, 26 arterioles in FL/HL representation). For both cases, the diameters were normalized by the average basal diameter of the vessel after vehicle infusion

5.3.2 **Astrocyte activity drives no significant changes in arterial diameter**

The importance of Type 1 nNOS neurons and local neural activity on the regulation of the vasculature (see Chapter 3) raises the question of whether other cell types, such as astrocytes, are involved in any indirect signaling pathways. We sought to manipulate the activity of astrocytes by injecting AAVs encoding hM3D(q) and hM4D(i) DREADDs under a DiO promoter in Aldh1l1-cre mouse. These transgenic mice were generated to selectively target astrocytes *in vivo* (Srinivasan *et al.*, 2016). The expression of the cre is tamoxifen dependent, which restricts the expression of the DREADDs to astrocytes.

Past work has shown that using chemogenetics to activate astrocytes increased Ca^{2+} transients (Agulhon *et al.*, 2013). Astrocyte-DREADD labeled cells colocalized with GFAP expression (Figure 5.3A). Expressing DREADDs in astrocytes produced non-significant changes in overall neural activity as measured with extracellular electrophysiology. Activating hM4D(i) DREADDs expressed in astrocytes with CNO caused no decrease in basal gamma-band power (CNO gamma-band power -12.1±9.3% relative to vehicle, Figure 5.3B, paired t-test p=0.63). When hM3D(q) DREADD receptors in astrocytes were activated, basal gamma-band power was unchanged (CNO gamma-band power increased by -13.0±13.3% relative to vehicle controls, Figure 5.3E, paired t-test p=0.36). When altering the activity of astrocytes using DREADDs, we expect no changes to neural activity, but if the

astrocyte activity is necessary for the regulation of the vasculature, we would expect to measure differences in vessel diameters after the astrocyte-DREADDs manipulations. There were no large changes in neural activity, and we did not see significant changes in the basal arterial diameters with manipulation of astrocyte activity (2.8±7.7%, LME p=0.64 for inhibition and +6.7±10%, LME p=0.44 for excitation) (Figure 5.3 C and F, respectively).

These results suggest that the regulation of the arteriole diameter is independent from the activity of astrocytes. It also suggests that the activity of the neurons affect the vasculature through direct signaling and not by indirect signaling through astrocytes.

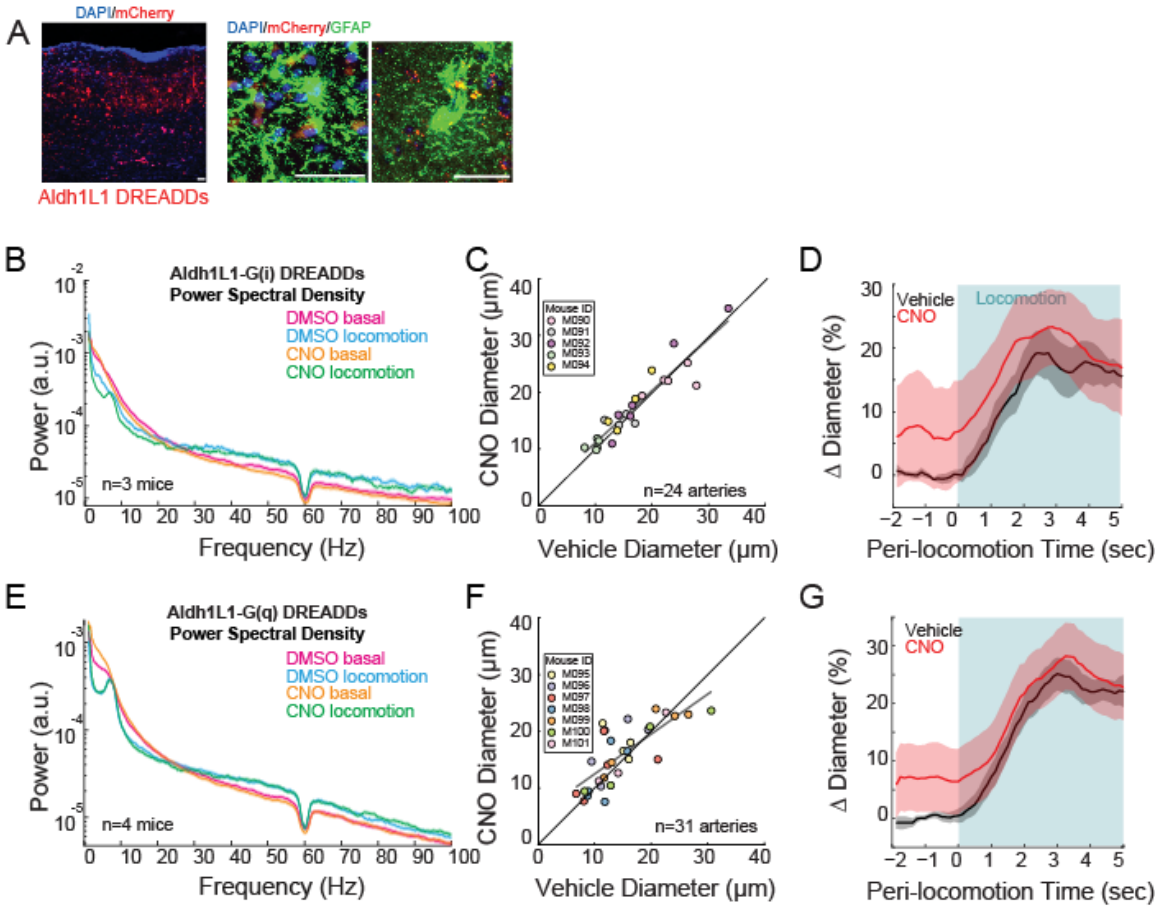

Figure 5.3 **Astrocytes do not mediate the control of the basal arteriole diameter.**

A. Representative image of cortex taken of AAV-hSyn-DIO-hM3D(Gq)-mCherry in Aldh1l1 (astrocyte)-cre mice, where DREADDs expressed in astrocytes. Left image is wide field image of astrocyte-mCherry DREADDs virus (red) in cortex with DAPI (blue) staining (scale bar 100μm). Right image is zoomed image of astrocyte -mCherry DREADDs virus (red) in cortex with DAPI (blue) and GFAP (green) staining (scale bar 30μm). Tissues sectioned to a 90μm thickness
Data in **B-D** are from Aldh1l1 (astrocyte)-cre mice injected with AAV-hSyn-DIO-hM4D(Gi)-mCherry, data in **E-G** is from Aldh1l1 (astrocyte)-cre injected with AAV-hSyn-DIO-hM4D(Gq)-mCherry.
B. LFP power spectra during stationary periods (basal) and locomotion after CNO injection in astrocyte G(i) DREADDs, normalized to vehicle injection in the same mouse. Aldh1l1 expression of G(i) DREADDs did not change neural activity in the gamma band (basal, -12.1±9.3%, paired t-test p=0.63; locomotion, -21.9±8.3 %, paired t-test p=0.17, n=3). Shading denotes mean ± standard deviation.
C. Plot of basal arteriole diameter after vehicle injection (x-axis) versus CNO injection (y-axis). CNO caused no significant change in arterial diameter (2.8±7.7%, LME p=0.64 Bonferroni corrected, n= 5 mice, 24 vessels)
D. Population locomotion-triggered average after vehicle (black) and CNO (red) injections (n=5 mice, 19 arterioles in FL/HL representation). For both cases, the diameters were normalized by the average basal diameter of the vessel after vehicle infusion
E. LFP power spectra during stationary periods (basal) and locomotion after CNO injection in astrocyte G(q) DREADDs, normalized to vehicle injection in the same mouse. Aldh1l1 expression of G(q) DREADDs did not change neural activity in the gamma band basal, 53.0±13.3%, paired t-test p=0.36; locomotion, +10.14±7.3 %, paired t-test p=0.16, n=4).
F. Plot of basal arteriole diameter after vehicle injection (x-axis) versus CNO injection (y-axis). CNO caused no significant change in arterial diameter (+6.7±10%, LME p=0.44 Bonferroni corrected, n= 7 mice, 31 vessels)
G. Locomotion-triggered averages after vehicle (black) and CNO (red) injections (n=7 mice, 20 arterioles in FL/HL representation). For both cases, the diameters were normalized by the average basal diameter of the vessel after vehicle infusion

5.4 **Discussion**

Increases in extracellular K^+ resulting from astrocyte or neuron activity, can cause the hyperpolarization of smooth muscle cells through inward rectifying K^+ (Kir) channels present on endothelial cells (Attwell *et al.*, 2010). This signaling of K^+ could contribute to a portion of the hemodynamic signals (Sonkusare *et al.*, 2016), with the increased conductance of K^+ eliciting outward current flow. The hyperpolarization that follows causes decreased Ca^{2+} influx through the smooth muscle cells and relaxation.

Our data point to an issue with the methods used to manipulate the K^+ signal *in vivo*. Many of the manipulations used to block the Kir channels that allows for K^+ transients in endothelial cells (ML-133 and $BaCl_2$) also affect the activity of neurons.

Blocking Kir channels affects neural excitability, and thus it is hard to untangle any direct effects K^+ signaling could have on the vasculature.

These results go against the results that past researchers have reported. This could be for multiple reasons that are all related to fundamental issues with the experimental design. Importantly, past data comes from applying the Kir blockers to affect extracellular K^+ *in vivo* at the surface of the brain. When using topical administration of pharmacology, the affected area of the manipulation is limited by its inability to diffuse to the relevant areas in deeper layers of cortex (Ferezou, Bolea and Petersen, 2006). There are also no available studies where there are measures of neural activity during the pharmacology manipulation. In our experiments, the use of pharmacology to block Kir channels caused a significant increase in vessel diameter showing potassium transients affect the vasculature. Unfortunately, these results have no straightforward interpretation because these K^+ transients also produces indirect neural changes.

Along with K^+ transients, some speculate that increases in astrocytic Ca^{2+} cause the release of vasoactive components that mediate changes in neurovascular coupling (Gu *et al.*, 2018). Astrocytes are conveniently located near the vasculature and neural synapses (Kacem *et al.*, 1998; Attwell *et al.*, 2010), and have receptors that could act as possible targets for the coupling between neurons and the vasculature (Zonta *et al.*, 2002; Peng *et al.*, 2004; Rosenegger, Ha, *et al.*, 2015). Astrocytes have the potential for the Ca^{2+}-dependent synthesis of vasodilators and constrictors (Nizar *et al.*, 2013). Glutamate-mediated Ca^{2+} elevation in astrocytes through mGluR cause the release of vasoactive compounds (Zonta *et al.*, 2002; Peng *et al.*, 2004). Briefly, the

astrocytic calcium increases (through IP3R-mediated increases in intracellular Ca^{2+}) activates the production of EETs from AA (Zonta *et al.*, 2002; Cauli and Hamel, 2010; Rosenegger, Ha, *et al.*, 2015). The release of EETs act as a vasodilators on the local cerebral arteries (Mishra *et al.*, 2016). However, others have shown these Ca^{2+} changes are delayed and might only contribute to the basal arteriole diameter (Nizar *et al.*, 2013; Gu *et al.*, 2018).

Alterations of the activity of astrocytes with DREADDs had little effect on either basal or evoked arterial diameter. Neither basal nor sensory-evoked changes in arterial diameter are mediated or controlled by local astrocyte activity.

It should be noted that DREADDs allow for local changes of Ca^{2+} in astrocytes and have been shown to inhibit and promote neuronal firing (Urban and Roth, 2015), but it is still not clear exactly how DREADDs affect astrocyte activity or astrocytic Ca^{2+} signaling. Astrocytes differ from neurons because they are not electrically excitable and do not have action potentials. We bi-directionally manipulated G-protein coupled signaling pathways in astrocytes with DREADDs, but this manipulation might not affect astrocytic pathways that drive vasodilation. We did not observe any effect of manipulating astrocyte activity using DREADDs on the vasculature, but the results do not rule out astrocyte signaling pathways not affected by our manipulation.

The alteration of astrocyte activity lacked any observable effect on arterial diameters, which suggests that these cells have a minimal role in regulating neurovascular coupling. Instead, cortical hemodynamic signals seem to be controlled primarily by NO produced by the activity of nNOS-positive neurons, as described in

Chapter 3, and not by the changes signaling pathways affected by our manipulation of astrocytes.

Chapter 6

6 Discussion and future directions

6.1 Discussion

For the previous chapters of this dissertation, we conducted experiments recording the dynamics of individual vessels, cerebral blood volume, and electrophysiological measurements in awake, head fixed mice. Our results have several implications for interpreting hemodynamic signals to infer the underlying neural sub-types and their activity. Understanding the coupling between neurons and the vasculature is important for understanding the basis of cerebral perfusion and neuroimaging (Logothetis, 2008; Attwell *et al.*, 2010).

While it is controversial whether capillaries dilate (Hall *et al.*, 2014; Hill *et al.*, 2015; Mishra *et al.*, 2016) and whether this dilation is active or passive (Mishra *et al.*, 2016; Rungta *et al.*, 2018), sensory stimulation drives reliable and large (~20%) dilations of cerebral arteries in animals (Drew, Shih and Kleinfeld, 2011; Hill *et al.*, 2015; Rungta *et al.*, 2018). The sensory-evoked dilation initiates in the deeper layers of the brain (Tian *et al.*, 2010; Rungta *et al.*, 2018), and rapidly propagates up to the surface arteries via conduction of an electrical signal (Chen *et al.*, 2014). Pial arteries dilate in response to sensory stimulation (Drew, Shih and Kleinfeld, 2011; Gao and Drew, 2016; Winder *et al.*, 2017), and to spontaneous or optogenetically-evoked increases in gamma-band power (Mateo *et al.*, 2017).

Population neural activity has been assumed to underlie hemodynamic signals, with neural activity increases thought to be linearly related with increases in

vessel dilation and cerebral blood flow. These assumptions can become problematic when this direct relationship might break down, like in neurological diseases or even the natural decrease in cerebral perfusion associated with aging. Recent *in vitro* evidence indicates neuronally-generated NO acts directly on arteries (Mishra *et al.*, 2016). In the cortex, there are two types of neuronal nitric oxide synthase (nNOS) expressing interneurons, type 1 and type 2.

6.1.1 **A small subset of interneurons controls neurovascular coupling**

We first show that local neural activity drives both basal and sensory-evoked changes in arterial diameter. Pyramidal neurons are the major source of activity for extracellular recordings of electrical signals and are the major energy consumers in cortex (Vazquez, Fukuda and Kim, 2018), but, unexpectedly, large alterations of pyramidal neural activity had little effect on either basal or evoked arterial diameter. Instead, nNOS-positive neural activity controls cortical hemodynamic signals primarily through the production of NO.

These results support a system where a certain sub-type of neurons, whose activity is not represented in population activity, control basal and evoked blood flow. This is obvious when we compare the relationship between the change in gamma-band power and basal arteriole diameter (Figure 3.12A). There is not a linear relationship between population neural activity and the hemodynamic response, meaning neural activity cannot always be interpreted directly from hemodynamic signals. This observation may resolve several past issues where there have been a mismatch between measured neural activity and hemodynamic signals (Sirotin and Das, 2009; Cardoso *et al.*, 2012).

The data we present is explained if the hemodynamic signals is controlled by a small group of neurons, instead of by overall local neural activity. The results suggest Type 1 nNOS neurons are largely directed by modulatory signals that are active after a sensory stimulus or by attention modulation (Boynton, 2011) and receive negligible local excitatory input. These Type 1 nNOS neurons are small in size and number so their activity is not the prominent signal in the local field potential (Buzsáki, Anastassiou and Koch, 2012). The activity of pyramidal and nNOS-expressing neurons usually change in parallel during natural behaviors, which is why there is a commonly perceived association between vasodilation and gamma band power (Goense and Nikos K Logothetis, 2008; Scholvinck *et al.*, 2010; Winder *et al.*, 2017).

6.1.2 The importance of basal perfusion for neuropathology and ratiometric imaging

In the experiments with muscimol and pan-neuronal DREADDs, we see that a change in basal local neural activity leads to a change in basal diameter of arteries (see Chapter 3). Variations in basal levels for arteriole diameter have the potential to confound ratiometric imaging modalities, especially because the activity of a small group of nNOS neurons can have such a profound effect on arteriole diameter without changes in neural activity. The basal arteriole diameter will greatly impact the magnitude of sensory-evoked responses in ratiometric signals.

Understanding this relationship is important because frequently used ratiometric imaging systems that measure hemodynamics can give an inconsistent representation of neural activity. An important implication for our data is that studies

using cerebral blood flow measurements should take into account the possible signals that are calculated using normalization to get at ratiometric changes. These quantitative measurements are key when comparing across populations (e.g., transgenic versus wildtype mice, diseased versus control humans).

There are also many likely influences that could alter basal neural activity and vasculature of a patient during neuroimaging (anxiety, medications, sleepiness), which has the potential to alter both the resting state fMRI and the BOLD responses to a sensory stimulus.

Our data, along with other research, have demonstrated that variations in the basal cerebral blood flow can shape the BOLD response, but we also wanted to investigate the cellular activity that regulates the basal state. We aimed to obtain the population of neurons that influence the arteriole baseline and determine if the basal condition is differentially regulated from the sensory evoked response. NO released from nNOS neurons contributed to a portion of the baseline arteriole diameter, as shown by experiments with NOS-inhibitors and the inhibition of nNOS neurons using DREADDs.

We predict that the problems with changes in basal state of the vasculature have the potential to affect the interpretation of BOLD imaging, as changes in baseline blood flow can change the magnitude or even the sign of the BOLD response without changes in the underlying neural activity (Cohen, Ugurbil and Kim, 2002; Kim and Ogawa, 2012).

6.1.3 No obvious role for K^+ transients and astrocyte signaling in neurovascular coupling

There are additional mechanisms that could be involved in the control of the remaining basal and evoked diameter changes remaining after modulating nNOS neural activity. This is especially important in the case of the regulation of basal perfusion and vascular tone. These mechanisms include voltage-gated potassium channels (Longden *et al.*, 2017) and signaling from astrocytes (Rosenegger, Tran, *et al.*, 2015).

Astrocyte or neural activity increases in response to a sensory stimuli lead to K^+ transients that precedes the activation of Kir channels present on endothelial cells (Longden *et al.*, 2017). The increased conductance of K^+ causes outward current flow and hyperpolarization in smooth muscle cells. This decreases Ca^{2+} influx through the smooth muscle cells and initiates vessel dilation. Previous research shows that potassium signaling is a possible mechanism in neurovascular coupling (Sonkusare *et al.*, 2016).

Blocking Kir channels to inhibit K^+ transients in endothelial cells caused a significant increase in vessel diameter showing potassium transients affect the vasculature. A major confound for the interpretation of these changes in vasculature is that the experimental design used to affect the K^+ signal *in vivo* (ML-133 and $BaCl_2$) also affect the activity of neurons. In past experiments, researchers fail to measure any off target affects the pharmacology might have on the neural activity. Unfortunately, these results have no straightforward interpretation because it is hard

to untangle any direct effects that K^+ might have on the vasculature from any indirect neural changes the pharmacology produces.

The activity of astrocytes and the role of astrocyte-derived vasoactive components has also been considered as mediating changes in neurovascular coupling (Gu *et al.*, 2018). Astrocytes are an appropriate possible indirect messenger in the signaling from neurons as they are conveniently positioned near both the arteries and neural processes (Kacem *et al.*, 1998; Attwell *et al.*, 2010). Astrocytes possess receptors as possible targets of messengers released during neural activity (Zonta *et al.*, 2002; Peng *et al.*, 2004; Rosenegger, Ha, *et al.*, 2015), along with the capability to produce vasodilators and constrictors (Nizar *et al.*, 2013).

In astrocytes glutamate-mediated Ca^{2+} elevation happen through mGluR and IP3R. The calcium transient initiates the production of vasoactive EETs from AA (Zonta *et al.*, 2002; Cauli and Hamel, 2010; Rosenegger, Ha, *et al.*, 2015). These Ca^{2+} changes are delayed and might only contribute to the basal arteriole diameter (Nizar *et al.*, 2013; Gu *et al.*, 2018). Our experimental setup allows us to probe the role of astrocytes on both basal and sensory evoked hemodynamics. Bi-directional manipulation of astrocyte activity using DREADDs had no significant effect on basal or evoked arterial diameter, which implies that the activity of astrocytes is not necessary in regulating neurovascular coupling.

The data suggests that there is no role for local astrocyte activity in controlling the basal or sensory-evoked changes in arterial diameter. While we did see an effect on the vasculature when altering K^+ signaling, it is hard to untangle any indirect effects caused by neural changes.

As our works shows that cerebral blood flow is controlled by a relatively small subset of neurons, and not by the average population activity. Any damage or dysfunction to this select group of neurons could result in decreased blood flow, regardless of the metabolic need. Importantly, changes in activity patterns of these neurons will alter basal diameter of arteries, which is known to affect the amplitude of fMRI signals (Cohen, Ugurbil and Kim, 2002). There is a decline in the number of interneurons, particularly nNOS-expressing interneurons, with aging (Miettinen *et al.*, 1993; Necchi *et al.*, 2002), and the removal of their tonic vasodilatory signal could elicit decreases in cerebral blood flow that are thought to contribute to dementia (F. Wolters *et al.*, 2017). Indeed, alterations of nNOS and TAC1 (encoding the precursor to Substance P) expression have been implicated in Alzheimer's disease (Li *et al.*, 2016; Han *et al.*, 2019). Protecting these blood-flow controlling neurons from insults and damage could be a promising strategy for preventing neurovascular disorders.

6.2 **Future directions**

The activity of nNOS-positive neurons produced after sensory stimuli or modulatory input can become uncorrelated from pyramidal neural activity. When the activity of different neural sub-types become uncorrelated this will drive neurovascular uncoupling, as has been seen in some studies (Shih *et al.*, 2009; Sirotin and Das, 2009; Huo, Smith and Drew, 2014). Type 1 nNOS neurons are centers for modulation, as they receive orexinergic, substance P input, and cholinergic input from the basal forebrain (Bacci, Huguenard and Prince, 2005; Lee *et al.*, 2010; Owen *et al.*, 2013; Williams, Black, *et al.*, 2018). Activating projections from the basal forebrain to the cortex is known to greatly increase nNOS neural activity and basal cortical blood

flow without cortical metabolic changes (Sato, Sato and Uchida, 2001; Hamel, 2004). These cholinergic projections of basal forebrain are topographically represented (Saper, 1984; J.-H. Kim *et al.*, 2016). Sensory stimulation and voluntary movement increases the activity of cholinergic projections from the basal forebrain and other modulatory regions (Eggermann *et al.*, 2014; Harrison *et al.*, 2016), in agreement with the vasodilation being associated with behaviors (Huo, Smith and Drew, 2014; Winder *et al.*, 2017). nNOS neurons have also been shown to be active during REM sleep, and may release vasoactive messengers responsible for the huge changes in cerebral blood flow during REM sleep (Gerashchenko *et al.*, 2008; Bergel *et al.*, 2018).

In light of these results, we propose fundamental changes in the way hemodynamic signals are interpreted to infer local neural activity. Further investigation of the projections from the basal forebrain to nNOS neurons and the role of these projections in neurovascular coupling needs to be conducted. Also relevant is dissecting the differential role of Type 1 vs Type 2 nNOS neurons in the control of basal and stimulus evoked hemodynamics. This would require a more detailed genetic targeting (using the co-expression of NOS and other peptides to target only Type 1 or Type 2 genetically). Also interesting is any role that nNOS neurons might have on the major dilations and fluctuations that are seen during sleep.

References

Aarts, E. *et al.* (2014) 'A solution to dependency: Using multilevel analysis to accommodate nested data', *Nature Neuroscience*, 17(4), pp. 491–496. doi: 10.1038/nn.3648.

Adams, M. D. *et al.* (2018) 'The pial vasculature of the mouse develops according to a sensory-independent program', *Scientific Reports*. Springer US, 8(1), p. 9860. doi: 10.1038/s41598-018-27910-3.

Agulhon, C. *et al.* (2013) 'Modulation of the autonomic nervous system and behaviour by acute glial cell Gq protein-coupled receptor activation in vivo', *Journal of Physiology*, 591(22), pp. 5599–5609. doi: 10.1113/jphysiol.2013.261289.

Alkayed, H. N. J. *et al.* (1996) 'Inhibition of brain P-450 arachidonic acid epoxygenase decreases baseline cerebral blood flow', *American Journal of Physiology -Heart and Circulatory Physiology*, 271(4), pp. 1541–1546. Available at: http://ajpheart.physiology.org/content/271/4/H1541#cited-by.

Alonso-Galicia, M. *et al.* (1999) 'Contribution of 20-HETE to Vasodilator Actions of Nitric Oxide in the Cerebral Microcirculation', *Stroke*, 30(12), p. 2734. Available at: http://login.ezproxy.library.ualberta.ca/login?url=http://ovidsp.ovid.com/ovidweb.cgi?T=JS&CSC=Y&NEWS=N&PAGE=fulltext&D=ovftd&AN=00007670-199912000-00039.

Anenberg, E. *et al.* (2015) 'Optogenetic stimulation of GABA neurons can decrease local neuronal activity while increasing cortical blood flow', *Journal of Cerebral Blood Flow and Metabolism*. Nature Publishing Group, 35(10), pp. 1579–1586. doi: 10.1038/jcbfm.2015.140.

Astrup, D. *et al.* (1976) 'Evidence against H+ and K+ as the Main Factors in the Regulation of Cerebral Blood Flow during Epileptic Discharges, Acute Hypoxemia, Amphetamine Intoxication, and Hypoglycemia A Microelectrode Study', *Ionic Actions on Vascular Smooth Muscle*, 1(February 1970), pp. 21–26.

Attwell, D. *et al.* (2010) 'Glial and neuronal control of brain blood flow.', *Nature*, 468(7321), pp. 232–43. doi: 10.1038/nature09613.

Bacci, A., Huguenard, J. R. and Prince, D. A. (2005) 'Modulation of neocortical interneurons: Extrinsic influences and exercises in self-control', *Trends in Neurosciences*, 28(11), pp. 602–610. doi: 10.1016/j.tins.2005.08.007.

Barth, M. and Poser, B. A. (2011) 'Advances in High-Field BOLD fMRI', *Materials*, 4(11), pp. 1941–1955. doi: 10.3390/ma4111941.

Bekar, L. K., Wei, H. S. and Nedergaard, M. (2012) 'The locus coeruleus-norepinephrine network optimizes coupling of cerebral blood volume with oxygen demand.', *Journal of cerebral blood flow and metabolism*. Nature Publishing Group, 32(12), pp. 2135–45. doi: 10.1038/jcbfm.2012.115.

Bergel, A. *et al.* (2018) 'Local hippocampal fast gamma rhythms precede

brain-wide hyperemic patterns during spontaneous rodent REM sleep', *Nature Communications*, 9(1), p. 5364. doi: 10.1038/s41467-018-07752-3.

Bharat Biswal, F. *et al.* (1995) 'Functional Connectivity in the Motor Cortex of Resting Human Brain Using Echo-Planar MRI', *Magnetic resonance in medicine*, 77(4), pp. 599–617. doi: 10.1016/j.evopsy.2012.05.001.

Biesecker, K. R. *et al.* (2016) 'Glial Cell Calcium Signaling Mediates Capillary Regulation of Blood Flow in the Retina', *The Journal of Neuroscience*, 36(36), pp. 9435–9445. doi: 10.1523/jneurosci.1782-16.2016.

Biesold, D. *et al.* (1989) 'Stimulation of the nucleus basalis of Meynert increases cerebral cortical blood flow in rats', *Neuroscience Letters*, 98(1), pp. 39–44. doi: 10.1016/0304-3940(89)90370-4.

Bland-Ward, P. A. and Moore, P. K. (1995) '7-Nitro indazole Derivatives are potent inhibitors of brain, endothelium and inducible isoforms of nitric oxide synthase', *Life Sciences*, 57(11), pp. 0–4. doi: 10.1016/0024-3205(95)02046-L.

de Blas, A. L., Vitorica, J. and Friedrich, P. (1988) 'Localization of the GABAA receptor in the rat brain with a monoclonal antibody to the 57,000 Mr peptide of the GABAA receptor/benzodiazepine receptor/Cl- channel complex.', *The Journal of neuroscience*, 8(2), pp. 602–14. Available at: http://www.ncbi.nlm.nih.gov/pubmed/2828565.

Blinder, P. *et al.* (2013) 'The cortical angiome: an interconnected vascular network with noncolumnar patterns of blood flow', *Nature Neuroscience*. Nature Publishing Group, 16(7), pp. 889–897. doi: 10.1038/nn.3426.

Boynton, G. M. (2011) 'Spikes, BOLD, Attention, and Awareness: A comparison of electrophysiological and fMRI signals in V1', *Journal of Vision*, 11(5), pp. 12–12. doi: 10.1167/11.5.12.

Bredt, D. S., Hwang, P. M. and Snyder, S. H. (1990) 'Localization of nitric oxide synthase indicating a neural role for nitric oxide', *Nature*, 347(6295), pp. 768–770. doi: 10.1038/347768a0.

Buerk, D. G. *et al.* (2003) 'Temporal dynamics of brain tissue nitric oxide during functional forepaw stimulation in rats', *NeuroImage*, 18(1), pp. 1–9. doi: 10.1006/nimg.2002.1314.

Busija, D. W. *et al.* (2007) 'Mechanisms Involved in the Cerebrovascular Dilator Effects of N-methyl-D-aspartate in Cerebral Cortex', *Brain Res Rev.*, 46(2), pp. 220–231. doi: 10.1016/j.freeradbiomed.2008.10.025.The.

Buxton, R. B. *et al.* (2004) 'Modeling the hemodynamic response to brain activation', *NeuroImage*, 23(SUPPL. 1), pp. 220–233. doi: 10.1016/j.neuroimage.2004.07.013.

Buzsáki, G., Anastassiou, C. A. and Koch, C. (2012) 'The origin of extracellular fields and currents-EEG, ECoG, LFP and spikes', *Nature Reviews Neuroscience*. Nature Publishing Group, 13(6), pp. 407–420. doi: 10.1038/nrn3241.

Cardoso, M. M. B. *et al.* (2012) 'The neuroimaging signal is a linear sum of neurally distinct stimulus-and task-related components', *Nature Neuroscience*. Nature Publishing Group, 15(9), pp. 1298–1306. doi: 10.1038/nn.3170.

Cauli, B. *et al.* (2004) 'Cortical GABA Interneurons in Neurovascular Coupling: Relays for Subcortical Vasoactive Pathways', *Journal of Neuroscience*, 24(41), pp. 8940–8949. doi: 10.1523/JNEUROSCI.3065-04.2004.

Cauli, B. and Hamel, E. (2010) 'Revisiting the role of neurons in neurovascular coupling.', *Frontiers in neuroenergetics*, 2(June), p. 9. doi: 10.3389/fnene.2010.00009.

Cha, C. I. *et al.* (1998) 'Immunocytochemical study on the distribution of NOS-immunoreactive neurons in the cerebral cortex of aged rats', *NeuroReport*, 9(10), pp. 2171–2174.

Chang, C. *et al.* (2016) 'Tracking brain arousal fluctuations with fMRI', *Proceedings of the National Academy of Sciences*, 113(16), pp. 4518–4523. doi: 10.1073/pnas.1520613113.

Chen, B. R. *et al.* (2014) 'A critical role for the vascular endothelium in functional neurovascular coupling in the brain', *Journal of the American Heart Association*, 3(3), pp. 1–14. doi: 10.1161/JAHA.114.000787.

Chen, K., Pittman, R. N. and Popel, A. S. (2008) 'Nitric oxide in the vasculature: where does it come from and where does it go? A quantitative perspective.', *Antioxidants & redox signaling*, 10(7), pp. 1185–98. doi: 10.1089/ars.2007.1959.

Cipolla, M. J. (2009) *The Cerebral Circulation*. Morgan & Claypool Life Sciences. Available at: https://www.ncbi.nlm.nih.gov/books/NBK53081/.

Cohen, E. R., Ugurbil, K. and Kim, S. (2002) 'Effect of Basal Conditions on the Magnitude and Dynamics of the Blood Oxygenation Level–Dependent fMRI Response', *Journal of Cerebral Blood Flow & Metabolism*, 10(1), pp. 57180–57180.

Cooke, S. F. *et al.* (2015) 'Visual recognition memory, manifested as long-term habituation, requires synaptic plasticity in V1', *Nature Neuroscience*, 18(2), pp. 262–271. doi: 10.1038/nn.3920.

Corfield, D. R. *et al.* (2001) 'Does Hypercapnia-Induced Cerebral Vasodilation Modulate the Hemodynamic Response to Neural Activation ?', 1211, pp. 1207–1211. doi: 10.1006/nimg.2001.0760.

Crochet, S. and Petersen, C. C. H. (2009) 'Cortical Dynamics by Layers', *Neuron*. Elsevier Inc., 64(3), pp. 298–300. doi: 10.1016/j.neuron.2009.10.024.

Desai, M. *et al.* (2010) 'Mapping brain networks in awake mice using combined optical neural control and fMRI', *Journal of Neurophysiology*, 105(3), pp. 1393–1405. doi: 10.1152/jn.00828.2010.

Dittrich, L. *et al.* (2012) 'Cortical nNOS neurons co-express the NK1 receptor and are depolarized by Substance P in multiple mammalian species', *Frontiers in Neural Circuits*, 6(June), pp. 1–11. doi: 10.3389/fncir.2012.00031.

Drew, P. J. *et al.* (2008) 'Finding coherence in spontaneous oscillations', *Nature Neuroscience*, 11(9), pp. 991–993. doi: 10.1038/nn0908-991.

Drew, Patrick J *et al.* (2010) 'Chronic optical access through a polished and reinforced thinned skull.', *Nature Methods*, 7(12), pp. 981–984. doi: 10.1038/nmeth.1530.

Drew, Patrick J. *et al.* (2010) 'Rapid determination of particle velocity from space-time images using the Radon transform', *Journal of Computational Neuroscience*, 29(1–2), pp. 5–11. doi: 10.1007/s10827-009-0159-1.

Drew, P. J., Shih, A. Y. and Kleinfeld, D. (2011) 'Fluctuating and sensory-induced vasodynamics in rodent cortex extend arteriole capacity.', *Proceedings of the National Academy of Sciences of the United States of America*, 108(20), pp. 8473–8478. doi: 10.1073/pnas.1100428108.

Drew, P. J., Winder, A. T. and Zhang, Q. (2018) 'Twitches, Blinks, and Fidgets: Important Generators of Ongoing Neural Activity', *The Neuroscientist*, p. 107385841880542. doi: 10.1177/1073858418805427.

Duvernoy, H. M., Delon, S. and Vannson, J. L. (1981) 'Cortical blood vessels of the human brain', *Brain Research Bulletin*, 7(5), pp. 519–579. doi: 10.1016/0361-9230(81)90007-1.

Edvinsson, L., Larsson, B. and Skarby, T. O. R. (1980) 'Effect of the GABA receptor agonist muscimol on regional cerebral blood flow in the rat', *Brain Research*, 185, pp. 445–448.

Eggermann, E. *et al.* (2014) 'Cholinergic Signals in Mouse Barrel Cortex during Active Whisker Sensing', *Cell Reports*. The Authors, 9(5), pp. 1654–1661. doi: 10.1016/j.celrep.2014.11.005.

Emerson, G. G. and Segal, S. S. (2000) 'Endothelial cell pathway for conduction of hyperpolarization and vasodilation along hamster feed artery', *Circulation Research*, 86(1), pp. 94–100. doi: 10.1161/01.RES.86.1.94.

Endo, T., Yanagawa, Y. and Komatsu, Y. (2016a) 'Substance P Activates Ca2+-Permeable Nonselective Cation Channels through a Phosphatidylcholine-Specific Phospholipase C Signaling Pathway in nNOS-Expressing GABAergic Neurons in Visual Cortex', *Cerebral Cortex*, 26(2), pp. 669–682. doi: 10.1093/cercor/bhu233.

Endo, T., Yanagawa, Y. and Komatsu, Y. (2016b) 'Substance P Activates Ca2+-Permeable Nonselective Cation Channels through a Phosphatidylcholine-Specific Phospholipase C Signaling Pathway in nNOS-Expressing GABAergic Neurons in Visual Cortex', *Cerebral Cortex*, 26(2), pp. 669–682. doi: 10.1093/cercor/bhu233.

Engelhardt, T. *et al.* (2006) 'Inhibition of neuronal nitric oxide synthase reduces the propofol requirements in wild-type and nNOS knockout mice', *European Journal of Anaesthesiology*, 23(3), pp. 197–201. doi: 10.1017/S0265021505002188.

Estabrooke, I. V. *et al.* (2018) 'Fos Expression in Orexin Neurons Varies with Behavioral State', *The Journal of Neuroscience*, 21(5), pp. 1656–1662. doi:

10.1523/jneurosci.21-05-01656.2001.

Estrada, C., Mengual, E. and Gonzalez, C. (1993) 'Local NADPH-diaphorase neurons innervate pial arteries and lie close or project to intracerebral blood vessels: A possible role for nitric oxide in the regulation of cerebral blood flow', *Journal of Cerebral Blood Flow and Metabolism*, 13(6), pp. 978–984. doi: 10.1038/jcbfm.1993.122.

Faraci, F. M. and Breese, K. R. (1993) 'Nitric oxide mediates vasodilatation in response to activation of N- methyl-D-aspartate receptors in brain', *Circulation Research*, 72(2), pp. 476–480. doi: 10.1161/01.RES.72.2.476.

Ferezou, I., Bolea, S. and Petersen, C. C. H. (2006) 'Visualizing the Cortical Representation of Whisker Touch: Voltage-Sensitive Dye Imaging in Freely Moving Mice', *Neuron*, 50(4), pp. 617–629. doi: 10.1016/j.neuron.2006.03.043.

Fergus, A. and Lee, Kevin S (1997) 'GABAergic regulation of cerebral microvascular tone in the rat.', *Journal of cerebral blood flow and metabolism : official journal of the International Society of Cerebral Blood Flow and Metabolism*, 17(9), pp. 992–1003. doi: 10.1097/00004647-199709000-00009.

Fergus, A. and Lee, Kevin S. (1997) 'Regulation of cerebral microvessels by glutamatergic mechanisms', *Brain Research*, 754(1–2), pp. 35–45. doi: 10.1016/S0006-8993(97)00040-1.

Fernandez-Klett, F. *et al.* (2010) 'Pericytes in capillaries are contractile in vivo, but arterioles mediate functional hyperemia in the mouse brain', *Proceedings of the National Academy of Sciences*, 107(51), pp. 22290–22295. doi: 10.1073/pnas.1011321108.

Fox, M. D. and Raichle, M. E. (2007) 'Spontaneous fluctuations in brain activity observed with functional magnetic resonance imaging', *Nature Reviews*, 8(september). doi: 10.1038/nrn2201.

Fox, P. and Raichle, M. (1986) 'Focal physiological uncoupling of cerebral blood flow and oxidative metabolism during somatosensory stimulation in human subjects', *PNAS*, 83(February), pp. 1140–1144. doi: 10.1007/978-3-319-48478-5_1.

Gao, Y.-R. and Drew, P. J. (2014) 'Determination of vessel cross-sectional area by thresholding in Radon space', *Journal of Cerebral Blood Flow & Metabolism*. Nature Publishing Group, 34(7), pp. 1180–1187. doi: 10.1038/jcbfm.2014.67.

Gao, Y.-R. and Drew, P. J. (2016) 'Effects of Voluntary Locomotion and Calcitonin Gene-Related Peptide on the Dynamics of Single Dural Vessels in Awake Mice', *Journal of Neuroscience*, 36(8), pp. 2503–2516. doi: 10.1523/JNEUROSCI.3665-15.2016.

Gao, Y. R., Greene, S. E. and Drew, P. J. (2015) 'Mechanical restriction of intracortical vessel dilation by brain tissue sculpts the hemodynamic response', *NeuroImage*. Elsevier B.V., 115, pp. 162–176. doi: 10.1016/j.neuroimage.2015.04.054.

Gerashchenko, D. *et al.* (2008) 'Identification of a population of sleep-active cerebral cortex neurons', *Proceedings of the National Academy of Sciences*, 105(29), pp. 10227–10232. doi: 10.1073/pnas.0803125105.

Goard, M. and Dan, Y. (2009) 'Basal forebrain activation enhances cortical coding of natural scenes', *Nature Neuroscience*, 12(11), pp. 1444–1449. doi: 10.1038/nn.2402.

Goense, J. B. M. and Logothetis, Nikos K (2008) 'Neurophysiology of the BOLD fMRI signal in awake monkeys.', *Current biology : CB*, 18(9), pp. 631–40. doi: 10.1016/j.cub.2008.03.054.

Goense, J. B. M. and Logothetis, Nikos K. (2008) 'Neurophysiology of the BOLD fMRI Signal in Awake Monkeys', *Current Biology*, 18(9), pp. 631–640. doi: 10.1016/j.cub.2008.03.054.

Gramaglia, I. *et al.* (2006) 'Low nitric oxide bioavailability contributes to the genesis of experimental cerebral malaria', *Nature Medicine*, 12(12), pp. 1417–1422. doi: 10.1038/nm1499.

Greensmith, J. E. and Duling, B. R. (1984) 'Morphology of the constricted arteriolar wall: physiological implications.', *The American journal of physiology*, 247(5 Pt 2), pp. H687-98. doi: 10.1017/S0003055410000110.

Griffith, T. M. (2004) 'Endothelium-dependent smooth muscle hyperpolarization: Do gap junctions provide a unifying hypothesis?', *British Journal of Pharmacology*, 141(6), pp. 881–903. doi: 10.1038/sj.bjp.0705698.

Gritti, I., Mainville, L. and Jones, B. E. (1993) 'Codistribution of GABA- with acetylcholine-synthesizing neurons in the basal forebrain of the rat', *Journal of Comparative Neurology*, 329(4), pp. 438–457. doi: 10.1002/cne.903290403.

Grothe, M. J. *et al.* (2014) 'Atrophy of the cholinergic basal forebrain in dementia with lewy bodies and alzheimer's disease dementia', *Journal of Neurology*, 261(1), pp. 1939–1948. doi: 10.1007/s00415-014-7439-z.

Gu, X. *et al.* (2018) 'Synchronized Astrocytic Ca 2+ Responses in Neurovascular Coupling during Somatosensory Stimulation and for the Resting State', *Cell Reports*. ElsevierCompany., 23(13), pp. 3878–3890. doi: 10.1016/j.celrep.2018.05.091.

Hall, C. N. *et al.* (2014) 'Capillary pericytes regulate cerebral blood flow in health and disease', *Nature*, 508(7494), pp. 55–60. doi: 10.1038/nature13165.Capillary.

Hall, C. N. and Garthwaite, J. (2009) 'What is the real physiological NO concentration in vivo?', *Nitric Oxide - Biology and Chemistry*. The Authors, 21(2), pp. 92–103. doi: 10.1016/j.niox.2009.07.002.

Hamel, E. (2004) 'Cholinergic modulation of the cortical microvascular bed', *Progress in Brain Research*, 145, pp. 171–178. doi: 10.1016/S0079-6123(03)45012-7.

Hamilton, N. B., Atwell, D. and Hall, C. N. (2010) 'Pericyte-mediated regulation of capillary diameter: a component of neurovascular coupling in health and disease', *Frontiers in Neuroenergetics*, 2(May), pp. 1–14. doi: 10.3389/fnene.2010.00005.

Han, S. *et al.* (2019) 'Identification of exon skipping events associated with Alzheimer ' s disease in the human hippocampus', *BMC Medical Genomics*, 12(Suppl 1).

Harnett, M. T. *et al.* (2013) 'Potassium channels control the interaction between active dendritic integration compartments in layer 5 cortical pyramidal neurons', *Neuron*. Elsevier Inc., 79(3), pp. 516–529. doi: 10.1016/j.neuron.2013.06.005.

Harrison, T. C. *et al.* (2016) 'Calcium Imaging of Basal Forebrain Activity during Innate and Learned Behaviors', *Frontiers in Neural Circuits*, 10(May), pp. 1–12. doi: 10.3389/fncir.2016.00036.

Henny, P. and Jones, B. E. (2008) 'Projections from basal forebrain to prefrontal cortex comprise cholinergic, GABAergic and glutamatergic inputs to pyramidal cells or interneurons', *Eur J Neurosci.*, 5(3), pp. 379–390. doi: 10.2217/FON.09.6.Dendritic.

Hill, R. A. *et al.* (2015) 'Regional Blood Flow in the Normal and Ischemic Brain Is Controlled by Arteriolar Smooth Muscle Cell Contractility and Not by Capillary Pericytes', *Neuron*. Elsevier Inc., 87(1), pp. 95–110. doi: 10.1016/j.neuron.2015.06.001.

Hillman, E. M. C. *et al.* (2007) 'Depth-resolved Optical Imaging and Microscopy of Vascular Compartment Dynamics During Somatosensory Stimulation Elizabeth', *Neuroimage*, 35(1), pp. 617–643.

Hoge, R. D. *et al.* (1999) 'Linear coupling between cerebral blood flow and oxygen consumption in activated human cortex', 96(August), pp. 9403–9408.

Huo, B.-X. B.-X., Smith, J. B. and Drew, P. J. (2014) 'Neurovascular coupling and decoupling in the cortex during voluntary locomotion.', *The Journal of Neuroscience*, 34(33), pp. 10975–81. doi: 10.1523/JNEUROSCI.1369-14.2014.

Huo, B.-X., Greene, S. E. and Drew, P. J. (2015) 'Venous cerebral blood volume increase during voluntary locomotion reflects cardiovascular changes', *NeuroImage*. Elsevier Inc., 118, pp. 301–312. doi: 10.1016/j.neuroimage.2015.06.011.

Huo, B. X., Gao, Y. R. and Drew, P. J. (2015) 'Quantitative separation of arterial and venous cerebral blood volume increases during voluntary locomotion', *NeuroImage*. Elsevier Inc., 105, pp. 369–379. doi: 10.1016/j.neuroimage.2014.10.030.

Iadecola, C. (1993) 'Regulation of the cerebral microcirculation during neural activity: is nitric oxide the missing link?', *Trends in Neurosciences*, 16(6), pp. 206–214. doi: 10.1016/0166-2236(93)90156-G.

Iadecola, C. *et al.* (1997) 'Local and Propagated Vascular Responses Evoked by Focal Synaptic Activity in Cerebellar Cortex', *Journal of Neurophysiology*, 78(2), pp. 651–659. doi: 10.1152/jn.1997.78.2.651.

Iadecola, C. (2004) 'Neurovascular regulation in the normal brain and in Alzheimer's disease.', *Nature reviews. Neuroscience*, 5(5), pp. 347–360. doi: 10.1038/nrn1387.

Iadecola, C. and Nedergaard, M. (2007) 'Glial regulation of the cerebral microvasculature', *Nature Neuroscience*, 10(11), pp. 1369–1376. doi: 10.1038/nn2003.

Iddings, J. A. *et al.* (2015) 'Enhanced parenchymal arteriole tone and astrocyte signaling protect neurovascular coupling mediated parenchymal arteriole vasodilation in the spontaneously hypertensive rat', *Journal of Cerebral Blood Flow and Metabolism*. Nature Publishing Group, 35(7), pp. 1127–1136. doi: 10.1038/jcbfm.2015.31.

Intaglietta, M. (1990) 'Vasomotion and flowmotion: physiological mechanisms and clinical evidence', *Vascular Medicine Review*, 1(2), pp. 101–112. doi: 10.1177/1358836x9000100202.

Jones, B. E. (2008) 'Modulation of cortical activation and behavioral arousal by cholinergic and orexinergic systems', *Annals of the New York Academy of Sciences*, 1129, pp. 26–34. doi: 10.1196/annals.1417.026.

Kacem, K. *et al.* (1998) 'Structural organization of the perivascular astrocyte endfeet and their relationship with the endothelial glucose transporter: A confocal microscopy study', *Glia*, 23(1), pp. 1–10. doi: 10.1002/(SICI)1098-1136(199805)23:1<1::AID-GLIA1>3.0.CO;2-B.

Kalinchuk, A. *et al.* (2012) 'The time course of adenosine, nitric oxide (NO) and inducible NO synthase changes in the brain with sleep loss and their role in the NREM sleep homeostatic cascade', *J Neurochem*, 116(2), pp. 260–272. doi: 10.1111/j.1471-4159.2010.07100.x.THE.

Kaneko, T. *et al.* (1994) 'Morphological and chemical characteristics of substand p receptor-immunoreactive neurons in the rat neocortex', *Neuroscience*, 60(I), pp. 199–211.

Kastrup, A. *et al.* (1999) 'Relationship between cerebral blood flow changes during visual stimulation and baseline flow levels investigated with functional MRI', *NeuroReport*, 10(8), pp. 1751–1756.

Kavdia, M., Tsoukias, N. M. and Popel, A. S. (2002) 'Model of nitric oxide diffusion in an arteriole: impact of hemoglobin-based blood substitutes', *American Journal of Physiology -Heart and Circulatory Physiology*, 21205, pp. 2245–2253.

Kawaguchi, Y. (2001) 'Distinct firing patterns of neuronal subtypes in cortical synchronized activities.', *The Journal of neuroscience*, 21(18), pp. 7261–72. Available at: http://www.ncbi.nlm.nih.gov/pubmed/11549736.

Kawaguchi, Y. and Kubota, Y. (1997) 'GABAergic cell subtypes and their synaptic connections in rat frontal cortex', *Cerebral Cortex*, 7(6), pp. 476–486. doi: 10.1093/cercor/7.6.476.

Kay, K. N., Naselaris, T., *et al.* (2008) 'Identifying natural images from human brain activity', *Nature Letters*, 452(7185), pp. 352–355. doi: 10.1038/nature06713.

Kay, K. N., David, S. V., *et al.* (2008) 'Modeling low-frequency fluctuation and hemodynamic response timecourse in event-related fMRI', *Human Brain Mapping*, 29(2), pp. 142–156. doi: 10.1002/hbm.20379.

Kim, J.-H. *et al.* (2016) 'Selectivity of Neuromodulatory Projections from the Basal Forebrain and Locus Ceruleus to Primary Sensory Cortices', *Journal of Neuroscience*, 36(19), pp. 5314–5327. doi: 10.1523/JNEUROSCI.4333-15.2016.

Kim, K. J. *et al.* (2016) 'Vasculo-Neuronal Coupling: Retrograde Vascular Communication to Brain Neurons', *The Journal of Neuroscience*. doi: 10.1523/JNEUROSCI.1300-16.2016.

Kim, S. G. and Ogawa, S. (2012) 'Biophysical and physiological origins of blood oxygenation level-dependent fMRI signals', *Journal of Cerebral Blood Flow and Metabolism*, 32(7), pp. 1188–1206. doi: 10.1038/jcbfm.2012.23.

Kimura, A., Sato, A. and Takano, Y. (1990) 'Stimulation of the nucleus basalis of Meynert does not influence glucose utilization of the cerebral cortex in anesthetized rats', *Neuroscience Letters*, 119(1), pp. 101–104. doi: 10.1016/0304-3940(90)90766-3.

Kleinfeld, D. *et al.* (2011) 'A guide to delineate the logic of neurovascular signaling in the brain', *Frontiers in Neuroenergetics*, 3(APRIL), pp. 1–9. doi: 10.3389/fnene.2011.00001.

Kocharyan, A. *et al.* (2008) 'Specific subtypes of cortical GABA interneurons contribute to the neurovascular coupling response to basal forebrain stimulation', *Journal of Cerebral Blood Flow and Metabolism*, 28(2), pp. 221–231. doi: 10.1038/sj.jcbfm.9600558.

Kövari, E. *et al.* (2007) 'Cortical microinfarcts and demyelination affect cognition in cases at high risk for dementia', *Neurology*, 68(12), pp. 927–931. doi: 10.1212/01.wnl.0000257094.10655.9a.

Kubota, Y. *et al.* (2011) 'Selective coexpression of multiple chemical markers defines discrete populations of neocortical gabaergic neurons', *Cerebral Cortex*, 21(8), pp. 1803–1817. doi: 10.1093/cercor/bhq252.

Lacroix, A. *et al.* (2015) 'COX-2-Derived Prostaglandin E2 Produced by Pyramidal Neurons Contributes to Neurovascular Coupling in the Rodent Cerebral Cortex.', *The Journal of neuroscience*, 35(34), pp. 11791–810. doi: 10.1523/JNEUROSCI.0651-15.2015.

Lauritzen, M. and Gold, L. (2003) 'Brain function and neurophysiological correlates of signals used in functional neuroimaging.', *The Journal of Neuroscience*,

23(10), pp. 3972–80. doi: 86/2/514 [pii].

Lecrux, C. *et al.* (2011) 'Pyramidal Neurons Are "Neurogenic Hubs" in the Neurovascular Coupling Response to Whisker Stimulation', *Journal of Neuroscience*, 31(27), pp. 9836–9847. doi: 10.1523/JNEUROSCI.4943-10.2011.

Lecrux, C. and Hamel, E. (2016) 'Neuronal networks and mediators of cortical neurovascular coupling responses in normal and altered brain states', *Royal Society Publishing*. doi: 10.1098/rstb.2015.0350.

Lee, M. G. *et al.* (2005) 'Cholinergic Basal Forebrain Neurons Burst with Theta during Waking and Paradoxical Sleep', *Journal of Neuroscience*, 25(17), pp. 4365–4369. doi: 10.1523/jneurosci.0178-05.2005.

Lee, S. *et al.* (2010) 'The Largest Group of Superficial Neocortical GABAergic Interneurons Expresses Ionotropic Serotonin Receptors', *Journal of Neuroscience*, 30(50), pp. 16796–16808. doi: 10.1523/JNEUROSCI.1869-10.2010.

Lee, S. *et al.* (2013) 'A disinhibitory circuit mediates motor integration in the somatosensory cortex', *Nature Neuroscience*. Nature Publishing Group, 16(11), pp. 1662–1670. doi: 10.1038/nn.3544.

Lein, E. S. *et al.* (2007) 'Genome-wide atlas of gene expression in the adult mouse brain', *Nature*, 445(7124), pp. 168–176. doi: 10.1038/nature05453.

Li, T., Moseley, M. E. and Glover, G. (1999) 'A FAIR Study of Motor Cortex Activation under Normo- and Hypercapnia Induced by Breath Challenge', 569, pp. 562–569.

Li, W. X. *et al.* (2016) 'Integrated analysis of Alzheimer's disease and schizophrenia dataset revealed different expression pattern in learning and memory', *Journal of Alzheimer's Disease*, 51(2), pp. 417–425. doi: 10.3233/JAD-150807.

Lindauer, U. *et al.* (1999) 'Nitric oxide: a modulator, but not a mediator, of neurovascular coupling in rat somatosensory cortex.', *The American journal of physiology*, 277(2 Pt 2), pp. H799-811. doi: http://www.ncbi.nlm.nih.gov/entrez/query.fcgi?cmd=Retrieve&db=PubMed&dopt=Citation&list_uids=10444508.

Lindauer, U. *et al.* (2010) 'Neurovascular coupling in rat brain operates independent of hemoglobin deoxygenation', *Journal of Cerebral Blood Flow and Metabolism*, 30(4), pp. 757–768. doi: 10.1038/jcbfm.2009.259.

Liu, X. *et al.* (2008) 'Interaction of nitric oxide, 20-HETE, and EETs during functional hyperemia in whisker barrel cortex', *American Journal of Physiology-Heart and Circulatory Physiology*, 295(2), pp. H619–H631. doi: 10.1152/ajpheart.01211.2007.

Logothetis, N. K. *et al.* (2001) 'Neurophysiological investigation of the basis of the fMRI signal', *Nature*, 412(6843), pp. 150–157. doi: 10.1038/35084005.

Logothetis, N. K. (2008) 'What we can do and what we cannot do with fMRI',

Nature Reviews. Nature Neuroscience, pp. 95–101. doi: 10.1016/j.anl.2012.11.003.

Longden, T. A. *et al.* (2017) 'Capillary K+-sensing initiates retrograde hyperpolarization to increase local cerebral blood flow', *Nature Neuroscience*, 20(5), pp. 717–726. doi: 10.1038/nn.4533.

Lopez, A. J. *et al.* (2016) 'Promoter-Specific Effects of DREADD Modulation on Hippocampal Synaptic Plasticity and Memory Formation', *Journal of Neuroscience*, 36(12), pp. 3588–3599. doi: 10.1523/JNEUROSCI.3682-15.2016.

Lourenço, C. F. *et al.* (2014) 'Neurovascular coupling in hippocampus is mediated via diffusion by neuronal-derived nitric oxide', *Free Radical Biology and Medicine*. Elsevier, 73, pp. 421–429. doi: 10.1016/j.freeradbiomed.2014.05.021.

Ma, Y. *et al.* (2016) 'Resting-state hemodynamics are spatiotemporally coupled to synchronized and symmetric neural activity in excitatory neurons', *Proceedings of the National Academy of Sciences*, 113(52), pp. E8463–E8471. doi: 10.1073/pnas.1525369113.

Mateo, C. *et al.* (2017) 'Entrainment of Arteriole Vasomotor Fluctuations by Neural Activity Is a Basis of Blood-Oxygenation-Level-Dependent "Resting-State" Connectivity', *Neuron*. Elsevier Inc., 96(4), pp. 936-948.e3. doi: 10.1016/j.neuron.2017.10.012.

Mesulam, M.-M. *et al.* (1983) 'Cholinergic Innervation of Cortex by the Basal Forebrain: Cytochemistry and Cortical Connections of the Septa Area, Diagonal Band Nuclei, Nucleus Basalis, and Hypothalamus in the Rhesus Monkey', *THE JOURNAL OF COMPARATIVE NEUROLOGY*, 197.

Miettinen, R. *et al.* (1993) 'Neocortical, hippocampal and septal parvalbumin- and somatostatin-containing neurons in young and aged rats: Correlation with passive avoidance and water maze performance', *Neuroscience*, 53(2), pp. 367–378. doi: 10.1016/0306-4522(93)90201-P.

Mishra, A. *et al.* (2016) 'Astrocytes mediate neurovascular signaling to capillary pericytes but not to arterioles', *Nature Neuroscience*, 19(October). doi: 10.1038/nn.4428.

Mitrovic, N. and Schachner, M. (1996) 'Transient expression of NADPH diaphorase activity in the mouse whisker to barrel field pathway.', *Journal of neurocytology*, 25(8), pp. 429–37. Available at: http://www.ncbi.nlm.nih.gov/pubmed/8899565.

Montague, P. *et al.* (1994) 'Role of NO Production in NMDA Receptor-Mediated Neurotransmitter Release in Cerebral Cortex', *Science*, 263(4), pp. 973–977. Available at: http://www.jstor.org/stable/2883276 (Accessed: 20 June 2018).

Nakaya, Y. *et al.* (1994) 'Immunohistochemical localization of substance P receptor in the central nervous system of the adult rat.', *The Journal of comparative neurology*, 347(2), pp. 249–74. doi: 10.1002/cne.903470208.

Necchi, D. *et al.* (2002) 'Regional alterations of the NO/NOS system in the

aging brain: A biochemical, histochemical and immunochemical study in the rat', *Brain Research*, 933(1), pp. 31–41. doi: 10.1016/S0006-8993(02)02302-8.

Nir, Y. *et al.* (2009) 'Interhemispheric correlations of slow spontaneous neuronal fluctuations revealed in human sensory cortex', 11(9), pp. 1100–1108. doi: 10.1038/nn.2177.Interhemispheric.

Nishimura, N. *et al.* (2007) 'Penetrating arterioles are a bottleneck in the perfusion of neocortex', *Proceedings of the National Academy of Sciences*, 6(5), pp. 587–591. doi: 10.1002/cpt196565587.

Niwa, K. *et al.* (2000) 'Cyclooxygenase-2 contributes to functional hyperemia in whisker-barrel cortex.', *The Journal of Neuroscience*, 20(2), pp. 763–70. Available at: http://www.ncbi.nlm.nih.gov/pubmed/10632605.

Nizar, K. *et al.* (2013) 'In vivo stimulus-induced vasodilation occurs without IP3 receptor activation and may precede astrocytic calcium increase.', *The Journal of Neuroscience*, 33(19), pp. 8411–22. doi: 10.1523/JNEUROSCI.3285-12.2013.

Ogawa A, S. *et al.* (1990) 'Brain magnetic resonance imaging with contrast dependent on blood oxygenation', *Proceedings of the National Academy of Sciences*, 87(6), pp. 9868–9872. doi: 10.7566/JPSJ.84.064704.

Owen, S. F. *et al.* (2013) 'Oxytocin enhances hippocampal spike transmission by modulating fast-spiking interneurons', *Nature*. Nature Publishing Group, 500(7463), pp. 458–462. doi: 10.1038/nature12330.

Parabucki, A. and Lampl, I. (2017) 'Volume Conduction Coupling of Whisker-Evoked Cortical LFP in the Mouse Olfactory Bulb', *Cell Reports*. ElsevierCompany., 21(4), pp. 919–925. doi: 10.1016/j.celrep.2017.09.094.

Peng, X. *et al.* (2004) 'Dependency of Cortical Functional Hyperemia to Forepaw Stimulation on Epoxygenase and Nitric Oxide Synthase Activities in Rats', *Journal of Cerebral Blood Flow & Metabolism*. doi: 10.1097/01.WCB.0000114702.97890.E0.

Perrenoud, Q. *et al.* (2012) 'Characterization of Type I and Type II nNOS-Expressing Interneurons in the Barrel Cortex of Mouse', *Frontiers in Neural Circuits*, 6(June), pp. 1–17. doi: 10.3389/fncir.2012.00036.

Peterson, E. C., Wang, Z. and Britz, G. (2011) 'Regulation of cerebral blood flow', *International Journal of Vascular Medicine*, 2011. doi: 10.1155/2011/823525.

Pfeffer, C. K. *et al.* (2013) 'Inhibition of inhibition in visual cortex: The logic of connections between molecularly distinct interneurons', *Nature Neuroscience*. Nature Publishing Group, 16(8), pp. 1068–1076. doi: 10.1038/nn.3446.

Phillips, E. A. and Hasenstaub, A. R. (2016) 'Asymmetric effects of activating and inactivating cortical interneurons', *eLife*, 5, pp. 1–22. doi: 10.7554/elife.18383.

Pigott, B., Bartus, K. and Garthwaite, J. (2013) 'On the selectivity of neuronal NOS inhibitors', *British Journal of Pharmacology*, 168(5), pp. 1255–1265. doi: 10.1111/bph.12016.

Pinto, L. *et al.* (2013) 'Fast modulation of visual perception by basal forebrain cholinergic neurons', *Nature Neuroscience*. Nature Publishing Group, 16(12), pp. 1857–1863. doi: 10.1038/nn.3552.

Pohl, U. *et al.* (1991) 'EDRF-mediated shear-induced dilation opposes myogenic vasoconstriction in small rabbit arteries', *American Journal of Physiology-Heart and Circulatory Physiology*, 261(6), pp. H2016–H2023. doi: 10.1152/ajpheart.1991.261.6.h2016.

Porter, J. T. and McCarthy, K. D. (1996) 'Hippocampal Astrocytes In Situ Respond to Glutamate Released from Synaptic Terminals', *The Journal of Neuroscience*, 29(8 SUPPL.), pp. 14–22.

Poulos, T. L. and Li, H. (2017) 'Nitric Oxide Synthase and Structure-Based Inhibitor Design Thomas', *Nitric Oxide.*, pp. 1–10. doi: 10.1109/EMBC.2016.7590696.Upper.

Powers, W. J., Hirsch, I. B. and Cryer, P. E. (1996) 'Effect of stepped hypoglycemia on regional cerebral blood flow response to physiological brain activation', *American Journal of Physiology-Heart and Circulatory Physiology*, 270(2), pp. H554–H559. doi: 10.1152/ajpheart.1996.270.2.h554.

Purves, D. and Williams, M. (2001) 'The Blood Supply of the Brain and Spinal Cord', in *Neuroscience*. 2nd Editio. Suderland, MA. Available at: https://www.ncbi.nlm.nih.gov/books/NBK11042/.

Raichle, M. E. (2009) 'A Paradigm Shift in Functional Brain Imaging', *Journal of Neuroscience*, 29(41), pp. 12729–12734. doi: 10.1523/JNEUROSCI.4366-09.2009.

Raichle, M. E. and Mintun, M. A. (2006) 'Brain Work and Brain Imaging', *Annual Review of Neuroscience*, 29(1), pp. 449–476. doi: 10.1146/annurev.neuro.29.051605.112819.

Regidor, J., Edvinsson, L. and Divac, I. (1993) 'NOS neurones lie under branchings of cortical arteriolae', *NeuroReport*.

Reiman, E. M. *et al.* (1996) 'Preclinical evidence of alzheimer's disease in persons homozygous for the allele for apolipoprotein E', *THE NEW ENGLAND JOURNAL OF MEDICINE*, pp. 752–758.

Reiner, A. and Zagvazdin, Y. (1998) 'On the selectivity of 7-nitroindazole as an inhibitor of neuronal nitric oxide synthase.', *Trends in pharmacological sciences*, 19(9), pp. 348–50. doi: S0165-6147(98)01194-8 [pii].

Reiter, C. D. *et al.* (2002) 'Cell-free hemoglobin limits nitric oxide bioavailability in sickle-cell disease', *Nature Medicine*, 8(12), pp. 1383–1389. doi: 10.1038/nm799.

Rogan, S. and Roth, B. (2011) 'Remote control of neuronal signaling', *Pharmacological Reviews*, 63(2), pp. 291–315. doi: 10.1124/pr.110.003020.291.

Rosenegger, D. G., Ha, C., *et al.* (2015) 'Tonic Local Brain Blood Flow Control by Astrocytes Independent of Phasic Neurovascular Coupling', *Journal of*

Neuroscience, 35(39), pp. 13463–13474. doi: 10.1523/JNEUROSCI.1780-15.2015.

Rosenegger, D. G., Tran, C. H. T., *et al.* (2015) 'Tonic Local Brain Blood Flow Control by Astrocytes Independent of Phasic Neurovascular Coupling', *Journal of Neuroscience*, 35(39), pp. 13463–13474. doi: 10.1523/JNEUROSCI.1780-15.2015.

Roy, C. S. and Sherrington, C. S. (1890) 'On the regulation of the blood supply of the brain', *Journal of Physiology*, 11(5), pp. 85–108. doi: 10.1113/jphysiol.1890.sp000321.

Ruland, S. and Aiyagari, V. (2007) 'Cerebral Autoregulation and Blood Pressure Lowering', *Hypertension*, 49(5), pp. 977–978. doi: 10.1161/hypertensionaha.107.087502.

Rungta, R. L. *et al.* (2018) 'Vascular Compartmentalization of Functional Hyperemia from the Synapse to the Pia', *Neuron*, pp. 1–14. doi: 10.1016/j.neuron.2018.06.012.

Saper, C. B. (1984) 'Organization of cerebral cortical afferent systems in the rat. II. Magnocellular basal nucleus', *Journal of Comparative Neurology*, 222(3), pp. 313–342. doi: 10.1002/cne.902220302.

Sato, A., Sato, Y. and Uchida, S. (2001) 'Regulation of regional cerebral blood flow by cholinergic fibers originating in the basal forebrain', *International Journal of Developmental Neuroscience*, 96(1), pp. 13–19. doi: 10.1016/S1566-0702(01)00367-8.

Scholvinck, M. L. *et al.* (2010) 'Neural basis of global resting-state fMRI activity', *Proceedings of the National Academy of Sciences*, 107(22), pp. 10238–10243. doi: 10.1073/pnas.0913110107.

Schubert, R., Lidington, D. and Bolz, S. S. (2008) 'The emerging role of Ca2+ sensitivity regulation in promoting myogenic vasoconstriction', *Cardiovascular Research*, 77(1), pp. 8–18. doi: 10.1016/j.cardiores.2007.07.018.

Schummers, J., Yu, H. and Sur, M. (2008) 'Tuned Responses of Astrocytes and Their Influence on Hemodynamic Signals in the Visual Cortex', *Science*, 320(June), pp. 1638–1644.

Scott, N. A. and Murphy, T. H. (2012) 'Hemodynamic responses evoked by neuronal stimulation via channelrhodopsin-2 can be independent of intracortical glutamatergic synaptic transmission', *PLoS ONE*, 7(1), pp. 1–10. doi: 10.1371/journal.pone.0029859.

Shih, A. Y. *et al.* (2012) 'Two-photon microscopy as a tool to study blood flow and neurovascular coupling in the rodent brain', *Journal of Cerebral Blood Flow and Metabolism*, 32(7), pp. 1277–1309. doi: 10.1038/jcbfm.2011.196.

Shih, Y.-Y. I. *et al.* (2009) 'A New Scenario for Negative Functional Magnetic Resonance Imaging Signals: Endogenous Neurotransmission', *Journal of Neuroscience*, 29(10), pp. 3036–3044. doi: 10.1523/JNEUROSCI.3447-08.2009.

Shmuel, A. and Leopold, D. a (2008) 'Neuronal correlates of spontaneous

fluctuations in fMRI signals in monkey visual cortex: Implications for functional connectivity at rest.', *Human brain mapping*, 29(7), pp. 751–61. doi: 10.1002/hbm.20580.

Sirotin, Y. and Das, A. (2009) 'Anticipatory haemodynamic signals in sensory cortex not predicted by local neuronal activity', *Nature Letters*. Nature Publishing Group, pp. 4843–4843.

Smiley, J. F., McGinnis, J. P. and Javitt, D. C. (2000) 'Nitric oxide synthase interneurons in the monkey cerebral cortex are subsets of the somatostatin, neuropeptide Y, and calbindin cells', *Brain Research*, 863(1–2), pp. 205–212. doi: 10.1016/S0006-8993(00)02136-3.

Sonkusare, S. K. *et al.* (2016) 'Inward rectifier potassium (Kir2.1) channels as end-stage boosters of endothelium-dependent vasodilators', *Journal of Physiology*, 12, pp. 3271–3285. doi: 10.1113/JP271652.

Srinivasan, R. *et al.* (2016) 'New Transgenic Mouse Lines for Selectively Targeting Astrocytes and Studying Calcium Signals in Astrocyte Processes In Situ and In Vivo', *Neuron*, pp. 1–15. doi: 10.1016/j.neuron.2016.11.030.

Steelman, S. M. *et al.* (2010) 'Perivascular tethering modulates the geometry and biomechanics of cerebral arterioles', *Journal of Biomechanics*. Elsevier Ltd, 43(14), pp. 2717–2721. doi: 10.1016/j.jbiomech.2010.06.024.

Stefanovic, B. *et al.* (2007) 'Functional uncoupling of hemodynamic from neuronal response by inhibition of neuronal nitric oxide synthase', *Journal of Cerebral Blood Flow and Metabolism*, 27(4), pp. 741–754. doi: 10.1038/sj.jcbfm.9600377.

Stefanovic, B. *et al.* (2008) 'Functional reactivity of cerebral capillaries', *Journal of Cerebral Blood Flow and Metabolism*, 28(5), pp. 961–972. doi: 10.1038/sj.jcbfm.9600590.

Takano, T. *et al.* (2006) 'Astrocyte-mediated control of cerebral blood flow', *Nature Neuroscience*, 9(2), pp. 260–267. doi: 10.1038/nn1623.

Takata, N. *et al.* (2013) 'Cerebral Blood Flow Modulation by Basal Forebrain or Whisker Stimulation Can Occur Independently of Large Cytosolic Ca2+ Signaling in Astrocytes', *PLoS ONE*, 8(6), pp. 4–9. doi: 10.1371/journal.pone.0066525.

Tasic, B. *et al.* (2016) 'Adult mouse cortical cell taxonomy revealed by single cell transcriptomics', *Nature Neuroscience*, 19(2), pp. 335–346. doi: 10.1038/nn.4216.

Tian, P. *et al.* (2010) 'Cortical depth-specific microvascular dilation underlies laminar differences in blood oxygenation level-dependent functional MRI signal', *Proceedings of the National Academy of Sciences*, 107(34), pp. 15246–15251. doi: 10.1073/pnas.1006735107.

Tomioka, R. *et al.* (2005) 'Demonstration of long-range GABAergic connections distributed throughout the mouse neocortex', *European Journal of*

Neuroscience, 21(6), pp. 1587–1600. doi: 10.1111/j.1460-9568.2005.03989.x.

Tomioka, R. and Rockland, K. (2007) 'Long-Distance Corticocortical GABAergic Neurons in the Adult Monkey White and Gray Matter', *Journal of Comparative Neurology*, 7(4), pp. 430–438. doi: 10.1002/cne.

Tricoire, L. and Vitalis, T. (2012) 'Neuronal nitric oxide synthase expressing neurons: a journey from birth to neuronal circuits', *Frontiers in Neural Circuits*, 6(December), pp. 1–16. doi: 10.3389/fncir.2012.00082.

Uhlirova, H., Kılıç, K., *et al.* (2016) 'Cell type specificity of neurovascular coupling in cerebral cortex', *eLife*, 5(MAY2016), pp. 1–23. doi: 10.7554/eLife.14315.

Uhlirova, H., Kılıc, K., *et al.* (2016) 'The roadmap for estimation of cell-type-specific neuronal activity from non- invasive measurements', *Proceedings Of The Royal Society Of London*, 371(August), p. 20150356. doi: 10.1098/rstb.2015.0356.

Urban, D. J. and Roth, B. L. (2015) 'DREADDs (Designer Receptors Exclusively Activated by Designer Drugs): Chemogenetic Tools with Therapeutic Utility', *Annual Review of Pharmacology and Toxicology*, 55(1), pp. 399–417. doi: 10.1146/annurev-pharmtox-010814-124803.

Vanlandewijck, M. *et al.* (2018) 'A molecular atlas of cell types and zonation in the brain vasculature', *Nature*. Nature Publishing Group, 554(7693), pp. 475–480. doi: 10.1038/nature25739.

Vaucher, E. *et al.* (2000) 'GABA neurons provide a rich input to microvessels but not nitric oxide neurons in the rat cerebral cortex: A means for direct regulation of local cerebral blood flow', *Journal of Comparative Neurology*, 421(2), pp. 161–171. doi: 10.1002/(SICI)1096-9861(20000529)421:2<161::AID-CNE3>3.0.CO;2-F.

Vaucher, E., Linville, D. and Hamel, E. (1997) 'Cholinergic basal forebrain projections to nitric oxide synthase- containing neurons in the rat cerebral cortex', *Neuroscience*, 79(3), pp. 827–836. doi: 10.1016/S0306-4522(97)00033-X.

Vazquez, A. L. *et al.* (2014) 'Neural and hemodynamic responses elicited by forelimb- and photo-stimulation in channelrhodopsin-2 mice: Insights into the hemodynamic point spread function', *Cerebral Cortex*, 24(11), pp. 2908–2919. doi: 10.1093/cercor/bht147.

Vazquez, A. L., Fukuda, M. and Kim, S.-G. (2018) 'Inhibitory Neuron Activity Contributions to Hemodynamic Responses and Metabolic Load Examined Using an Inhibitory Optogenetic Mouse Model', *Cerebral Cortex*, (November), pp. 4105–4119. doi: 10.1093/cercor/bhy225.

Vruwink, M. *et al.* (2001) 'Substance P and nitric oxide signaling in cerebral cortex: Anatomical evidence for reciprocal signaling between two classes of interneurons', *Journal of Comparative Neurology*, 441(4), pp. 288–301. doi: 10.1002/cne.1413.

Williams, R. H., Vazquez-derose, J., *et al.* (2018) 'Cortical nNOS / NK1 Receptor Neurons are Regulated by Cholinergic Projections From the Basal

Forebrain', *Cerebral Cortex*, pp. 1–28.

Williams, R. H., Black, S. W., *et al.* (2018) 'Excitation of Cortical nNOS/NK1R Neurons by Hypocretin 1 is Independent of Sleep Homeostasis', *Cerebral Cortex*, (February), pp. 1–19. doi: 10.1093/cercor/bhy015.

Winder, A. T. *et al.* (2017) 'Weak correlations between hemodynamic signals and ongoing neural activity during the resting state', *Nature Neuroscience*. Springer US, 20(12), pp. 1761–1769. doi: 10.1038/s41593-017-0007-y.

Winship, I. R., Plaa, N. and Murphy, T. H. (2007) 'Rapid Astrocyte Calcium Signals Correlate with Neuronal Activity and Onset of the Hemodynamic Response In Vivo', *Journal of Neuroscience*, 27(23), pp. 6268–6272. doi: 10.1523/jneurosci.4801-06.2007.

Wolf, T. *et al.* (1997) 'Excessive oxygen or glucose supply does not alter the blood flow response to somatosensory stimulation or spreading depression in rats', *Brain Research*, 761(2), pp. 290–299. doi: 10.1016/S0006-8993(97)00354-5.

Wölfle, S. E. *et al.* (2011) 'Non-linear relationship between hyperpolarisation and relaxation enables long distance propagation of vasodilatation', *Journal of Physiology*, 589(10), pp. 2607–2623. doi: 10.1113/jphysiol.2010.202580.

Wolters, F. *et al.* (2017) 'Cerebral Perfusion and the Risk of Dementia', *Circulation*, 136, pp. 719–728. doi: 10.1161/CIRCULATIONAHA.117.027448.

Wolters, F. J. *et al.* (2017) 'Cerebral perfusion and the risk of dementia: A population-based study', *Circulation*, 136(8), pp. 719–728. doi: 10.1161/CIRCULATIONAHA.117.027448.

Yaksh, T. L., Wang, J. Y. and Go, V. L. W. (1987) 'Cortical vasodilatation produced by vasoactive intestinal polypeptide (VIP) and by physiological stimuli in the cat', *Journal of Cerebral Blood Flow and Metabolism*, 7(3), pp. 315–326. doi: 10.1038/jcbfm.1987.69.

Yousef, T. *et al.* (2004) 'Nitric oxide synthase in rat visual cortex: An immunohistochemical study', *Brain Research Protocols*, 13(1), pp. 57–67. doi: 10.1016/j.brainresprot.2004.01.004.

Zaldivar, D. *et al.* (2018) 'Two distinct profiles of fMRI and neurophysiological activity elicited by acetylcholine in visual cortex', *Proceedings of the National Academy of Sciences*, 115(51), pp. E12073–E12082. doi: 10.1073/pnas.1808507115.

Zhao, F. *et al.* (2006) 'Cortical layer-dependent BOLD and CBV responses measured by spin-echo and gradient-echo fMRI: Insights into hemodynamic regulation', *NeuroImage*, 30(4), pp. 1149–1160. doi: 10.1016/j.neuroimage.2005.11.013.

Zonta, M. *et al.* (2002) 'Neuron-to-astrocyte signaling is central to the dynamic control of brain microcirculation', *Nature Neuroscience*, 6(1), pp. 43–50. doi: 10.1038/nn980.

Vita

Christina Echagarruga

EDUCATION

Pennsylvania State University 2015-2019
Ph.D. Bioengineering, Advisor: Patrick Drew

University of Miami 2008-2012
B.S. Biomedical Engineering

PUBLICATIONS

Echagarruga C, Gheres K, Drew P. "An oligarchy of NO-producing interneurons controls basal and evoked arterial dilation in the cortex." *In prep.*

Winder A, **Echagarruga C,** Zhang Q, Drew P. "Spontaneous hemodynamic signals report a mixture of behavior, local neural activity, and putatively non-neural processes." Nature Neuroscience. September 2017

Newman J D, **Echagarruga C,** … Berger J. "Hyperglycemia enhances arsenic-induced platelet and megakaryocyte activation." Journal of Translational Medicine. March 2017.

Montenont E, **Echagarruga C, …** Berger JS. "Platelet WDR1 suppresses platelet activity and associates with cardiovascular disease." Blood. September 2016.

Shah B, Allen N, Harchandani B, Pillinger M, Katz S, Sedlis SP, Echagarruga C, … Berger JS. "Effect of Colchicine on Platelet-Platelet and Platelet-Leukocyte Interactions: A Pilot Study in Healthy Subjects" Inflammation August 2015.

SELECTED PRESENTATIONS

Echagarruga C, Drew P. Dissecting the neural contribution to vascular tone in the brain. Society for Neuroscience Conference; San Diego, CA, November 2018.
Echagarruga C, Drew P. Dissecting the neural control of baseline and evoked vascular tone in the brain. World Congress for Microcirculation; Vancouver Canada, September 2018.
Echagarruga C, Zhang Q, Drew P. Dissecting neuronal cell-type specific control of neurovascular coupling using DREADDs. Society for Neuroscience Conference; Washington DC, November 2017.
Winder A, **Echagarruga C**, Drew P. Spontaneous hemodynamic fluctuations have behavioral and non-neuronal origins. Society for Neuroscience Conference; San Diego, CA, November 2016.